the STEEL centre

STABILITY OF EXTENDED SHEAR TAB CONNECTIONS UNDER COMBINED LOADING

Victoria Buffam

Robert G. Driver

Logan Callele

UNIVERSITY OF ALBERTA

cisc icca

External Sponsor

NSERC CRSNG

Steel Centre Industry Partners

cisc icca

SUPREME GROUP

COLLINS STEEL EST. 1984

WF STEEL & CRANE

Waiward

DIALOG®

S-FRAME SOFTWARE

TSE TSE STEEL LTD.

ECA EDMONTON CONSTRUCTION ASSOCIATION

PRICE STEEL LTD.

Stability of Extended Shear Tab Connections Under Combined Loading

by

Victoria Buffam
Robert G. Driver
and
Logan Callele

Steel Centre Engineering Report No. 012

Department of Civil and Environmental Engineering
University of Alberta
Edmonton, Alberta, Canada

March 2018

ABSTRACT

Extended shear tab connections are efficient for both fabrication and erection where a beam would otherwise need to be coped to clear the flanges of the supporting member, and are therefore used extensively in industry. Stability issues can arise as the plate becomes longer and more slender, as may be required in skewed connections or other complex geometries. Therefore, this research aims to determine when stability of the extended shear tab governs the behaviour and capacity of the connection as opposed to strength, considering the interaction of shear, axial and bending stresses.

A parametric study using finite element simulations was conducted in which the length of the extended shear tab was increased until instability of the plate became the governing failure mode. A full-scale experimental testing program was also completed to further validate the results of the numerical analysis. The study investigated the effect of plate depth, plate thickness and level of applied axial compression. The shear capacity of the connection is discussed and a design procedure for the critical length is proposed. The recommendation includes the effect of varying levels of axial load and initial imperfections.

ACKNOWLEDGEMENTS

University of ALBERTA   cisc icca

iii

TABLE OF CONTENTS

LIST OF TABLES

LIST OF FIGURES

LIST OF SYMBOLS

C_b	=	Moment gradient coefficient for lateral–torsional buckling in AISC
D	=	Fillet weld leg size
d	=	Depth of extended shear tab plate
E	=	Modulus of elasticity
e_b	=	Bolt group shear load eccentricity
$e_{eff\text{-}cs}$	=	Clear span effective eccentricity
e_g	=	Geometric eccentricity
F_{cr}	=	Flexural local buckling stress
F_y	=	Plate nominal yield stress
G	=	Shear modulus
I_y	=	Weak-axis moment of inertia
J	=	St. Venant torsional constant
L_b	=	Unbraced length of plate
L_{cr}	=	Critical length of plate (measured from the support to the first vertical bolt line)
M	=	Applied moment
M_{BG}	=	Moment about the centroid of the bolt group
M_{cr}	=	Elastic lateral–torsional buckling moment capacity
M_n	=	Nominal flexural strength
M_p	=	Plastic moment of shear tab plate
$M_{p(reduced)}$	=	Plastic moment capacity reduced for shear and axial stresses
M_S	=	Moment at support
M_y	=	Yield moment of shear tab plate
P	=	Applied axial load
P_y	=	Axial yield load
Q	=	Yield stress reduction factor for plate buckling
s	=	Bolt spacing in horizontal direction
S_x	=	Elastic section modulus

t	=	Extended shear tab plate thickness
t_{min}	=	Minimum plate thickness
V	=	Applied shear load
V_{LTB}	=	Nominal shear force that can be applied without stiffeners
V_{MN}	=	Flexural shear capacity of the plate
V_n	=	Nominal shear strength
V_p	=	Plastic shear strengh
X_u	=	Ultimate tensile strength of weld filler material
Z_x	=	Strong-axis plastic section modulus
λ	=	Slenderness parameter
σ_n	=	Normal stress
τ	=	Shear stress
κ	=	Ratio of smaller end moment to larger, positive for double curvature
$\psi_{Axial(10\%)}$	=	Reduction factor for 10% axial load
$\psi_{Axial(25\%)}$	=	Reduction factor for 25% axial load
ψ_{II}	=	Reduction factor for initial imperfections
ω_2	=	Moment gradient coefficient for lateral–torsional buckling in S16
$\omega_{2(10\%)}$	=	Moment gradient coefficient for 10% axial load
$\omega_{2(25\%)}$	=	Moment gradient coefficient for 25% axial load

CHAPTER 1: INTRODUCTION

1.1 Statement of Problem

Shear tab connections are commonly used in steel building construction to transfer gravity loads from beams to supporting members. The connection consists of a vertical plate welded to a column or girder and bolted to the supported beam; as such, they are efficient for both fabrication and erection and are extensively used in industry. Extended shear tabs have a similar configuration, but with an increased plate length in order to clear the flanges of the supporting member, and eliminate the need for coping the beam as shown in Figure 1-1(b). This reduces fabrication time and costs.

<center>(a)   (b)</center>
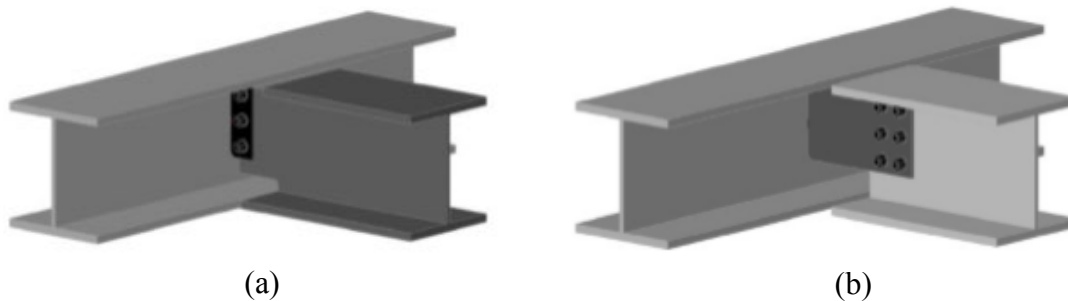
Figure 1-1: Shear tab configurations (Salem et al. 2016):
(a) Conventional shear tab with double-coped beam; (b) Extended shear tab

The behaviour of extended shear tabs differs from that of the conventional configuration, as the increased length of the plate introduces potential stability concerns. Since this behaviour is not well understood, designers have typically adopted a conservative approach wherein the plate thickness is increased or stiffeners (stabilizer plates) added to prevent plate buckling, reducing or eliminating the economic advantage of the connection. Figure 1-2 illustrates both configurations of the extended shear tab. Recent research at the University of Alberta by Thomas et al. (2014) determined that installing stiffeners alters the behaviour of the connection significantly and can cause failure to occur as a result of out-of-plane deformations.
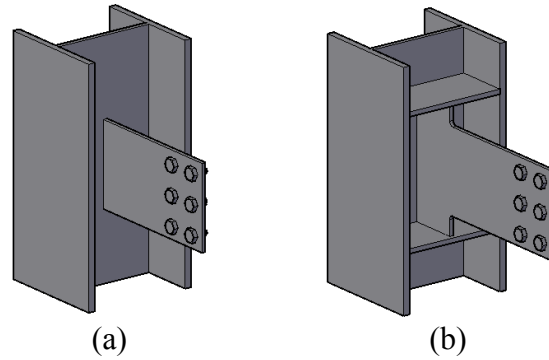
Figure 1-2: Extended shear tab configurations:
(a) Unstiffened; (b) Stiffened

Extended shear tab connections with either rigid or semi-rigid supports were later investigated by Salem et al. (2016) through experimental tests and finite element simulations. Nearly all specimens developed their full cross-sectional plastic capacity prior to failure caused by bolt fracture or out-of-plane deformations. The results were compared to capacity and failure mode predictions using the method in the 14th edition of the *Steel Construction Manual* (AISC 2011). The procedure under-predicted the ultimate capacity in all cases, but also incorrectly predicted plate buckling as the failure mode for some specimens. AISC (2011) indicates that stiffeners must be added to the connection in the event of this type of failure. However, no stiffeners were present in the experimental program, and the shear tab plates did not buckle prior to reaching their full plastic capacity. This indicates that extended shear tab plates are much more stable than predicted by the AISC design method.

Shear connections are increasingly being required to transfer axial loads (compressive or tensile). These loads can occur as a result of member orientation, as in the case of stair stringers, lateral loads (wind and seismic), or industrial equipment. Compressive loads were observed to reduce the shear capacity of unstiffened extended shear tab connections (Thomas et al. 2014) and are also expected to have a detrimental effect on plate stability.

Despite their common use, the effects of stability on the behaviour of extended shear tab connections are not well understood. Few research programs have reported stability failures of these connections when the supported beam is laterally braced, as is common practice in building construction. Additionally, combined loading creates complex stress states that

are not currently accounted for in design procedures. Therefore, a research program consisting of numerical and experimental tests is required to better understand stability of extended shear tabs.

1.2 Objectives and Scope

The main objective of this research program is to investigate the effects of stability on the behaviour of extended shear tab connections of a laterally supported beam. A parametric study has been conducted to determine when instability becomes the governing failure mode, as opposed to cross-sectional strength. A secondary objective is to study the behaviour of the connection when it is subjected to combined rotation, shear loading, and an axial compressive load. The effects of certain geometric parameters on the connection behaviour and capacity are also investigated and quantified.

The parametric study was conducted using a finite element model developed during previous research on extended shear tabs that was modified to meet the requirements of this study. Twenty-seven models were analyzed varying the plate depth, plate thickness, and level of axial compression. The results were used to create an experimental test matrix, and six specimens were tested in the laboratory at three different lengths. The loading beam was braced near the connection in order to focus on local stability of the plate. Finally, the results of the experimental tests were used to further validate the finite element model. Ultimately, the results are used to propose a method for determining the length at which instability becomes the governing design limit state.

1.3 Organization of Thesis

This thesis is organized into six chapters. Chapter 2 is a review of recent literature regarding extended shear tab connections. Design methodologies and equations for stability limit states from the 14th and 15th editions of the *Steel Construction Manual* (AISC 2011; 2017) are outlined and discussed.

The finite element model and corresponding parametric study are included in Chapter 3. Details regarding the development and modification of the model such as: model assembly, boundary conditions, and loading are presented. The methodology for the parametric study

is discussed, including the selection of variables. Finally, the results of the study are presented and vertical load–displacement response, bending moment variation, and deformed shapes are used to draw conclusions regarding the stability behaviour of extended shear tabs.

The full-scale experimental testing program is outlined in Chapter 4, which discusses the creation of the test matrix. Specimen geometries and material properties are presented and the test set-up, instrumentation, and loading procedure are discussed. A summary of the test results is presented by reporting the connection capacity, bending moment ratios, failure modes, and shear load eccentricity. The results are also compared to those obtained from finite element models having identical geometry and material properties.

A discussion regarding the importance of the critical length is contained in Chapter 5. Additionally, a design equation is proposed, along with relevant reduction factors, based on the numerical test results. The shear load design philosophy for extended shear tabs is also discussed.

Conclusions drawn from this study are included in Chapter 6, along with recommendations for future work. Vertical load–displacement, bending moment ratio–displacement and eccentricity ratio–displacement curves extracted from the numerical models are contained in Appendix A. Stress–strain curves obtained from the experimental tension coupon tests are in Appendix B. Finally, Appendix C includes the same displacement responses as Appendix A, but for the experimental test specimens. Appendix D contains comparisons of the numerical and experimental bending moment ratio–displacement responses.

CHAPTER 2: LITERATURE REVIEW

2.1 Introduction

Research relating to steel extended shear tab connections has become more widespread in recent years due to their frequent use. Despite this, concerns regarding the stability of this connection still exist, leading to conservatively designed connections. As such, a review of recent research studies was conducted to summarize existing knowledge and identify parameters worth investigating. An overview of research relating to the behaviour and design of extended shear tabs, using both finite element analysis and experimental test data, is presented. Additionally, design guidelines and equations currently used to check plate stability are discussed.

2.2 Extended Shear Tabs

2.2.1 Sherman and Ghorbanpoor (2002)

The behaviour of extended shear tabs when welded to the web of a girder or column was investigated by Sherman and Ghorbanpoor (2002). The objective of the study was to develop a comprehensive design procedure, including the evaluation of connection capacity, the identification of the shear load eccentricity, and the determination of critical limit states.

The study consisted of an experimental testing program in three phases, with all extended shear tab specimens having a single vertical line of bolts. In the first phase, 17 physical tests were conducted on either stiffened or unstiffened extended shear tab specimens supported by either column or girder webs. The second phase consisted of four tests and investigated the use of snug-tight bolts in short slotted holes, as well as the effect of stiffener (stabilizer) plates and their behaviour. Ten tests were performed in the third phase on deeper connections—those having six or eight bolts—and included both stiffened and unstiffened connections. The parameters used to evaluate the connection behaviour are as follows: span-to-depth ratio of the supported beam, depth-to-thickness ratio of the support member web, geometry of the shear tab, number and type of bolt holes, and presence of lateral bracing of the supported beam.

In order to determine ultimate shear capacities and failure modes, shear–displacement, shear–twist, and shear–rotation curves were constructed for each test. In most tests, the curves became non-linear due to several simultaneous conditions such as shear distortion of the shear tab, twisting of the shear tab, and a yield line mechanism in the supporting member web. The ultimate capacity was taken as the point where the curve slope approached zero, or the highest load achieved. The shear load eccentricity, which is defined as the distance from the bolt line to the point of zero moment, was also measured. Sherman and Ghorbanpoor (2002) observed that this eccentricity varied with the shear load, with the largest variations occurring at low loads. The measured eccentricities did not correlate well with the AISC *Steel Construction Manual LRFD* (1994) recommended values for either rigid or flexible supports for the stiffened and unstiffened connections. The researchers considered the standard limit states to be: bolt shear, bolt bearing, gross shear yielding, net section rupture, block shear rupture, and weld shear. However, additional failure modes were observed during testing and include weld tearing, plate buckling, tearing of the extended shear tab, bolt fracture, and web shear (Sherman and Ghorbanpoor 2002).

The following conclusions were drawn from the results of the physical testing program:

- For connections with three to five bolts, the use of the measured eccentricity to calculate ultimate capacity correlated better with the experimental capacity results as opposed to the AISC (1994) recommended values. However, for deeper connections, the AISC (1994) eccentricities gave values closer to the experimental capacities.

- The critical failure mode predicted using the AISC (1994) eccentricity was always bolt shear; however, using the measured eccentricity resulted in an accurate prediction of the observed failure mode.

- The capacity of the connection was not affected by lateral bracing of the beam.

- Yield-line mechanism failure of the supporting web must be considered an additional limit state for column webs with a large depth-to-thickness ratio.

- Unstiffened extended shear tabs have much lower capacities when compared to conventional shear tabs.

- Plate twist is an additional potential failure mode due to the lateral eccentricity between the supported beam web and the extended shear tab. Twisting deformations are also present when beam bracing is used.

Sherman and Ghorbanpoor (2002) developed a design procedure for extended shear tabs within the geometric constraints of the experimental testing program. They reported, however, that the pertinent AISC committee decided that the procedure should include only stiffened connections, as the deformations of unstiffened connections were observed to be excessive at the ultimate limit state.

2.2.2 Metzger (2006)

The performance and behaviour of shear tabs designed in accordance with the 13th edition of the *Steel Construction Manual* (AISC 2005) were experimentally determined by Metzger (2006). A full-scale testing program was developed that consisted of four conventional shear tabs and four extended shear tabs. The parameters varied were: number of horizontal bolt lines, number of vertical bolt lines, and length of plate between the weld and bolt group centre. The maximum length that was investigated is 267 mm (10.5 in.). The results were used to determine the ultimate shear capacity, the failure modes, and rotational ductility of the connection.

The shear tab connections were tested under a combination of rotation and vertical loading that was stopped once the loading beam reached its plastic moment. Shear–rotation curves were plotted for each test and exhibited linear behaviour until the beam began to yield. The longest extended shear tabs showed twisting of the plate about its longitudinal axis and large in-plane moments at the column support; therefore, additional lateral bracing was added to the beam near the connection. Yielding was observed in the plate near the bolts; however, failure occurred due to local buckling of the beam at midspan. Metzger (2006) concluded that the design method of the 13th edition *Steel Construction Manual* (AISC 2005) is conservative in its prediction of the connection capacity and bolt group strength. Additionally, the weld size requirement is adequate for both conventional and extended shear tab configurations.

2.2.3 Rahman et al. (2007)

A 3D finite element model was created by Rahman et al. (2007) to study the behaviour of unstiffened extended shear tabs. The model was validated using the results of the physical testing program of Sherman and Ghorbanpoor (2002). The objective of the study was to determine the parameters necessary to represent connection behaviour accurately.

The finite element software ANSYS was used to create the unstiffened extended shear tab model. Eight-node brick elements were used for the beam, support, and shear tab and ten-node tetrahedral elements for the bolts, pretension elements, and contact elements. Elements were positioned in the same locations as the instrumentation of the experimental tests to facilitate strain comparisons. Mesh optimization was completed by refining the mesh until no change was seen in the results, although the optimization methods were not described. Finally, the load was applied in three separate steps, starting with bolt pretension and bolt locking. The final step consisted of the shear load application and required many sub-steps to achieve convergence.

Rahman et al. (2007) used the same parameters as Sherman and Ghorbanpoor (2002) to study the connection behaviour including: vertical displacement of the connection, shear load eccentricity, plate twist, nonlinearity, and failure modes. The vertical displacement of the connection was represented by using shear–displacement curves and good correlation was observed between the finite element analysis and experimental results. The shear load eccentricity was determined at each load increment; however, agreement was only observed at the ultimate load. At early stages, the eccentricity fluctuated due to bolt slip, which led to the discrepancy with the finite element analysis results (Rahman et al. 2007). Twist was observed in the unstiffened extended shear tab by monitoring the lateral displacement at the top and bottom of the plate. Discrete decreases in the slope of the shear–displacement curves were used to identify the progression of failure modes and these were verified through the calculation of stresses and plastic deformations. The critical failure modes—where the slope of the curve levelled off—were then identified both visually and by monitoring stress and displacement values at critical locations. Overall, there was good correlation between the finite element analysis output and the results of the physical testing program completed by Sherman and Ghorbanpoor (2002).

2.2.4 Muir and Hewitt (2009)

A design procedure for extended shear tab connections was included in the 13th edition of the *Steel Construction Manual* (AISC 2005) to address common design concerns such as the influence of support rigidity, which could cause unanticipated additional demand on the supporting member or sudden bolt or weld failure. The development of this general design procedure is outlined by Muir and Hewitt (2009), including a description of the model used for connection design and anticipated behaviour.

Moment distribution in an extended shear tab connection is dependent on the stiffness of the plate, bolt slip, bearing deformation, and other factors. As a result, predicting the connection behaviour can be difficult and instead the design procedure assumes a pinned-end beam model. This model is based on a lower bound theorem and only applies if all limit states are satisfied and ductility exists in the connection. The required ductility is achieved by designing the plate as a fuse; if the connection is subjected to a moment in excess of the yield strength of the plate, all additional load is shed towards the supported beam.

Muir and Hewitt (2009) focus on three aspects of the design procedure: sizing the plate, sizing the bolt group, and rotation of the support. Both a maximum and minimum plate thickness limit are specified in order to ensure the plate has sufficient strength and ductility. The minimum plate thickness is based on the limit states of gross shear yielding, net shear rupture, gross flexural yielding, net flexural rupture, and block shear, but the plate must also satisfy a stability check. The maximum plate thickness ensures that the plate will yield prior to a bolt shear failure; therefore, it is governed by the moment capacity of the bolt group. To address weld failure, a new requirement was proposed that ensures plate yielding occurs prior to weld rupture. This will be the case for welds greater than or equal to 5/8 of the plate thickness. The requirement was discussed by Muir and Hewitt (2009) and verified by testing completed by Metzger (2006).

Since the design procedure assumes a pinned-end beam, only shear is delivered to the face of the support and the bolt group can be designed using the instantaneous centre of rotation method. The rotation of the support is considered in terms of serviceability as opposed to strength, as the other components were already designed for the anticipated loads. When a

rigid support is used, all rotation is accommodated by the plate and bolt group; therefore, support rotation does not need to be considered.

The design procedure was compared to physical tests conducted by Sherman and Ghorbanpoor (2002) and Metzger (2006). An average factor of safety of 4.29 is implied when comparing the predicted capacities to tests conducted by Sherman and Ghorbanpoor (2002). Limitations to the design procedure exist; however, it was recommended by the authors for design of all cases without axial force (Muir and Hewitt 2009).

2.2.5 Thornton and Fortney (2011)

The lateral–torsional stability of extended shear tab connections is not included in the 13th edition of the *Steel Construction Manual* (AISC 2005). Research on double-coped beams was used to estimate the behaviour of extended shear tab connections as their geometry is similar. The lateral–torsional buckling capacity is only dependent on the coped portion for laterally braced beams and assumes that the coped section is subjected to pure moment. For convenience, a constant shear over the unbraced length of plate was also assumed, even though it is inconsistent with the assumption of a constant moment. Thornton and Fortney (2011) proposed a stability equation, later adopted as part of the design method in the 14th edition of the *Steel Construction Manual* (AISC 2011), to investigate the limit state of lateral–torsional buckling for extended shear tabs and to determine the need for stiffeners should the connection not satisfy the check. Design examples were provided to illustrate the implementation of the method.

2.2.6 Mirzaei (2014)

The *Handbook of Steel Construction* (CISC 2016) is limited in its application to conventional shear tab connections with a single vertical line of bolts, with a depth not exceeding that required for seven bolts, and subjected to shear loading only. Mirzaei (2014) set out to address these limitations with emphasis on the application of combined shear and axial tension and compression forces on conventional shear tab connections. As this research considered the effects of axial load, it is included in the literature review even though the shear tabs are not considered "extended".

A full-scale testing program was developed that consisted of four tests, with each connection using two vertical bolt lines. The test matrix varied the axial load amplitude and type (compression or tension) for two different shear tab configurations. These configurations differed in all three shear tab dimensions, weld size, bolt size, and number of bolts per vertical line. An experimental testing program that investigated conventional shear tabs subjected to vertical loading only was previously conducted by Marosi (2011). In order to compare results, the tests in this study were conducted under a combination of rotation, shear and axial loading and used the same vertical loading protocol as Marosi (2011). Each specimen was subjected to rotation and vertical loading simultaneously until the connection reached a service-level shear load selected based on a statistical study. At this point, the vertical load application was paused and the horizontal load was gradually applied until the desired force was achieved. With the horizontal load held constant, the vertical load was once again increased until failure was observed (Mirzaei 2014). Results showed that under combined shear and axial compression, cracks developed in the net area between bolt holes and excessive bearing was observed. However, the strength of the connection was governed by the weld under combined shear and axial tension.

A finite element model was also developed in the Abaqus program and verified using both the physical tests completed by Marosi (2011) and those conducted for this study. The model was used to conduct a parametric study that varied the horizontal load level, the number of vertical bolt lines, and the number of bolts per line to expand on the results of the physical testing program. The finite element model included a damage simulation in order to model weld tearing accurately, and the analysis was stopped once a sudden failure was observed. At low levels of axial compression, the behaviour and failure progression of the connection was similar to that under pure shear. As the axial load was increased, the bottom of the shear tab showed distortion, and out-of-plane deformation of the plate and beam web were observed. Additionally, the connections with two vertical bolt lines were seen to be more sensitive to compression than connections with a single line. Mirzaei (2011) used the results of the physical tests and finite element parametric study to develop a design approach for conventional shear tabs subjected to shear and axial tension or compression.

2.2.7 Abou-zidan and Liu (2015)

Abou-zidan and Liu (2015) conducted a numerical analysis of unstiffened extended shear tabs in order to investigate the strength and behaviour of the connection. A finite element analysis was undertaken using ANSYS and the model was verified using the results of physical tests on conventional and extended shear tabs completed by Asteneh (1989) and Sherman and Ghorbanpoor (2002), respectively. It was found that the model was able to capture connection failure modes and predict ultimate shear loads accurately. The model consisted of a beam framing into the web of a supporting column, creating a flexible support condition for the extended shear tab. A mesh density study was conducted and a non-linear static analysis was used. This consisted of a two-step load application system: first, the bolts were loaded to simulate a snug-tightened condition and, second, a concentrated vertical load was applied. The location of this load was chosen such that the shear and rotation of the extended shear tab are similar to those when the beam is uniformly loaded (Abou-zidan and Liu 2015).

A parametric study was conducted and investigated the influence of the web slenderness of the supporting column, distance from the weld to the first vertical bolt line, plate thickness, number of bolts, number of vertical bolt lines, and the type and location of beam lateral restraint (Abou-zidan and Liu 2015). All connections failed due to bolt fracture, except for two cases that failed by shear tab yielding. It was observed that an increase in support flexibility corresponds to a higher shear load eccentricity due to rotations, causing high stresses in the bolts. Five different distances from the weld to the first bolt line were investigated, with the maximum being 250 mm. Abou-zidan and Liu (2015) found that a larger distance corresponded to a decrease in connection shear capacity due to large rotations and shear stresses in the bolts.

The plate thickness did not have a significant effect on the shear load eccentricity; however, the thinnest plate tested (6 mm) did not reach shear stresses large enough to cause bolt fracture and failed due to yielding instead (Abou-zidan and Liu 2015). As expected, an increase in the number of bolts led to an increase in eccentricity and connection capacity. Similarly, the addition of a second vertical bolt line created a stiffer connection, also leading to higher connection capacities. Lastly, the effect of beam lateral bracing was investigated

using three cases: a fully laterally restrained beam, a beam braced at midspan, and a beam braced both at midspan and the connection. The case where the beam is braced only at midspan failed immediately after yielding due to twisting of the extended shear tab. The fully braced beam yielded at a load greater than the other two cases; however, it was observed that employing lateral restraint only at the connection is equally effective in preventing twist as a fully braced beam.

Abou-zidan and Liu (2015) also examined the accuracy of the design procedure outlined in the 14th edition of the *Steel Construction Manual* (AISC 2011) using the results of their finite element parametric study. AISC (2011) predicted bolt fracture as the failure mode for all cases and consistently underestimated the bolt group shear strength. This underestimation is due to the difference in the eccentricity used in the calculation; using the shear load eccentricity determined from ANSYS and the AISC procedure resulted in good correlation with the results. However, once the connection depth reached six bolts, this approach results in an over-prediction of the connection capacity, as previously determined by Sherman and Ghorbanpoor (2002). Abou-zidan and Liu (2015) found the AISC (2011) procedure (including the use of the full geometric eccentricity for design of the bolt group) to be adequate for deep connections and those with two vertical bolt lines, but recommended reducing the eccentricity for connections with a single vertical bolt line and fewer than six bolts.

2.2.8 Thomas et al. (2014; 2016)

The research program conducted by Thomas et al. (2014; 2016) aimed to examine the behaviour of extended shear tabs under shear load only, as well as combined shear and axial loading. A full-scale laboratory testing program was developed that considered the following geometric parameters: number of horizontal bolt lines, plate depth, plate thickness, and presence of stiffeners. In addition, the magnitude and direction of the axial load was varied. All specimens were welded to the web of a W310×107 stub column using a 6 mm fillet weld (designed based on the assumption of pure shear loading), had two vertical bolt lines, and the plate length was kept constant. For the specimens with stiffeners, the stiffener dimensions were chosen to represent what is typically used in industry. The

loading beam was laterally braced near the connection and was reused in subsequent tests. The test set-up is shown schematically in Figure 2-1.
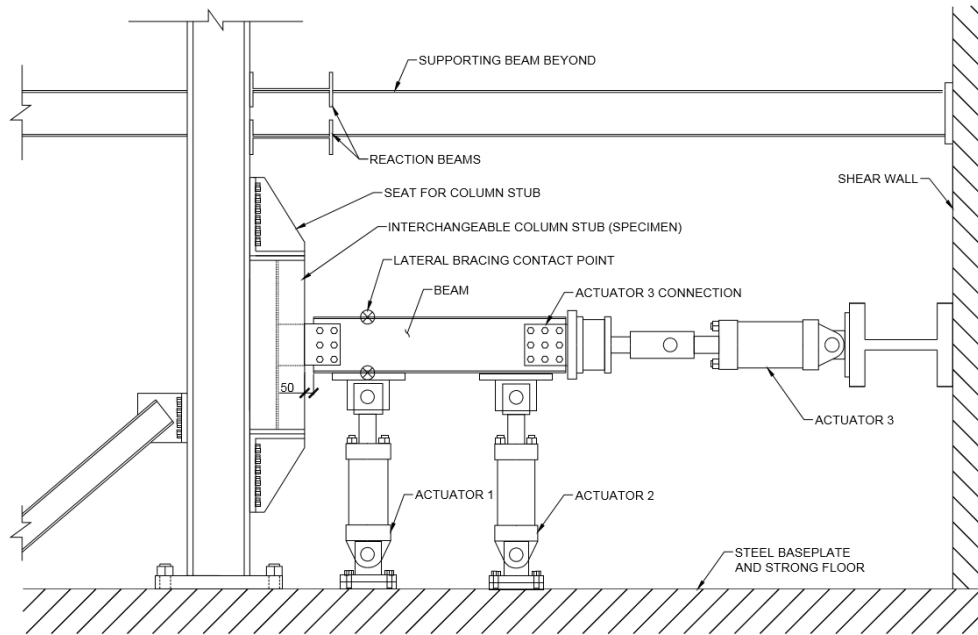
Figure 2-1: Test set-up used by Thomas et al. (2016)

The testing procedure was divided into three distinct steps and required the use of three different actuators. Loading began with the application of a 0.03 radian rotation, to reflect the expected end rotation of a typical simply supported beam when the plastic moment is reached at mid-span, and then the horizontal load was applied. The vertical load in the connection was kept at or near zero during this first stage (Thomas et al. 2016). Once the desired horizontal load was reached, the vertical load was applied to the connection while keeping the rotation and horizontal load constant. The tests concluded with the failure of the specimen, which was considered to be when the vertical load decreased substantially from its peak value.

Vertical load–deformation curves were used to identify the connection capacity and failure modes, in addition to visual inspection during and after the test. The unstiffened extended shear tab connections had three possible critical failure modes: weld rupture, bolt fracture, and column web tearing. Weld rupture was observed in all specimens and began at the tension tip of the weld, although in most cases the tear was highly localized and considered not to have influenced the overall response. Cases where tearing was the critical failure

mode were those tested without axial load or with axial tension. Bolt fracture was the critical failure mode for the majority of unstiffened specimens. When it occurred after weld rupture, it was due to the increased bolt shear caused by the redistribution of stresses. Similarly, column web yielding was observed in all tests, and column web tearing was observed in one specimen.

In addition to the three critical failure modes stated above, gross section yielding and out-of-plane deformations were also observed in the tests. Yielding through the full cross section occurred at the bolt line closest to the welded support and caused the plate to kink, as shown in Figure 2-2. Plate twisting was not observed due to lateral bracing of the loading beam; however, some out-of-plane deformations did occur.
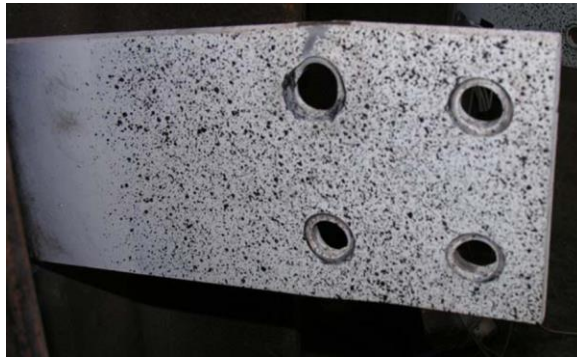
Figure 2-2: Kink deformation observed by Thomas et al. (2014)

Thomas et al. (2014) confirmed that in general the addition of axial load (tensile or compressive) reduces the shear capacity of extended shear tab connections. The effects are amplified with deeper connections and tensile loads, as more demand is placed on the weld. It was observed that applying a small compressive load actually increased the shear capacity, but additional compression resulted in a reduced capacity. It was speculated that there may be a range of compression within which the shear capacity of the connection is not affected significantly.

The results of the experimental study were also compared to existing design procedures including the 14th edition of the *Steel Construction Manual* (AISC 2011), which is outlined in Section 2.3.1. All methods investigated under-predict the strength of unstiffened extended shear tab connections significantly, and the majority predict an incorrect failure mode.

The stiffened connections differed greatly from the unstiffened ones as the stiffeners reduced the stress concentration in the weld and thus prevented a weld rupture failure. The critical failure mode for all stiffened tests was out-of-plane deformation. These deformations began prior to reaching the peak shear load and continued throughout the rest of the test. Bolt fracture, gross section yielding, and plate rupture were also observed. With stiffened connections, the addition of a horizontal compression load accelerated the out-of-plane displacement and resulted in a reduced capacity.

Thomas et al. (2016) concluded that eight failure modes must be considered in the design of extended shear tabs. Design recommendations were made to better represent the behaviour of unstiffened and stiffened connections, while continuing to ensure a ductile failure. A main takeaway of the design procedure is the recommendation to use 75% and 50% of the geometric eccentricity (measured from the centre of the bolt group to the support) for unstiffened and stiffened specimens, respectively, for design of the bolt group. This was defined as the effective eccentricity as it better represents the actual loads the bolts are subjected to in the connection. Maximum and minimum plate thicknesses were specified to ensure plate yielding and to prevent excessive out-of-plane deformations, respectively. The equation for minimum plate thickness was derived by equating the critical lateral–torsional buckling moment and the plastic moment of extended shear tabs and is as follows:

$$t_{min} = 0.663 \sqrt{\frac{F_y d L_b}{E}}$$

2-1

where F_y is the yield stress of the plate material, d is the plate depth, L_b is the unbraced length of the plate (length from the weld to the first vertical bolt line), and E is the modulus of elasticity.

A weld capacity equation was specified to ensure that the plate yields prior to weld rupture. The equation considers the presence of shear, moment, and axial loading and results in a minimum weld size, D, of:

$$D \geq 1.155 \frac{F_y}{X_u} t$$

2-2

where X_u is the nominal ultimate strength of the weld metal and t is the plate thickness. Thomas et al. (2014) also developed an equation to predict the flexural capacity of unstiffened extended shear tabs in the presence of axial force. It is expressed as the shear force required to cause the plate to reach its plastic moment capacity. This shear capacity, V_{MN}, is as follows:

$$V_{MN} = \frac{\sigma_n t d^2}{4e_{\text{eff-cs}}} - \frac{P^2}{4\sigma_n t e_{\text{eff-cs}}}$$ 2-3

$$\sigma_n = \min\left[F_y, 6.25(0.66F_y - \tau)\right]$$ 2-4

where P is the applied axial force, $e_{\text{eff-cs}}$ is the clear span effective eccentricity (calculated by subtracting the distance from the bolt group centroid to the first vertical bolt line from the effective eccentricity), τ is the applied shear force divided by the gross cross-sectional area of the plate, and t and d are as described above. Equation 2-4 defines the maximum permissible normal stress, σ_n, in order to account for the interaction of shear and normal stress as per CSA Standard S16 (CSA 2014). Further research, including a parametric study to investigate the influence of plate length, column web thickness, stiffener configuration, and back-to-back extended shear tabs, was suggested by Thomas et al. (2014) to validate the results presented.

2.2.9 Salem et al. (2016)

Salem et al. (2016) aimed to evaluate the behaviour of cantilever plate connection elements with the main objective being the development of a unified design approach for a wide range of steel connections. Finite element models were developed for both extended shear tab connections and double-coped beams and validated using experimental results from Thomas et al. (2014) and Johnston et al. (2015), respectively. A full-scale test program on extended shear tabs only was also carried out to increase the available experimental data. Only the results and conclusions for extended shear tabs are discussed here, as they are the most relevant to the current study.

The full-scale testing program consisted of 17 specimens and used the same set-up and loading procedure as did Thomas et al. (2014), and described in Section 2.2.8. Two boundary conditions were investigated: a stiff support, where the extended shear tab was

welded to a one-inch-thick plate, and a semi-rigid support, where it was instead welded to the web of a stiffened W310×107 column stub. While the latter case used a stiffened column web to reduce the support flexibility, the extended shear tabs themselves were unstiffened as the stiffener plates were on the opposite side of the column. Salem et al. (2016) varied the plate length, thickness, bolt configuration, and level of axial load. Several limit states were observed:

- Gross section plasticity was observed in almost all of the tests but was not considered in itself to constitute failure of the connection. Net section plasticity at the bolt line closest to the support was also observed; however, it did not ultimately contribute to loss of vertical load capacity.

- Out-of-plane deformations, illustrated in Figure 2-3, began prior to reaching the peak capacity and were seen in all tests. In some cases, this was identified as the primary failure mode.

- The majority of tests failed due to bolt fracture after significant plasticity and out-of-plane deformations had occurred.

- Weld rupture occurred in all specimens tested with a semi-rigid support and this occurred prior to any noticeable out-of-plane deformations.

Figure 2-3: Out-of-plane deformation of extended shear tab specimen with stiff support
(Salem et al. 2016)

Salem et al. (2016) investigated the measured in-plane bending moments at the support and first vertical bolt line. The moments were normalized using the plastic moment capacity of the plate and were observed to be variable during the test. The moment at the support was reported to be greater than the plastic moment capacity of the plate for all connections tested with the stiff boundary condition, and an average bending moment ratio of 1.25 is reported. There is one exception to this statement: the 230 mm-deep, 9.5 mm-thick plate subjected to 200 kN of compression had a maximum bending moment ratio at the support of 0.86 due to its high compressive demand. The bending moment ratio at the first vertical bolt line was more variable and only approximately half of the connections with a stiff boundary condition reached the plastic moment capacity on the net section at this location.

The effects of the key variables were investigated and it was found that the length of the extended shear tab impacts the overall capacity significantly: shorter plates have a reduced unrestrained length and thus a higher resistance to out-of-plane deformations (Salem et al. 2016). Additionally, increasing the depth and thickness of the plate resulted in a higher peak vertical load, as expected.

In addition to the experimental test program, Salem et al. (2016) developed a finite element model using the Abaqus program. The model was verified using the results of the complementary experiments, as well as those of Thomas et al. (2014). Internal load diagrams, deformed shapes, and failure modes were all examined and it was determined that there was good correlation between the experimental and numerical results.

The model consisted of the extended shear tab plate, 19 mm diameter ASTM A325 bolts, a short beam section to represent the loading beam, a support plate, and a rigid loading plate. The loading plate was used to ensure that all loads and displacements were applied uniformly to the beam cross section. Quadratic elements with reduced integration were used to mesh all solid parts. Material properties for the plate and bolts were obtained from tension coupon and bolt shear tests done in parallel with the experimental test program. The loading procedure and boundary conditions were also modelled to represent the experimental set-up; loading was therefore applied in three steps and the beam was laterally braced at both flanges near the connection.

The model was used to conduct a parametric study on extended shear tab connections with 36 simulations varying the plate length, thickness, depth, and support condition. The primary failure mode for all models was either out-of-plane deformation or bolt fracture. The majority of models experienced gross or net section yielding prior to the primary failure occurring. Gross section plasticity is characterized by the development of plasticity throughout the whole depth of the plate and is illustrated by the darker grey in Figure 2-4. It occurred in all models with a stiff support condition; however, gross section plasticity was never a critical failure mode.
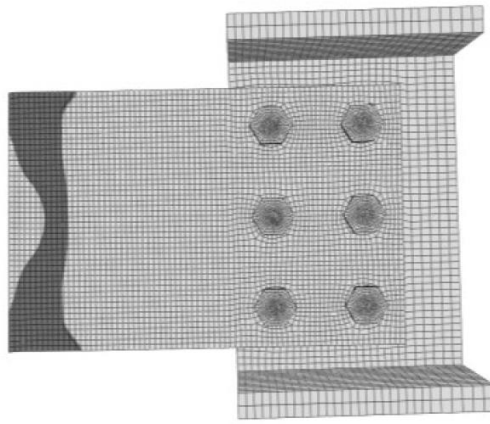
Figure 2-4: Gross section plasticity of specimen with stiff support (Salem et al. 2016)

Plasticity in the connection was evaluated at both the support and the vertical bolt line closest to the support using the plastic strain contour in the Abaqus program and Neal's (1961) interaction equation, which is as follows:

$$\frac{M}{M_p} + \left(\frac{P}{P_y}\right)^2 + \frac{\left(\frac{V}{V_p}\right)^4}{1 - \left(\frac{P}{P_y}\right)^2} \leq 1.0 \qquad\qquad 2\text{-}5$$

where M, P and V are the applied moment, axial and shear loads respectively, M_p is the plastic moment capacity, P_y is the axial yield capacity, and V_p is the plastic shear strength. Salem et al. (2016) observed that this equation was capable of predicting the development of both gross and net section plasticity. Since shear load eccentricity is such an important parameter in the design of extended shear tabs, Salem et al. (2016) investigated the ratio of the bolt group eccentricity (measured from the centre of the bolt group to the point of

inflection) to the geometric eccentricity when gross section plasticity, net section plasticity and bolt fracture occurred. At the occurrence of gross section plasticity, the point of inflection was located at or near the centre of the bolt group. When net section plasticity and bolt fracture occur, the ratio of bolt group eccentricity to geometric eccentricity was 0.55 and 0.56, respectively. As such, Salem et al. (2016) recommended that Equation 2-5, with the moment, M, substituted by the product of the shear load and eccentricity, be used to determine the shear load that causes net section plasticity at the first line of bolts and gross section plasticity at the support. The recommended eccentricity values are:

For gross section plasticity: $\quad\quad\quad\quad\quad\quad\quad e = e_g$ 2-6

For net section plasticity with flexible support: $e = 0.6e_g - 0.5s$ 2-7

For net section plasticity with stiff support: $\quad e = 0.5e_g - 0.5s$ 2-8

where e_g is the geometric eccentricity and s is the horizontal bolt spacing. The study concluded by comparing the results of the parametric finite element analysis with the design procedure recommended by Thomas et al. (2014). They found that the capacity was under-predicted in most cases and the failure mode was often incorrectly identified. Further research into the effect of axial load and flexible support conditions was recommended.

2.3 AISC Design Manual

The *Handbook of Steel Construction* (CISC 2016) only contains a recommended design procedure for conventional shear tabs that are limited to a geometric eccentricity of 75 mm. The *Steel Construction Manual* (AISC 2011; 2017) does, however, include a design method for extended shear tabs and the parts relating to connection stability are discussed in this section. The general design procedure is similar in both editions; however, the checks relating to plate buckling and stiffeners have changed and therefore both editions are presented.

2.3.1 AISC Steel Construction Manual, 14th Edition

The 14th edition of the *Steel Construction Manual* (AISC 2011) states that extended shear tab connections should be checked for the limit state of buckling using the double-coped beam procedure. This procedure is based on classical plate buckling theory and was recommended by Muir and Thornton (2004). The buckling stress, F_{cr}, is calculated based

on a plate slenderness parameter and a response relationship that depends on the slenderness zone within which it falls, using Equations 2-9 to 2-13. The parameter Q allows the method to be applicable for both elastic and inelastic buckling behaviour. The buckling stress is calculated as:

$$F_{cr} = QF_y \qquad\qquad 2\text{-}9$$

where F_y is the specified minimum yield stress of the plate material.

The slenderness zones are as follows:

When $\lambda \le 0.7$: $\qquad\qquad Q = 1 \qquad\qquad$ 2-10

When $0.7 < \lambda \le 1.41$: $\qquad Q = (1.34 - 0.486\lambda) \qquad$ 2-11

When $\lambda > 1.41$ $\qquad\qquad Q = \dfrac{1.30}{\lambda^2} \qquad\qquad$ 2-12

The slenderness parameter, λ, is defined as:

$$\lambda = \frac{d\sqrt{F_y}}{10t\sqrt{475 + 280\left(\dfrac{d}{L_b}\right)^2}} \qquad\qquad 2\text{-}13$$

where d and t are the plate depth and thickness, respectively, L_b is the distance from the support to the first vertical bolt line, and F_y is expressed in ksi. Note that the resulting parameter, λ, is unitless.

The 14th edition of the *Steel Construction Manual* (AISC 2011) also includes a check to determine whether stiffeners (stabilizer plates) are required. The procedure was developed by Thornton and Fortney (2011), as described in Section 2.2.5. It states that stiffeners are required if the applied shear is greater than the resisting force, as given by:

$$V_{LTB} = \frac{\pi}{2L_b^2}\sqrt{EGI_yJ} \qquad\qquad 2\text{-}14$$

where E is the modulus of elasticity, G is the shear modulus, I_y is the weak-axis moment of inertia, and J is the St. Venant torsional constant.

2.3.2 AISC Steel Construction Manual, 15th Edition

As in the previous edition, the 15th edition of the *Steel Construction Manual* (AISC 2017) advises designers to use the double-coped beam procedure to check the limit state of buckling. However, the procedure has been updated to reflect recent research conducted by Dowswell and Whyte (2014). The local flexural strength and lateral–torsional buckling strength are calculated in accordance with Equations 2-15 to 2-19 from the AISC Specification (AISC 2016), Section F11.

When $\dfrac{L_b d}{t^2} \leq \dfrac{0.08E}{F_y}$:

$$M_n = F_y Z_x \leq 1.6 F_y S_x \qquad\qquad 2\text{-}15$$

and lateral–torsional buckling does not apply.

When $\dfrac{0.08E}{F_y} < \dfrac{L_b d}{t^2} \leq \dfrac{1.9E}{F_y}$:

$$M_n = C_b \left[1.52 - 0.274 \left(\dfrac{L_b d}{t^2} \right) \dfrac{F_y}{E} \right] M_y \leq M_p \qquad\qquad 2\text{-}16$$

where C_b is calculated per Dowswell and Whyte (2014), as modified by setting the cope depth to zero to represent extended shear tab geometry:

$$C_b = 3 + \ln \left(\dfrac{L_b}{d} \right) \geq 1.84 \qquad\qquad 2\text{-}17$$

When $\dfrac{L_b d}{t^2} > \dfrac{1.9E}{F_y}$:

$$M_n = F_{cr} S_x \leq M_p \qquad\qquad 2\text{-}18$$

where the critical stress F_{cr} is:

$$F_{cr} = \dfrac{1.9 E C_b}{\dfrac{L_b d}{t^2}} \qquad\qquad 2\text{-}19$$

and C_b is determined according to Equation 2-17. Additionally, the 15th edition of the *Steel Construction Manual* (AISC 2017) no longer requires a check of the need for stiffeners.

2.4 Summary

Extended shear tabs have been the focus of several research programs in recent years. Finite element analysis has increasingly been used to supplement physical test data to investigate the behaviour of the connection. The influences of different geometric parameters and boundary conditions have been considered; however, the length of the extended shear tab is rarely varied. The plates investigated by Salem et al. (2016) with a stiff boundary condition were relatively long and it was observed that the majority of connections reached their plastic moment capacity at the support. As this was not an expected outcome, it indicates that further research is required to determine at what length instability begins to govern the strength and behaviour of extended shear tab connections.

Another concern with extended shear tab connections is whether current AISC design methods are able to assess their stability capacity accurately when the plates become long, and this has not been adequately addressed in previous studies. This is evidenced by the use of the double-coped beam design procedure to check buckling of extended shear tab connections and illustrates a need to investigate the stability of extended shear tab connections. In particular, to facilitate the design process there is a need to develop a simple method for determining the length below which geometric instability is not a plausible failure mode.

CHAPTER 3: FINITE ELEMENT INVESTIGATION

3.1   Introduction

A finite element model previously developed and validated by Salem et al. (2016) was used to investigate stability of extended shear tab connections. The development of the model and how it was modified for this study are addressed in this chapter. The model was used to conduct a parametric study to determine the longest length of plate that could reach its plastic moment capacity. The study investigated the effects of parameters such as the plate thickness, plate depth, and level of applied axial compression. The methodology is presented and the analysis results are examined and used to determine how stability affects the behaviour and capacity of extended shear tab connections.

3.2   Finite Element Model

The general-purpose finite element software Abaqus (Dassault Systèmes, 2014) was used by Salem et al. (2016) to create a model capable of predicting the behaviour of extended shear tabs, although it was validated mostly with tests on connections that failed by reaching the full plastic flexural capacity of the plate. It was modified in the current research in order to investigate stability of the connection.

The model consists of an extended shear tab plate of varying dimensions, ASTM A325 bolts with a 19 mm (3/4 in.) diameter and a 200 mm long loading beam stub. All components were modelled as solid parts and the assembly is depicted in Figure 3-1. Threads were not modelled as they are not intercepted by any shear planes in this study (Salem et al. 2016). The depth of the beam varied to accommodate the differing geometries of extended shear tab, but had a constant web thickness of 13.1 mm to match that used in the experimental testing program. Only a short length of the loading beam near the connection was modelled to save computational effort.
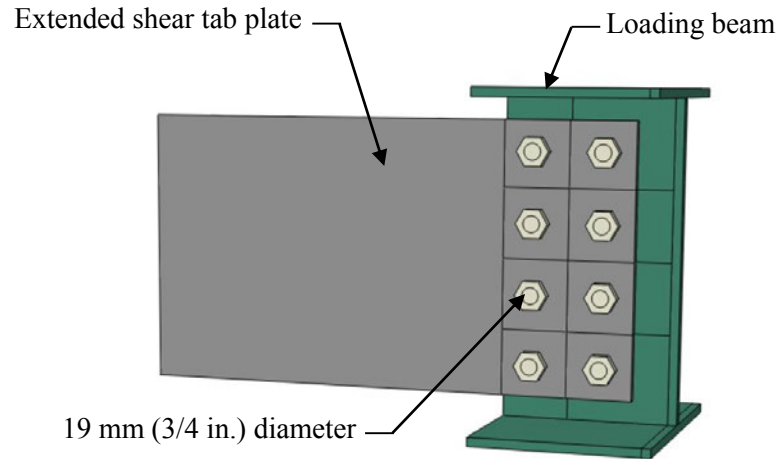
Figure 3-1: Model assembly in Abaqus

3.2.1 Elements and Meshing

Quadratic elements were used for the plate, beam, and bolts as they have an improved convergence rate as compared to tetrahedral elements (Salem et al. 2016). The elements also used reduced integration as it reduces the number of required computations per element, and thus offers savings in regards to computational resources. However, it does result in a slight reduction in accuracy compared to using full integration elements.

A structured hex mesh was created for the plate and beam using solid eight-node brick elements. Mesh size varied for the different parts of the model and was selected based on a balance between computational time and model behaviour. A mesh refinement study was undertaken in order to optimize the mesh density of the extended shear tab for the parametric study. Four different mesh sizes were investigated: 3 mm, 5 mm, 10 mm, and 15 mm, representing the maximum dimension of the element. All models used three elements across the thickness of the plate to model bending deformations accurately. Figure 3-2 illustrates the relationship between mesh size and ultimate shear capacity of the four models. It was observed that decreasing the element size also decreases the vertical load capacity, indicating that an improperly-sized mesh can over-predict the capacity of this connection. The capacity obtained with the 3 mm and 5 mm meshes differ by less than one percent; therefore, an element width of 5 mm was selected for the remainder of the study.

The bolts used a sweep technique with a medial axis algorithm to mesh the circular shaft and have an increased mesh density in the bolt shank. A larger mesh size was used for the beam, except around bolt holes in the web due to steep strain gradients at these locations, which were meshed using the same technique as for the bolts.
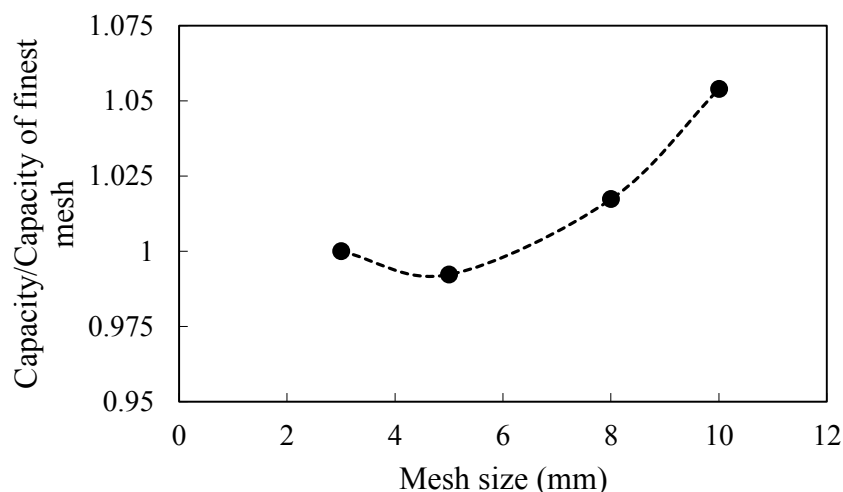
Figure 3-2: Mesh sensitivity analysis

3.2.2 Material Properties

Results from tension coupon tests previously completed at the University of Alberta were used to create a bilinear stress–strain curve that was then used to model the material properties of the steel plate for the parametric study. The curve consists of an elastic portion and a plastic portion. A yield stress of 385 MPa was chosen, as it represents the probable strength of 350W steel. The slope of the plastic portion was chosen such that it was approximately parallel to the true stress–strain distribution of the tension coupons. This resulted in a line with a slope of approximately 0.5% of the modulus of elasticity, which was taken as 200 GPa for this study (Salem et al. 2016). ASTM A325 bolts were also modelled using the stress–strain relationship developed experimentally by Salem et al. (2016).

3.2.3 Boundary Conditions and Interaction

The model was created with a fixed boundary condition for the extended shear tab (i.e., the support was restrained against translation and rotation in all directions). In order to ensure that the entire cross section of the plate was restrained at the support, a support plate was

modelled in the Abaqus program using a "discrete rigid" part. Welding of the extended shear tab plate to the support was not modelled explicitly, but rather represented using a "tie" constraint between these two parts. Additionally, the flanges of the loading beam were laterally braced to examine localized failure in the extended shear tab.

All of the parts in the model were in contact in some manner and this was captured using the "general contact" feature in the Abaqus program. Behaviour in the tangential direction was defined using the "penalty friction" formulation with a coefficient of 0.3. In the normal direction, hard contact was used to simulate the interaction and slip between parts and allow for force transmission in the model.

3.2.4 Loading

Loading was applied in three or four separate steps using a loading plate that was tied to all nodes at the far end of the loading beam. This was used to apply the loads uniformly to the cross section and avoid any local stress concentrations (Salem et al. 2016). The first step applied an internal tensile force of 15 kN to the bolts in order to simulate a snug-tight condition. In subsequent steps, the bolt was fixed at its new current length to maintain this nominal level of prestress.

Next, a rotation of 0.03 radians was applied to the supported beam, which represents the upper limit on rotational demand of shear connections when the plastic moment is reached in a typical beam (Thomas et al. 2016). If axial load was a parameter in the model, it was applied next as a horizontal point load to the loading plate. The bolt tensile force, the beam rotation and horizontal load were then held constant while the vertical force was applied to the connection as a displacement at the end of the supported beam. A displacement control loading scheme was used as it is more stable than force-controlled loading and is also able to capture the post-peak behaviour of the structure. The displacement was increased until the load in the connection began to decrease, signifying failure of the extended shear tab.

Generally, shear connections are subjected to downward shear forces; however, the Abaqus model analyzes the connection using an upward vertical force, as the model was developed to mimic the loading procedure of the experimental tests in order to facilitate model

verification. An upward vertical force is used in the laboratory as it is more convenient for the test set-up (Salem et al. 2016).

3.2.5 Model Verification

Salem et al. (2016) used results of their experimental tests, as well as those conducted by Thomas et al. (2014; 2016), to validate the finite element model. The model accounted for the actual material properties of the specimens. Load–displacement curves, deformed shapes, and failure modes were used to compare the results.

There was good correlation between the experimental and finite element results for the majority of tests. An example is shown in Figure 3-3 for the vertical load–displacement response. The qualitative comparisons also showed good agreement between the deformed shapes and plasticity development. From this, Salem et al. (2016) concluded that the model was capable of simulating the actual behaviour of extended shear tab connections. The only exception is tests that failed due to weld rupture, as the weld was not modelled and therefore the model could not predict its capacity. A comprehensive account of the tests and validation process can be found in Salem et al. (2016).
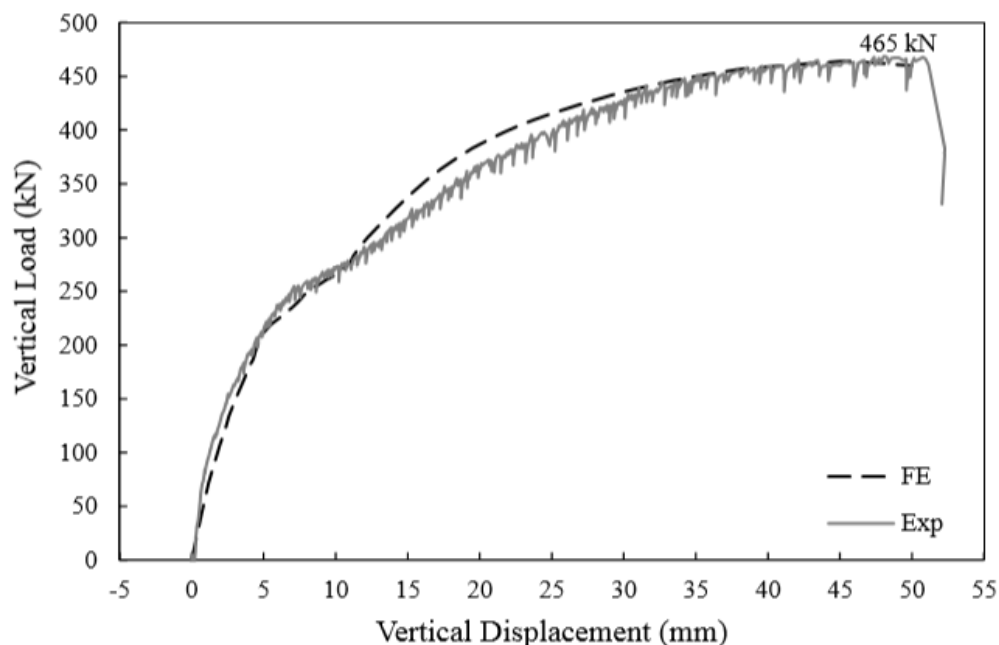
Figure 3-3: Load–displacement response comparing finite element and experimental test results (Salem et al. 2016)

3.3 Parametric Study

A parametric study using the validated finite element model was completed in order to investigate the behaviour of extended shear tabs and the effect of certain geometric parameters on their stability. The objective of the parametric study was to determine the longest length of plate that could reach its plastic moment capacity prior to failure. Plates with lengths longer than this would inherently undergo a stability-type failure and would no longer conform to the assumptions of the AISC (2017) design methods.

3.3.1 Parameters

As mentioned in Section 3.2.3, the extended shear tab is fixed against all translations and rotations at the support, creating a fixed boundary condition. The boundary condition was not chosen as a parameter in this study based on results of the parametric study conducted by Salem et al. (2016) and listed in Table 3-1. The models in Table 3-1 are the only ones in the previous study where the critical failure mode was out-of-plane deformations and not bolt fracture. It was reported that the cases with a fixed support failed at a lower ultimate shear capacity than those analyzed with a flexible support. Since the current study is only concerned with stability failures, a fixed support was chosen as it is conservative in terms of the shear capacity and is also simpler to implement in the model.

Table 3-1: Comparison of shear capacities for 6.35 mm
thick shear tabs (Salem et al. 2016)

Depth (mm)	Ultimate Capacity (kN)	
	Fixed Support	Flexible Support
150	104	141
230	199	262
310	294	371

The thickness, depth, and length of the shear tab plate can vary, and this study aimed to determine how these parameters affect connection stability. Buckling resistance of a connection plate element is primarily based on the weak-axis moment of inertia of the plate (Dowswell 2016). Therefore, the depth and thickness of the plate are of primary importance and the values selected for the study are presented in Table 3-2. In addition to varying the

geometry of the plate, the effect of axial loads is investigated. Only compression was considered for this study as it is expected to exacerbate a stability failure. The value of the horizontal load was chosen to reflect what has been observed in industry and is represented as a percentage of the plate nominal axial capacity.

As the depth and thickness of the plate vary, other geometric parameters were held constant. The edge and end distances from the nearest bolts are both 35 mm and the horizontal and vertical bolt spacing is 80 mm.

Table 3-2: Parametric study matrix

Depth (mm)	Thickness (mm)	Horizontal Compression Load
150	6.35	0%
230	9.50	10%
310	12.7	25%

3.3.2 Methodology

In order to find the longest length of plate that could reach its plastic cross-sectional capacity, the plate length was varied in the numerical model and the results at the support and bolt line were analyzed. Stresses were always taken at the vertical bolt line closest to the support, as shown in Figure 3-4, and therefore the length reported is the unsupported length of plate. Neal's (1961) interaction equation (Equation 2-5) was evaluated at both the support (gross section) and the first vertical bolt line (net section), and used to determine whether full plasticity had occurred. This equation considers the interaction of bending, axial, and shear stresses in the connection plate. In order to focus on a plate failure, it was assumed that both the weld at the support and the bolts were adequately designed.
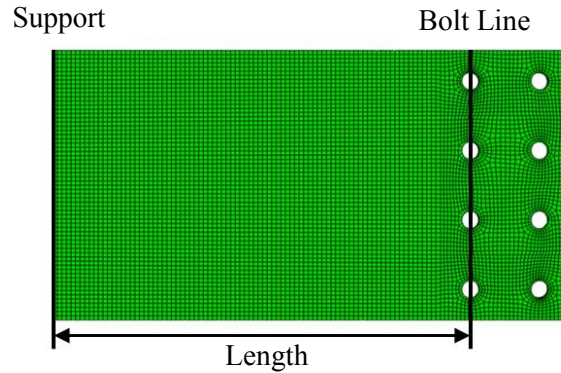
Figure 3-4: Locations of analyzed section cuts

For each model within the matrix, the total plate length was varied in 25 mm increments until a value close to 1.0 was obtained from Equation 2-5 at either the support or bolt line. This was taken as the critical length for the given connection geometry. A critical length for every permutation of the values listed in Table 3-2 was found, resulting in 27 individual models. Due to large computational processing times, a length was accepted if the value was within 3% of the target.

An alphanumeric model ID was used to identify the specimens based on their varying geometric parameters. The first two characters represent the depth, specified by the number of horizontal bolt lines followed by the letter "B", while the second number indicates the plate thickness rounded to the nearest whole number. The last number is the amount of horizontal compression that was applied to the connection and is expressed as a percent of the plate's nominal axial yield capacity. For example, specimen 3B-10-0 is a 9.5 mm thick extended shear tab with three horizontal bolt lines and no applied horizontal load.

3.4 Results and Discussion

The critical length was found for each geometry as the longest length at which the plate reached its plastic capacity. This value is presented and discussed, as it represents the limit between a strength and stability failure. The shear capacity of the plate and bending moment distribution over the plate length are presented, and, finally, the influence of the geometric and loading parameters on the critical length, capacity, and failure mode are discussed.

3.4.1   Connection Behaviour

It has generally been assumed in design that the extended shear tab connection transfers no moment to the supporting member and the moment increases linearly from the support to the bolt line. However, previous tests have shown that this is generally inaccurate, and significant moment can be developed at the support. The magnitude of this moment is, however, dependent on the rotational stiffness of the support (Salem et al. 2016). In this study the support was fixed, creating a significant bending moment at this location. As a result, gross section yielding occurs and the first plastic hinge is formed at the support. The first peak observed in Figure 3-5, at approximately 5 mm of vertical displacement, represents this yielding and the subsequent decrease is caused by softening of the system. The first peak also corresponds to the onset of out-of-plane deformations.

Based on the form of Equation 2-5, bending stresses have a greater effect on section plasticity than shear stresses. Variations of the bending moment ratio at both the support and bolt line were also plotted to analyze connection behaviour and are shown in Figure 3-6. In the figure, the bending moments are normalized by dividing the value obtained from the numerical model, M, by the reduced plastic moment, $M_{p(reduced)}$, of either the gross or net section. The reduced plastic moment is obtained by manipulating Neal's equation (Equation 2-5), which results in Equation 3-1. Figure 3-6 also indicates that the plastic moment was first reached at the support early in the analysis, at a low vertical displacement.

$$M_{p(reduced)} = M_p \left[1 - \left(\frac{P}{P_y} \right)^2 - \frac{\left(V/V_p \right)^4}{1 - \left(P/P_y \right)^2} \right] \qquad \text{3-1}$$

After the reduction in stiffness caused by the formation of the plastic hinge at the support, the load is shed towards the bolt line. This corresponds to an increase in connection strength, as seen in Figure 3-5. However, due to the length of the extended shear tab, instability causes the plate to fail prior to the formation of a second plastic hinge at the bolt line. Again, this is confirmed as the plate did not reach its plastic capacity at the bolt line per Figure 3-6.

Analyzing the two graphs together further supports the above conclusions regarding the behaviour of the connection. Initially, the capacity is influenced by the stiffness of the

support, as the two curves have an identical shape and reach a peak at the same vertical displacement. However, once the load is redistributed to the bolt line, the bending moment ratio curve for the bolt line mirrors the vertical load–displacement curve. Additionally, the peak moment at the bolt line occurs at the same vertical displacement as the ultimate shear capacity.
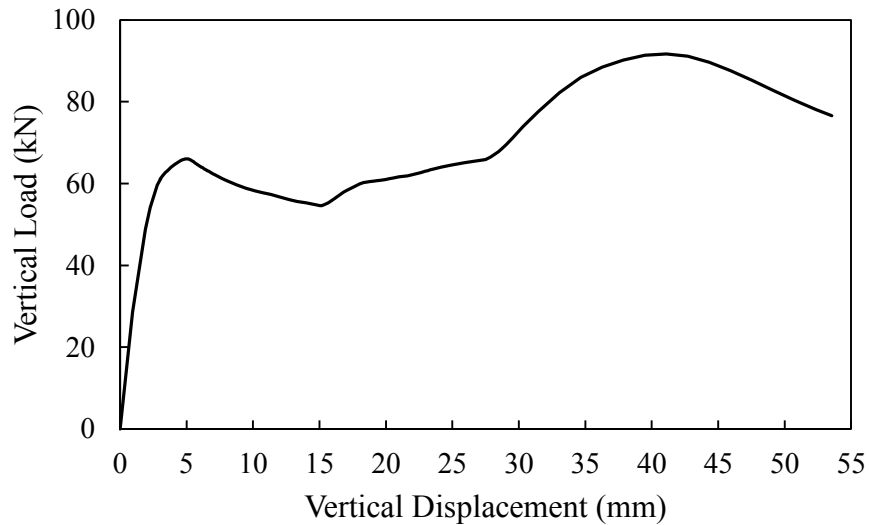
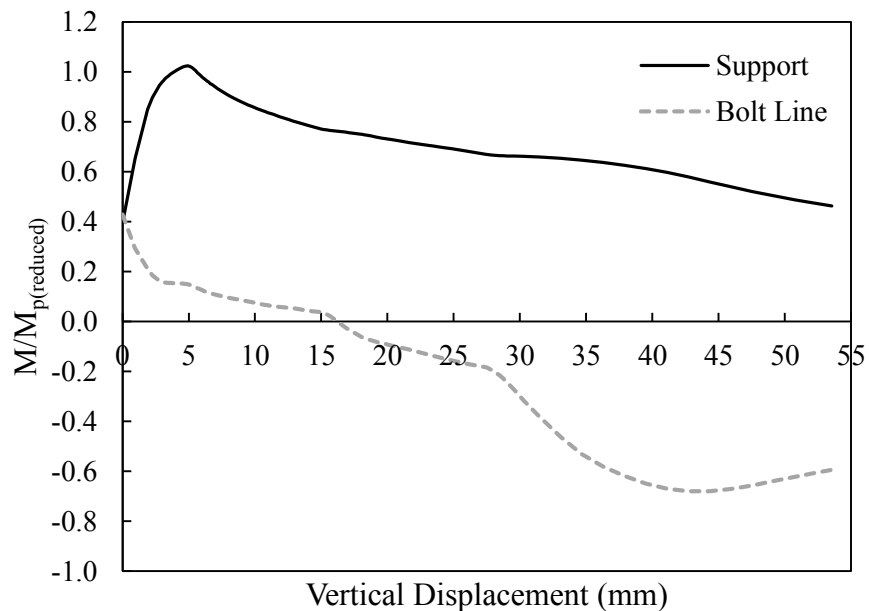Figure 3-5: Load–displacement response of model 3B-10-0

Figure 3-6: Bending moment ratio variation of model 3B-10-0

The extended shear tab connection was modelled similarly to an idealized cantilever beam in the Abaqus program; the support is fixed against all rotations and translations, and the far end of the loading beam is only laterally braced. Therefore, the applied rotation of 0.03 radians causes an upwards vertical displacement of the free end. The magnitude of this displacement is dependent on the plate length and moment of inertia. Since extended shear tabs are primarily used to resist shear forces, the displacement caused by the initial rotation was deemed not to be part of the shear response. As a result, the curves were shifted to begin at zero vertical displacement for all models. The largest shift was 5.65 mm for model 3B-13-0, where the peak capacity occurred at 93 mm of vertical displacement, and the majority of models were shifted by less than 2 mm.

3.4.2 Beam Longitudinal Displacement

No restraint was imposed on the horizontal movement of the beam towards the support. This movement occurs as a result of the applied rotation, and horizontal and vertical loads. This displacement was investigated in order to ensure that the model accurately represents a real-world application, where the supported beam is restrained due to its connection at the far end. The horizontal displacement was measured at the peak vertical load, just prior to connection failure, and was always taken at a point on the top flange of the loading beam. Due to the rotation, the top flange experienced the largest horizontal movement. A maximum displacement of 15.9 mm was observed with the 4B-13-10 model, with a mean displacement over all models of 10.1 mm. This was deemed acceptable, as allowing the horizontal movement of the connection only exacerbates a stability failure of the extended shear tab.

3.4.3 Critical Length

The critical length was determined using Neal's interaction equation (Equation 2-5), which is in terms of the resultant moment and horizontal and vertical forces at the cut location. The forces and moments were extracted from the model by using the "free body cuts" feature in the Abaqus program. This allows a cut to be a made at a specific location and the magnitude and direction of the resultant forces and moments are displayed. Abaqus

integrates the internal forces in the elements over the selected section and all moments are taken about the area centroid of the cut face (Dassault Systèmes, 2014).

As described above, the support is rotationally stiff and, therefore, the higher end moment occurs at this location. This means that the critical length is always governed by plasticity at the support and not at the bolt line. It is important to note that this occurs at the first peak in the load–displacement curve, rather than at the ultimate load. (If the connection is longer than the critical length, full plasticity at the support will not be achieved.) The critical length, measured from the support to the first vertical bolt line, was obtained for each model and is presented in Table 3-3. The lengths required to cause a stability failure of the extended shear tabs tend to be quite long, and some considerably exceed the practical range for this connection.

Due to the trial-and-error methodology used for the parametric study, models at multiple lengths were analyzed to find the critical length. Figure 3-7 illustrates the relationship between the plate length and the value obtained from Neal's interaction equation (Equation 2-5) for models without applied horizontal load. A line has been drawn at a value of 1.0, as it was the target for the parametric study. Symbols and colors have been used to facilitate comparisons; each symbol corresponds to a different plate thickness, and each depth is represented by a different color. It is evident that there is a linear relationship, where the value from Equation 2-5 decreases as the plate length increases. As the connection becomes deeper and thinner, the slope of the line becomes steeper and a small change in length can result in a large variation in the value of Neal's equation. For example, a 50 mm change in length for the model 4B-6-0 resulted in a 12% change in the value of Neal's equation, whereas the length of model 2B-10-0 must be varied by 550 mm to achieve this same difference.

Table 3-3: Critical lengths and failure modes

Specimen ID	Critical Length (mm)	Failure Mode
2B-6-0	535	OPD
2B-6-10	410	Buckling
2B-6-25	285	Buckling
2B-10-0	1385	OPD
2B-10-10	710	Buckling
2B-10-25	485	Buckling
2B-13-0	>2385*	OPD
2B-13-10	1135	Buckling
2B-13-25	760	Buckling
3B-6-0	285	OPD
3B-6-10	235	OPD
3B-6-25	160	OPD
3B-10-0	685	OPD
3B-10-10	535	Buckling
3B-10-25	360	Buckling
3B-13-0	1435	OPD
3B-13-10	835	Buckling
3B-13-25	610	Buckling
4B-6-0	185	OPD
4B-6-10	160	OPD
4B-6-25	135	OPD
4B-10-0	485	OPD
4B-10-10	385	OPD
4B-10-25	260	Buckling
4B-13-0	985	OPD
4B-13-10	685	Buckling
4B-13-25	460	Buckling

*The critical length was not obtained for this model as it exceeds the practical range for the connection. However, the length is greater than the presented value.
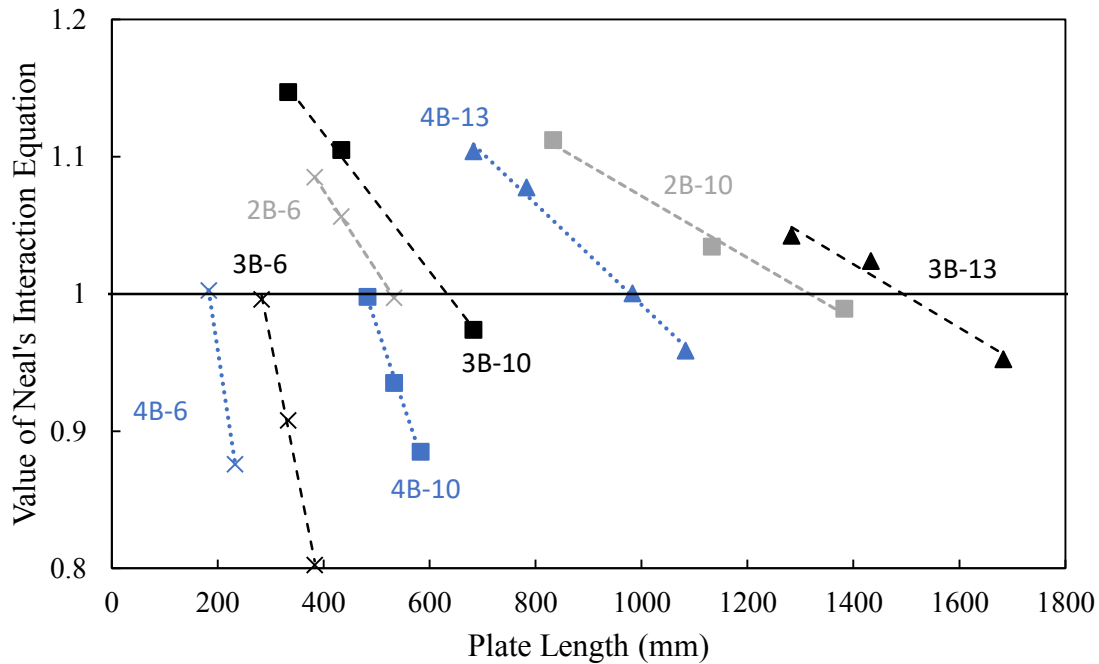
Figure 3-7: Relationship between plate length and plasticity at the support for models with no applied horizontal load

3.4.4 Failure Mode

As previously mentioned, only stability failures were observed in the parametric study, as the weld was not modelled and the 19 mm (3/4 in.) diameter bolts were assumed to be adequately designed for the applied loads. This assumption was checked and found to be true for all models. The two failure modes that were observed during the parametric study are out-of-plane deformations and buckling. They were identified by monitoring the deformed shape throughout the analysis and reviewing the load–displacement curves. The critical failure mode is the one that caused the load to drop after the ultimate vertical load was reached and is presented for each model in Table 3-3.

Out-of-plane deformations (OPD) were observed in all models. The out-of-plane displacements first occurred at the top of the plate near the support, at very low levels of vertical displacement. This displacement then gradually increased as the vertical load was applied. When out-of-plane deformations were the critical failure mode, the bottom of the plate, near the bolts, also displaced out-of-plane in the opposite direction from that at the support, causing a reverse twist deformation in the plate. This is illustrated in Figure 3-8.

This failure mode was easily identified using load–displacement curves because the post-peak reduction in capacity was smooth and gradual.

(a)

(b)
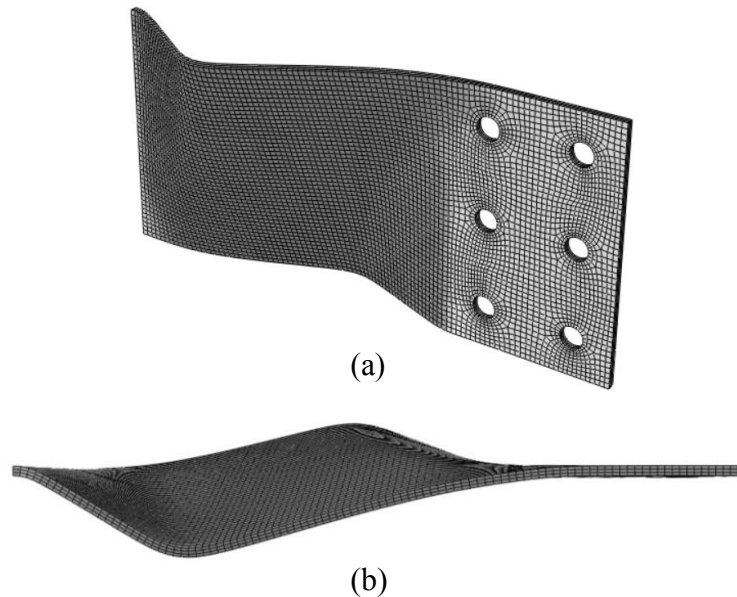
Figure 3-8: Out-of-plane (reverse twist) deformations of model 3B-6-0:
(a) Isometric view; (b) Top view

Buckling failure of the plate was observed in some models with axial compression. However, buckling never occurred as a result of the horizontal load alone (i.e., prior to the application of vertical load). Figure 3-9 shows the buckled shape of model 3B-10-10, where the plate folded near its centre. The fold location corresponds to where the plate initially deformed out-of-plane. In this case, buckling occurs prior to full load redistribution; therefore, no out-of-plane displacement is observed near the bolt line. This failure was distinguished from an out-of-plane deformation failure as it caused a sudden and significant drop in the vertical load. A load–displacement graph is presented in Figure 3-10 to show the difference in the curves created by an out-of-plane deformation failure and a buckling failure.

(a)

(b)
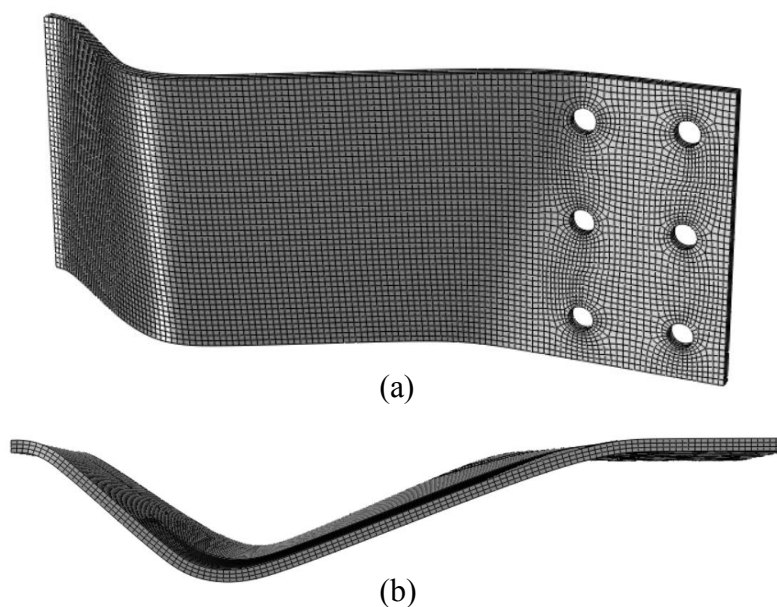
Figure 3-9: Buckled shape of model 3B-10-10:
(a) Isometric view; (b) Top view
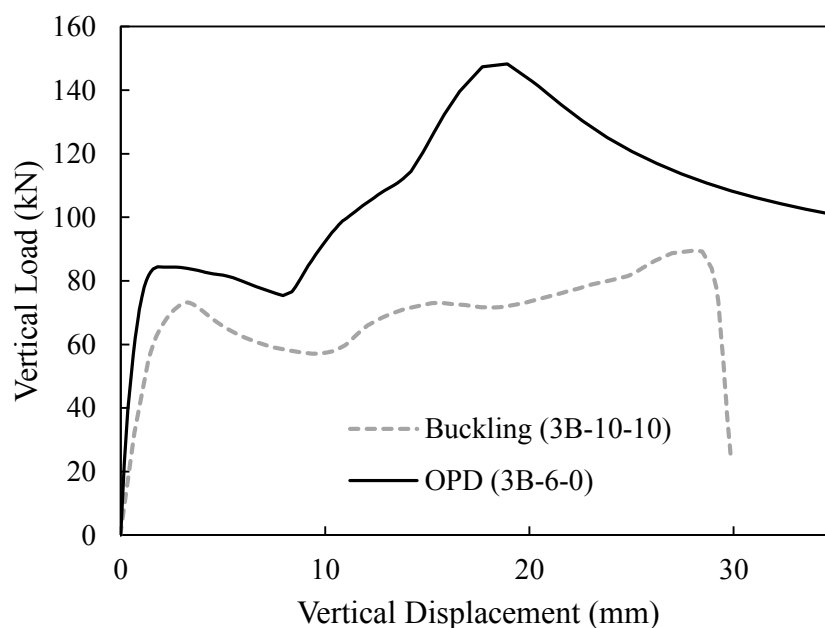
Figure 3-10: Load–displacement graph illustrating an out-of-plane deformation
failure and a buckling failure

3.4.5   Connection Capacity

The shear capacity of the connection was obtained using the load–displacement curves that
were created for each model and was taken as the peak vertical reaction force that was
developed at the reference point on the rigid loading plate, which is tied to the nodes at the

far end of the loading beam. The displacement is always measured at a point on the bottom beam flange aligned with the vertical line of bolts closest to the support.

Two peaks were observed in some of the load–displacement curves, corresponding to the redistribution of load, as mentioned in Section 3.4.1. The first peak occurs at a low level of vertical displacement, whereas a lot of ductility is required to reach the second peak. All models analyzed without horizontal load exhibited this double-peak behaviour. An example is provided in Figure 3-11, where model 4B-10-0 reached capacities of 157 kN and 233 kN at the first and second peaks, respectively. However, some of the models with an applied horizontal compression load either buckled after the first peak, or the second peak was lower than the first. In these cases, the ultimate capacity is equal to the capacity at the first peak. All model capacities are reported in Table 3-4 and load–displacement curves for all models are provided in Appendix A.
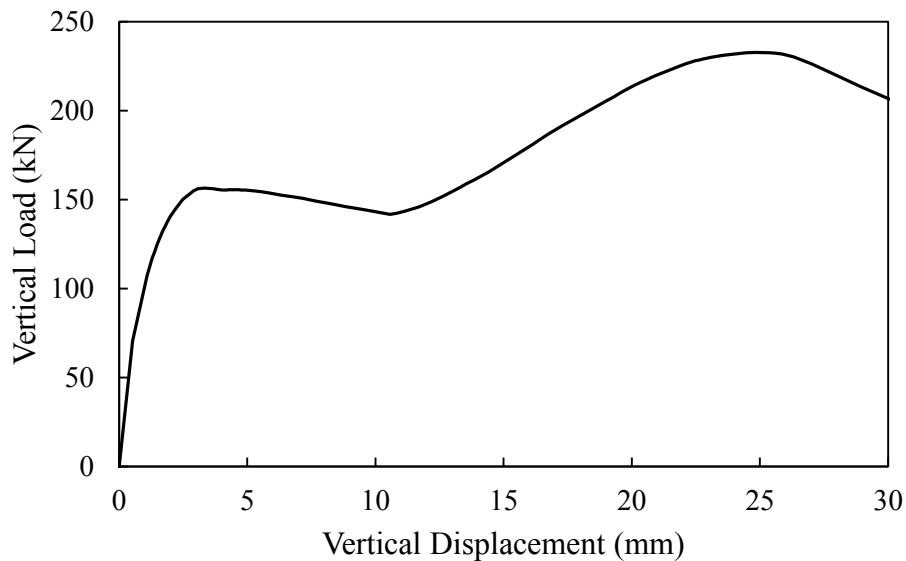
Figure 3-11: Load–displacement response for model 4B-10-0

Table 3-4: Model shear capacities at the critical length

Specimen ID	Capacity at First Peak (kN)	Ultimate Capacity (kN)
2B-6-0	26.6	30.4
2B-6-10	30.4	30.4
2B-6-25	33.0	33.0
2B-10-0	16.2	20.1
2B-10-10	26.9	28.2
2B-10-25	32.4	32.4
2B-13-0	15.5*	15.5*
2B-13-10	24.2	24.2
2B-13-25	33.3	33.3
3B-6-0	83.3	148.2
3B-6-10	103.5	163.9
3B-6-25	116.0	218.1
3B-10-0	66.0	91.7
3B-10-10	73.2	89.6
3B-10-25	89.5	94.7
3B-13-0	47.3	57.1
3B-13-10	69.9	69.9
3B-13-25	75.7	75.7
4B-6-0	230.9	354.5
4B-6-10	243.3	368.3
4B-6-25	221.4	385.8
4B-10-0	156.5	232.7
4B-10-10	182.0	263.6
4B-10-25	210.3	335.5
4B-13-0	114.4	146.3
4B-13-10	150.4	191.1
4B-13-25	164.7	201.1

*The critical length was not obtained for this model as it exceeds the practical range for the connection. Therefore, the capacity for the longest length analyzed is reported.

3.4.6 Bending Moment Distribution

The bending moment was obtained from the numerical model by making a cut at the desired locations, as described in Section 3.4.3. At the support, the cut was made at a distance of 8 mm from the rigid support plate. This was done to reflect the moment that would be developed at the weld toe in a real-world application, and also to exclude any discontinuities at the support. The cut at the vertical bolt line closest to the support was made through the plate only, not the entire system consisting of the bolts and beam web. Therefore, the resultant moments are those resisted by the plate alone. For this reason, the moment at the bolt line was normalized using the reduced plastic moment capacity (Equation 3-1) of the net section.

The moment ratio at both locations varies throughout the analysis and an example is presented in Figure 3-12 for model 4B-10-0, where a positive bending moment ratio corresponds to compression in the fibres above the neutral axis and tension in those below. The moments are not initially zero because some moment is created during the rotation step. It can be observed that the maximum moment is always reached early in the analysis at the support. The moment then gradually decreases as more vertical load is applied. However, the highest moment at the bolt line is only reached once a significant amount of vertical displacement has occurred, and it never reaches the reduced plastic moment capacity of the net section. When the ratio is positive at both the support and bolt line, the plate is in single curvature. However, as vertical load is applied, the bending moment ratio at the bolt line changes sign and the plate transitions into double curvature. Bending moment ratio–displacement curves for all models are provided in Appendix A.
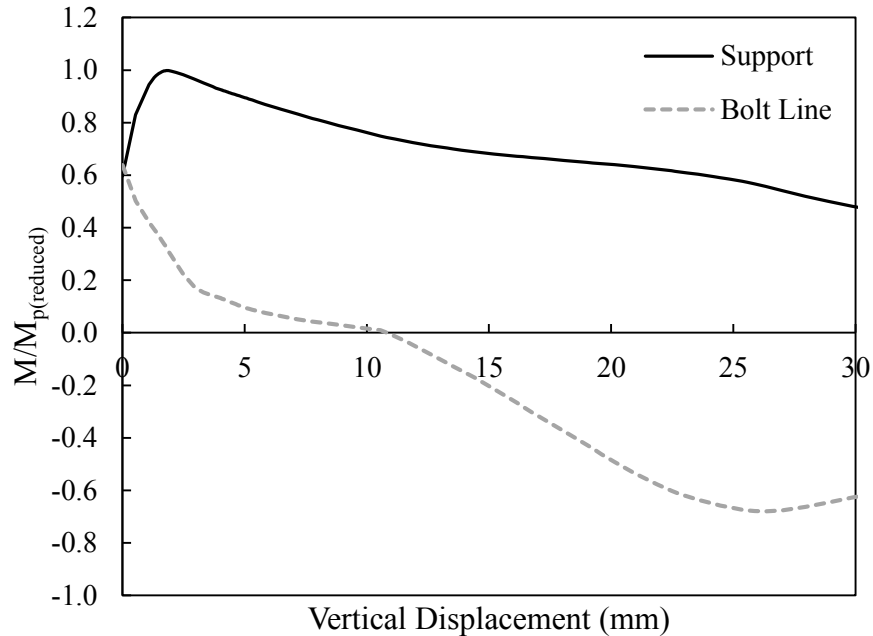
Figure 3-12: Bending moment ratio variation for model 4B-10-0

The bending moment ratio at the support corresponding to the first peak in the load–displacement curve is always approximately 1.0, as this location governed the determination of the critical length. However, the corresponding bending moment ratio at the bolt line at the first peak is extremely variable. It ranges from 0.01 in model 3B-13-0 to 0.61 for model 4B-6-0, as shown in Table 3-5. The large variation is due to the differing lengths of the extended shear tabs in this study; the longer plates have a smaller initial bending moment ratio at both the support and bolt line due to their higher flexibilities, and thus the moment at the bolt line at the first peak is much smaller as well.

Table 3-5 also lists the bending moment ratios at the support and bolt line just prior to failure of the connection. The values vary considerably, indicating that the bending moment is influenced by the applied loads and failure mode of the connection. The models with no applied horizontal load generally have similar, higher ratios at the support and bolt line. Also, there are still significant bending moments present at the support at failure, which must be accounted for in design.

Table 3-5: Model bending moment and eccentricity ratios

Specimen ID	M/M$_{p(reduced)}$ at First Peak		M/M$_{p(reduced)}$ at Failure		e$_b$/e$_g$ at Failure
	Support	Bolt Line	Support	Bolt Line	
2B-6-0	1.00	0.01	0.51	-0.63	0.56
2B-6-10	1.00	0.15	0.35	-0.41	0.57
2B-6-25	0.97	0.30	0.08	-0.13	0.55
2B-10-0	0.99	-0.06	0.64	-0.77	0.52
2B-10-10	1.02	0.11	0.43	-0.39	0.48
2B-10-25	1.02	0.15	0.48	-0.19	0.23
2B-13-0	1.03*	-0.26*	-*	-*	-*
2B-13-10	1.01	-0.05	0.56	-0.31	0.35
2B-13-25	1.00	-0.06	0.62	-0.20	0.22
3B-6-0	1.00	0.45	0.53	-0.68	0.62
3B-6-10	0.98	0.45	0.39	-0.69	0.67
3B-6-25	1.03	0.48	0.19	-0.80	0.81
3B-10-0	1.02	0.15	0.58	-0.68	0.55
3B-10-10	1.01	0.21	0.38	-0.61	0.62
3B-10-25	1.01	0.28	0.32	-0.28	0.51
3B-13-0	1.02	0.01	0.61	-0.62	0.51
3B-13-10	1.03	0.12	0.39	-0.43	0.54
3B-13-25	0.98	0.17	0.23	-0.14	0.32
4B-6-0	1.00	0.61	0.55	-0.74	0.69
4B-6-10	1.01	0.53	0.40	-0.71	0.75
4B-6-25	0.99	0.55	0.20	-0.74	0.82
4B-10-0	1.00	0.32	0.56	-0.68	0.55
4B-10-10	1.01	0.29	0.50	-0.66	0.60
4B-10-25	1.02	0.38	0.22	-0.75	0.75
4B-13-0	1.00	0.08	0.55	-0.64	0.53
4B-13-10	1.02	0.14	0.42	-0.69	0.62
4B-13-25	0.99	0.28	0.36	-0.33	0.56

*The critical length was not obtained for this model as it exceeds the practical range for the connection. Therefore, bending moment ratios are reported for the longest length analyzed.

3.4.7 Shear Load Eccentricity

The shear load eccentricity was determined for each model as it is an important parameter in the design of extended shear tabs. The eccentricity ratio is equal to the bolt group shear load eccentricity over the geometric eccentricity (e_b/e_g). The bolt group shear load eccentricity is equal to the distance from the centre of the bolt group to the point of inflection. It is divided by the geometric eccentricity, which is the distance from the support face to the centre of the bolt group, as this value is commonly used in design procedures (AISC 2017).

The eccentricity ratio varied substantially as the vertical load was applied to the connection, as shown in Figure 3-13 for model 4B-10-0. Negative values indicate that the point of inflection was not in the plate, but rather in the loading beam and, therefore, the plate was in single curvature. With further vertical loading, the point of inflection migrated towards the support and at approximately 8 mm of vertical displacement it reached the centre of the bolt group. After this, the eccentricity ratio continued to increase and eventually reached a value of 0.55. This behaviour is characteristic of all models, as shown by the eccentricity ratio–displacement graphs in Appendix A.
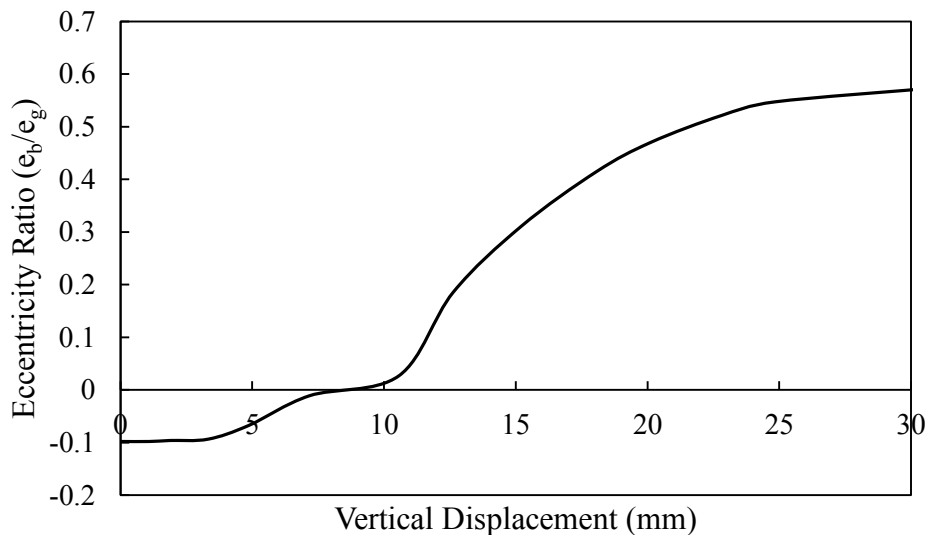

Figure 3-13: Eccentricity ratio variation for model 4B-10-0

The eccentricity ratio corresponding to the first peak in the load–displacement curve was found for all models. The ratio ranged from -0.29 in model 3B-6-25 to 0.08 in model

2B-10-0, and the majority are approximately zero. Therefore, the point of inflection is either in the loading beam or very close to the bolt group centre at this load level, indicating that the shear load eccentricity for the support would be approximately equal to the geometric eccentricity.

The bolt group shear load eccentricity just prior to failure was extracted from the model and the values are reported in Table 3-5. The average for all models is 0.56, indicating that the point of inflection is approximately midway between the support and bolt group centre. This value is in line with the mean eccentricity ratio reported by Salem et al. (2016) of 0.60 at bolt fracture for models with a stiff support. The lowest eccentricity ratio in this study was 0.22 for model 2B-13-25 and is caused by the buckling failure of the connection. The high axial compression caused the plate to fail while the point of inflection was still fairly close to the bolt group.

3.4.8 Influence of Parameters

The parametric study considered three different plate thicknesses and plate depths with varying levels of horizontal compression: 0%, 10% and 25% of the plate nominal axial yielding capacity. The critical length of the extended shear tab is heavily dependent on both the depth and thickness of the plate. Observations regarding the effect of these parameters on the critical length, failure mode, and capacity of the connection are discussed in the following sections. Direct comparisons between models in terms of ultimate capacity are difficult, as no two models have the same plate length.

3.4.8.1 Plate Thickness

The critical length increases with an increased thickness, as expected. As previously stated, the failure modes in this study are out-of-plane deformation and buckling. Increasing the plate thickness has a large impact on the resistance of the connection, as it increases the weak-axis properties. This is also demonstrated in Figure 3-14, which shows the approximately linear relationship between critical length and plate thickness for models with no applied horizontal load. There is little difference in the plate length obtained for the three depths at a thickness of 6.35 mm; however, the spread increases with plate

thickness. For thicker plates, the connection has an increased resistance to out-of-plane deformations and plate depth has a greater influence on the stability limit.

A similar, almost linear relationship was also observed for the models analyzed with an applied horizontal compression load. However, there is less variation in the critical length at the larger plate thicknesses, as shown in Figure 3-15. Since the critical length is longer for thicker plates, the corresponding shear capacity decreased.
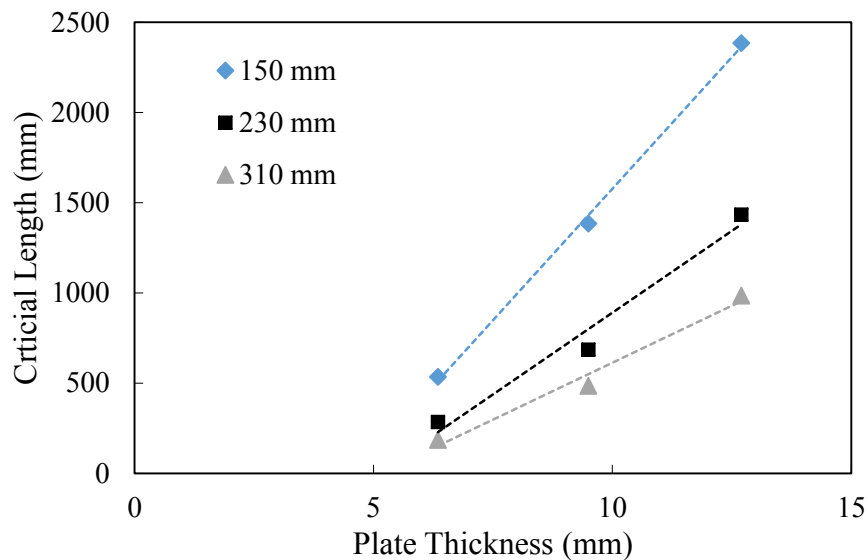

Figure 3-14: Effect of plate thickness on critical length for models with no applied horizontal compression load
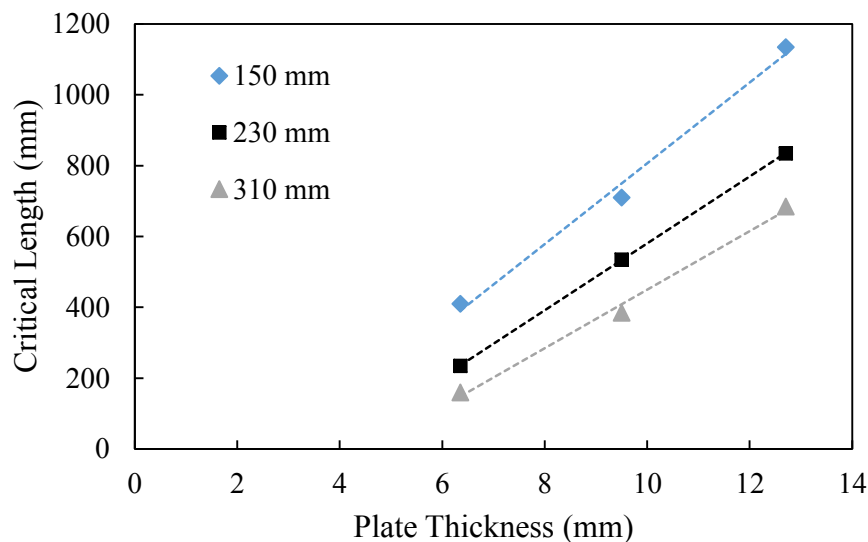

Figure 3-15: Effect of plate thickness on critical length for models with 10% applied horizontal compression load

3.4.8.2 Plate Depth

Table 3-3 shows that increasing the connection depth results in a smaller critical length. This relationship is also represented in Figure 3-16, where the parameters have a parabolic relationship and the steeper slope is attributed to the thicker extended shear tab plates. There is a larger spread in the data at a connection depth of 150 mm, indicating that the stability of shallow connections is greatly affected by plate thickness. The data converges as the connection depth increases, indicating that depth begins to govern the behaviour of the connection. This is in line with what was observed in Figure 3-14, where the deeper the section, the less the thickness affected the critical length.

The shear capacity of the connection also increases with increasing depth and shorter plate length, as illustrated in Figure 3-17 for 10% applied horizontal compression load, because less shear load is required for a shallow, long plate to reach a value of 1.0 using Equation 2-5. The reason for this is two-fold: longer plates have a greater moment arm, creating a larger moment at the support for the same vertical load, and the plastic moment of the plate is smaller for a shallower section. Also, all models with a depth of 150 mm had approximately the same ultimate shear capacity regardless of differing plate thicknesses and lengths.
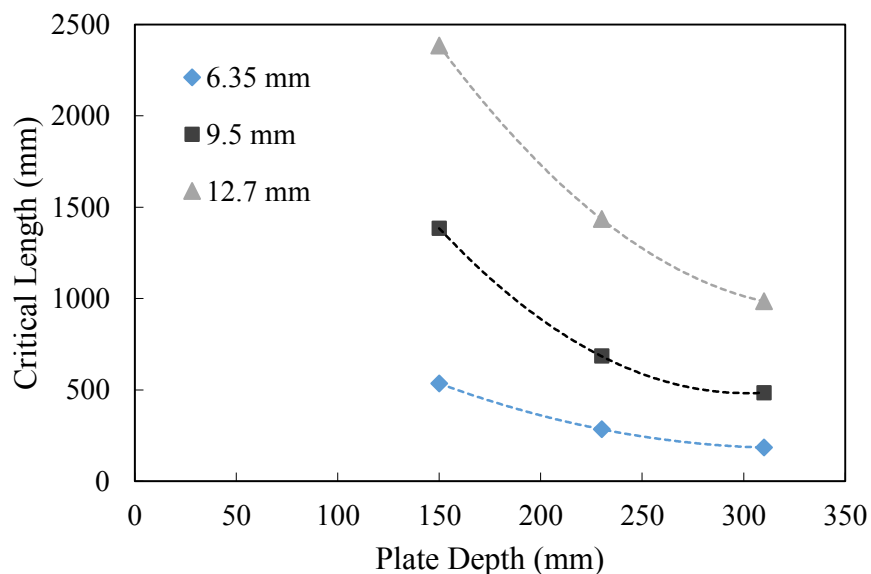

Figure 3-16: Effect of plate depth on critical length for models with no applied horizontal load
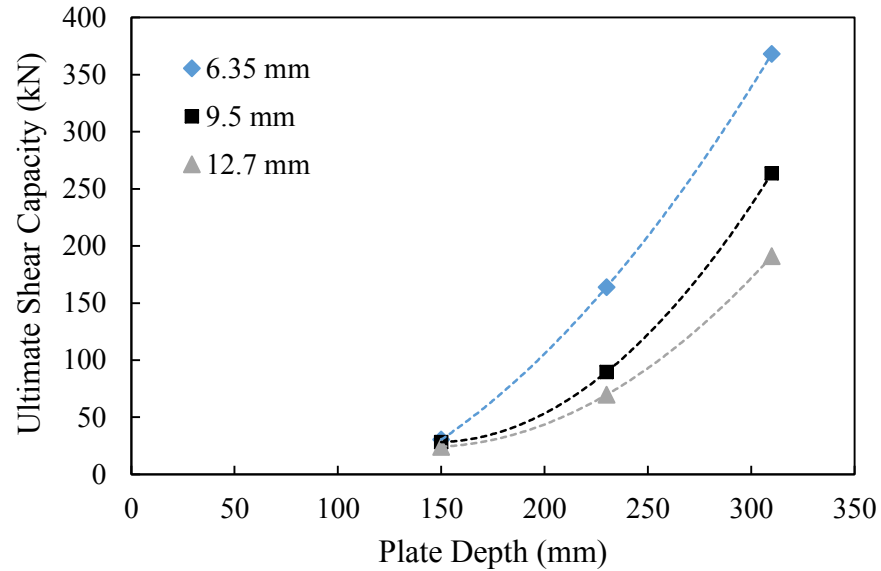
Figure 3-17: Effect of plate depth on ultimate shear capacity for models with 10% applied horizontal compression load

3.4.8.3 Axial Compression

Axial compression was applied as a percentage of the plate's nominal axial yielding capacity and the horizontal load ranged between 36.7 kN and 378.9 kN for models 2B-6-10 and 4B-13-25, respectively. The effect of the horizontal compression load on the critical length is presented in Figure 3-18. It is evident that the critical length decreases with axial compression. With zero applied horizontal load, the spread in the critical lengths is quite large, indicating that it is more sensitive to variations in the depth of the plate. Conversely, with higher compressive loads the critical length does not vary as much among the three depths. This is because the depth of the section becomes less influential as the failure mode changes.
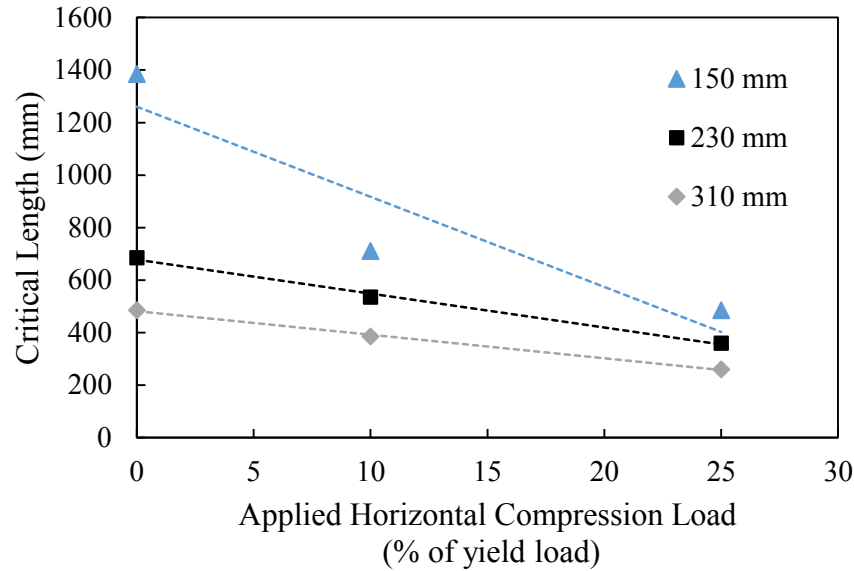
Figure 3-18: Effect of horizontal load on critical length for models with a plate thickness of 9.5 mm

As per Table 3-3, all models with no applied horizontal load failed due to out-of-plane deformations and those subjected to a horizontal load of 25% of the plate's nominal axial yield capacity failed due to buckling. Models 3B-6-25 and 4B-6-25 are the exception to this statement; because their critical lengths are short, 160 mm and 135 mm respectively, the plate buckling strength is high and they fail due to out-of-plane deformations.

The addition of axial compression changed the stress distribution in the plate and, therefore, affected the critical failure mode of the connection. Figure 3-19 shows yielding patterns for model 3B-10 at all levels of horizontal load considered. The shaded contours show the equivalent plastic strain (PEEQ in Abaqus) distribution, which is commonly used to detect yielding in finite element analysis, with the lightest grey indicating elastic material and increasingly darker shading signifying higher strains. In all cases, yielding developed at three distinct locations in the plate. The first is the support, since it is fixed, and yielding began at the top of the plate due to the direction of the rotation. Figure 3-19(a), which represents the connection with no applied horizontal load, also yielded where the out-of-plane deformations originated at the top and bottom of the plate.

Figure 3-19(c) shows the deformed shape of the connection subjected to a horizontal compressive load of 25%. Yielding is concentrated around the centre of the plate where it

folded due to buckling, and also at the first bolt line since the clamping effect of the bolts restricts any lateral displacement. Finally, the connections analyzed with a moderate horizontal load (10%) deformed as per Figure 3-19(b), and exhibited characteristics from each of the two bounding cases. Due to the axial compression, yielding of the full cross-section occurred near the centre of the plate. However, out-of-plane displacements occurred at the bottom of the plate near the bolts, causing some twist in the plate.

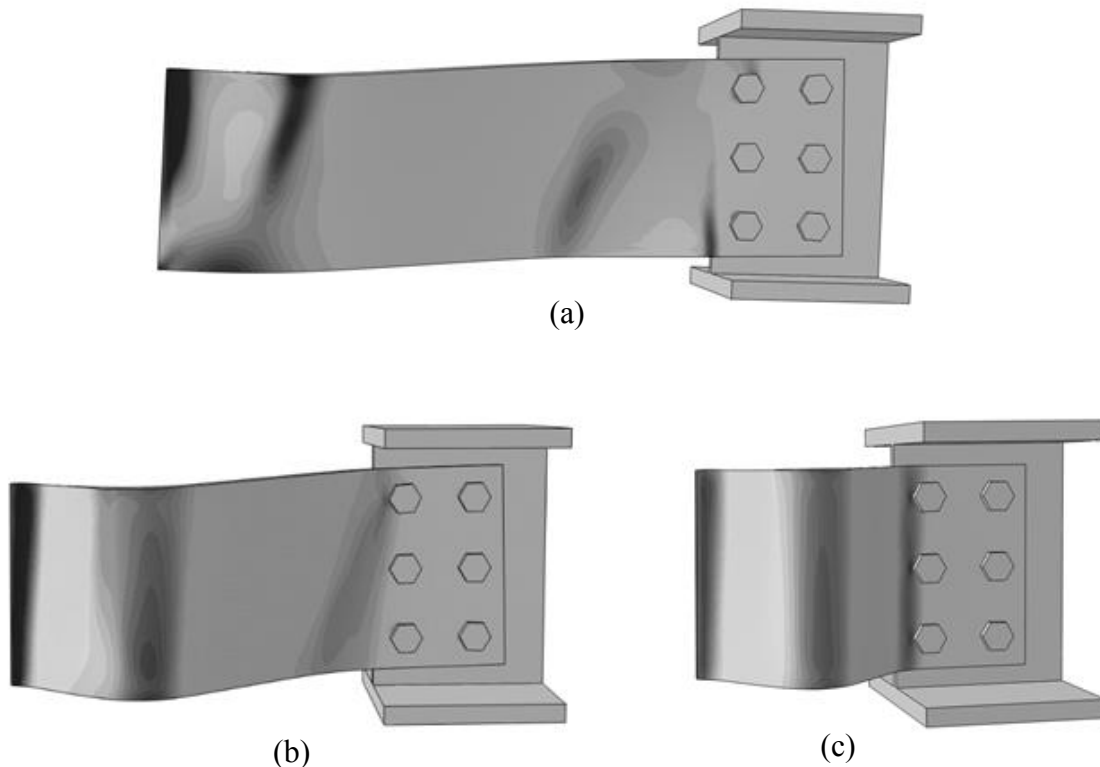(a)

(b)   (c)

Figure 3-19: Deformed shapes and plasticity development of models:
(a) 3B-10-0; (b) 3B-10-10; (c) 3B-10-25

The capacity of the connection was also affected by the axial compression as illustrated in Figure 3-20, which only shows connections with a depth of 230 mm. The ultimate shear capacity of the thin, 6.35 mm plates was more affected by the axial compression than the thicker plates. The reason for this is because as the horizontal load is increased, the plate length gets shorter and the connection is less susceptible to a stability failure. The reduced shear load eccentricity offsets the effect of an increased axial load. As previously mentioned, the stability of thicker plates is predominately governed by their depth, which

explains why the capacity of the 9.5 mm and 12.7 mm thick plates are approximately the same at all levels of horizontal load.
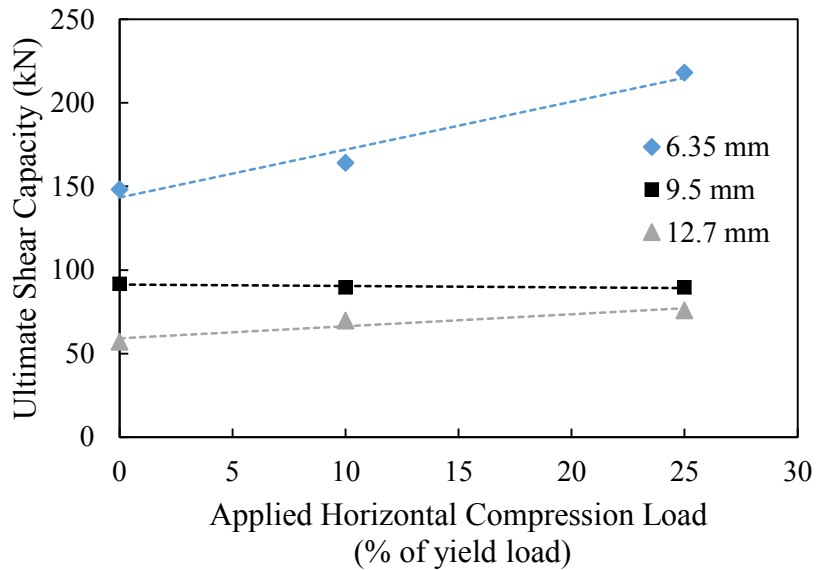

Figure 3-20: Effect of horizontal load on the ultimate shear capacity for models with a plate depth of 230 mm

3.5 Summary

An extended shear tab finite element model was created and validated by Salem et al. (2016) using results from three full-scale experimental tests conducted at the University of Alberta. This model was then modified in order to investigate connection stability under the combined loading of rotation, horizontal force, and vertical force. The model considered the support of the extended shear tab to be fully fixed against all rotations and translations and the loading beam was restrained against any lateral displacements.

A parametric study was then conducted in which the plate thickness, the plate depth, and the level of axial compression were varied. The length of the plate was increased until a stability failure occurred prior to the development of cross-sectional plasticity in the plate. Plasticity was determined using Neal's equation (Equation 2-5) to account for the interaction of bending, shear, and axial stresses. The behaviour of the connection was analyzed, and plasticity always developed at the support prior to the bolt line due to the high rotational stiffness of a fixed boundary condition. As the vertical force was increased further, load was shed towards the bolt line. Due to the length of the plates in this study, a

stability failure occurred prior to plasticity at the bolt line. This caused a double-peak to be observed in the load–displacement response curves. In some cases, the addition of a high compressive horizontal load caused the plate to either fail after the first peak or resulted in a lower capacity at the second peak.

Stability of extended shear tabs is dependent on plate thickness and depth; however, the lengths required to cause a stability failure are quite long, and in some cases longer than any practical application. Additionally, the ultimate shear capacity of the connection decreased as the length increased, but as plate thickness increases, so too does the critical length. Conversely, deeper plates fail by instability at shorter lengths than shallow plates of the same thickness. It has also been observed that the critical lengths for thin (6.35 mm) plates are less sensitive to connection depth than the two thicker plates analyzed.

Two different failure modes were observed in this study, out-of-plane deformations (more ductile) and buckling (less ductile). The failure mode was heavily influenced by the amount of horizontal load applied to the connection. The plates analyzed without horizontal load exhibited reverse twist deformation and failed due to gradually increasing out-of-plane deformations. With the addition of a horizontal compression load of 10% of the plate nominal axial yield capacity, the deformed shape is similar to those with no horizontal load; however, the compression caused a buckling failure in longer plates. Finally, those with high (25%) horizontal loads failed due to buckling soon after the application of vertical load began.

CHAPTER 4: EXPERIMENTAL PROGRAM

4.1 Introduction

In order to validate the results of the finite element analysis, an experimental full-scale testing program was carried out. The objective of the program was to obtain experimental results investigating the stability of extended shear tabs, as few previous tests have captured this behaviour. The influence of geometric parameters such as plate thickness, plate depth, and plate length were studied along with varying levels of axial compression. In this chapter, the experimental program is outlined, the methodology regarding the testing program is presented, and the experimental test results are discussed. Additionally, a comparison with results from the finite element model is presented.

4.2 Experimental Testing Program

In this section, the design of the extended shear tab specimens is discussed. A description of the ancillary tests used to determine the material properties is also presented, along with an overview of the test set-up, instrumentation, and loading procedure that was employed.

4.2.1 Test Specimens

A total of six extended shear tab specimens were tested. The specimens were fabricated and donated by Waiward Steel LP of Edmonton, Alberta, and the drawings are provided in Figure 4-1. Each extended shear tab specimen was welded to a 25 mm (1 in.) thick 700 mm×250 mm plate to represent the fixed support condition used in the finite element analysis. Two vertical bolt lines were used, as this is common in industry applications (Thomas et al. 2014). The horizontal and vertical end and edge distances are 35 mm, and both the pitch and gauge are 80 mm. The required number of standard bolt holes were drilled for 19 mm (3/4 in.) diameter ASTM A325 bolts. This size of bolt is consistent with previous studies conducted at the University of Alberta. The fillet welds were designed using Equation 2-2, and thus all specimens used an 8 mm weld. The plate thickness was kept constant at 9.5 mm (3/8 in.) for all tested extended shear tabs, and the plate depth, plate length, and level of axial compression were varied. An alphanumeric ID was given to each specimen to facilitate identification and data collection. The ID system is similar to

the one used for the finite element parametric study, described in Chapter 3, where the first two characters represent the number of horizontal bolt lines. As the plate thickness is constant for the tested extended shear tabs, this is not used in the ID. The last value represents the horizontal compression load that was applied and it is expressed as a percent of the plate's nominal axial yielding capacity.
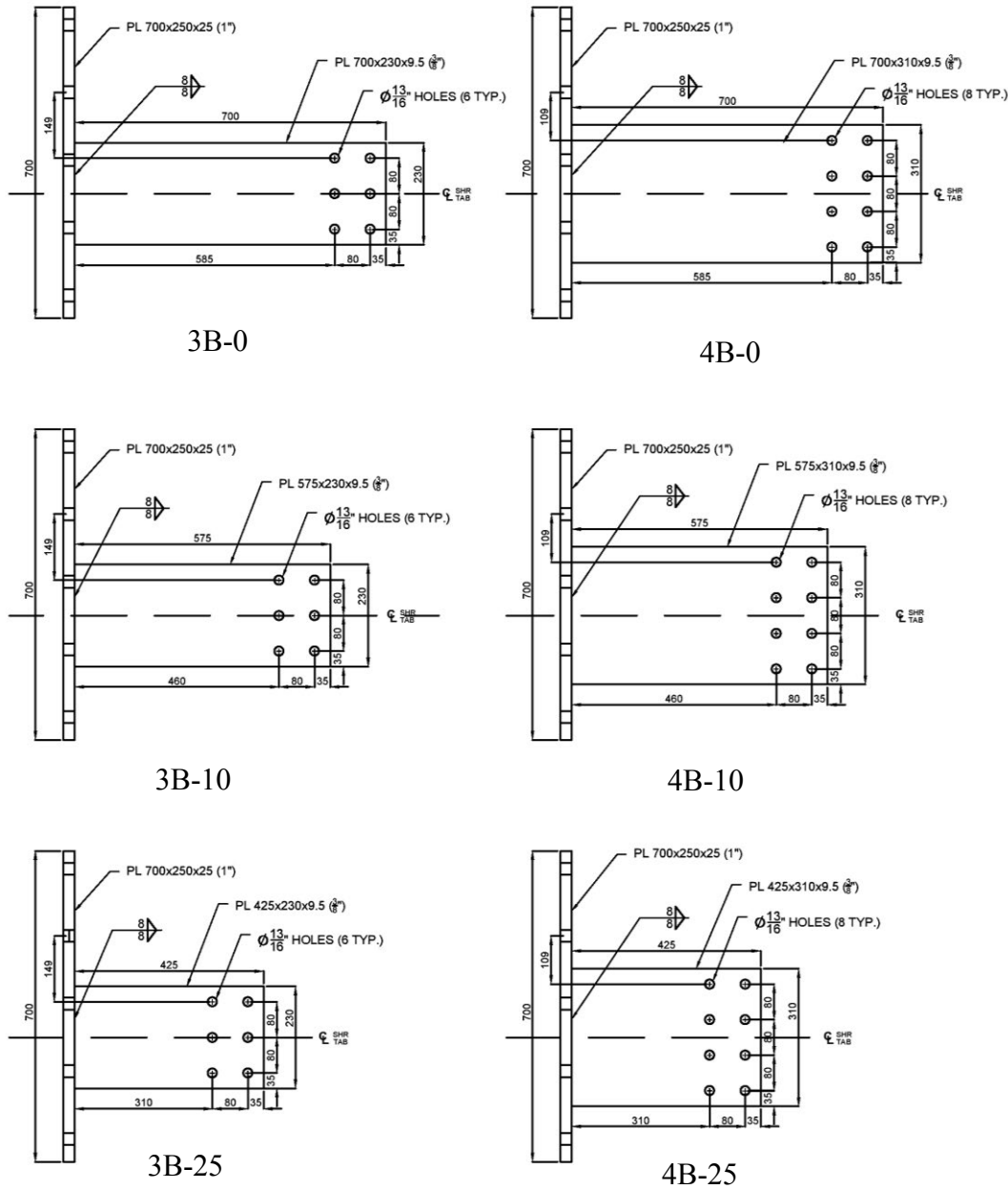

Figure 4-1: AutoCAD drawings of tested specimens

The dimensions of the specimens were chosen based on results of the parametric study conducted in Abaqus as well as lab constraints. The lab set-up required modification for each individual length; therefore, limiting the number of different lengths in the testing program is advantageous. As previously mentioned, 27 models were analyzed to find the critical lengths for different extended shear tab configurations, where the critical length represents the limit between a strength- and stability-governed failure. From these, six geometries were chosen to be tested in the lab, and are presented in Table 4-1. This table lists the critical length for each specimen as determined from the finite element parametric study. The table column adjacent to the critical length lists the tested length of the extended shear tab. The tested lengths were chosen to be the same for each level of horizontal load, and were taken as the midpoint between the critical lengths obtained for each depth.

A distinction between critical length and tested length was necessary because a limit is hard to obtain experimentally. This is principally due to potential differences from the finite element model. It was hypothesized that these differences or imperfections could result in a change in both the capacity and moment distribution of the extended shear tab plate. This would then impact the interaction of stresses and the value of Neal's equation (Equation 2-5) that was initially used to find the critical length, as described in Section 3.4.3. By testing the extended shear tabs at lengths either longer or shorter than their critical length, their anticipated behaviour could more easily be predicted. The shallow (3B) specimens are expected to reach their plastic capacity as they are tested at shorter lengths, whereas the deeper (4B) specimens are not. This prevents any ambiguity associated with testing plates right at the critical length.

Table 4-1: Experimental test matrix

Specimen ID	Thickness (mm)	Depth (mm)	Critical Length from FEA (mm)	Tested Length (mm)	Applied Horizontal Compression Load
3B-0	9.5	230	685	585	0%
4B-0	9.5	310	485		
3B-10	9.5	230	535	460	10% of nominal axial yield capacity
4B-10	9.5	310	385		
3B-25	9.5	230	360	310	25% of nominal axial yield capacity
4B-25	9.5	310	260		

As-built dimensions were measured for each specimen and averages are presented in Table 4-2. This ensured that the specimens were fabricated as specified and that the dimensions were within an acceptable tolerance. The measured dimensions match those requested in Figure 4-1 closely, and thus specified dimensions were used for any calculations in the following sections.

Table 4-2: As-built dimensions

Specimen ID	Plate Thickness (mm)	Plate Depth (mm)	Plate Length (mm)
3B-0	9.56	231.3	585.3
4B-0	9.40	311.3	583.8
3B-10	9.61	231.3	459.0
4B-10	9.56	311.5	459.8
3B-25	9.55	230.1	309.7
4B-25	9.50	310.8	311.0

4.2.2 Material Properties

To determine the material properties of the tested specimens, ancillary tests were conducted on tension coupons cut from a 540 mm×400 mm plate. This was cut from the same plate as the extended shear tabs. All material for this study was fabricated from CAN/CSA-G40.20/G40.21 grade 350W steel. Figure 4-2 shows the orientation of the coupons, where three are taken in the longitudinal direction and three in the transverse direction with respect

to the axis of the tested plate. This was done in order to capture any changes in behaviour and material properties resulting from steel grain orientation. The coupons were labelled sequentially, and the ID indicates the direction.

The tension coupons were tested in accordance with ASTM standard A370-14 (ASTM 2014). The initial cross-sectional dimensions were measured and recorded prior to the test. The tests were conducted using an MTS 1000 testing machine, which measured the applied force and an extensometer was used to measure strain. The engineering stress was calculated using the recorded force and the initial cross-sectional area of the dog-bone specimen. During the test, loading was paused in order to obtain three static points on the yield plateau. These static points were then averaged to calculate the static yield stress of the material. An additional static point was taken at the ultimate load level in order to calculate the ultimate static capacity. The results from tension coupon L-3 were invalidated due to a large initial flaw in the reduced section of the dog-bone specimen. A photograph of this flaw is provided in Figure 4-3. Engineering stress–strain curves for the remaining five tension coupons are provided in Appendix B.
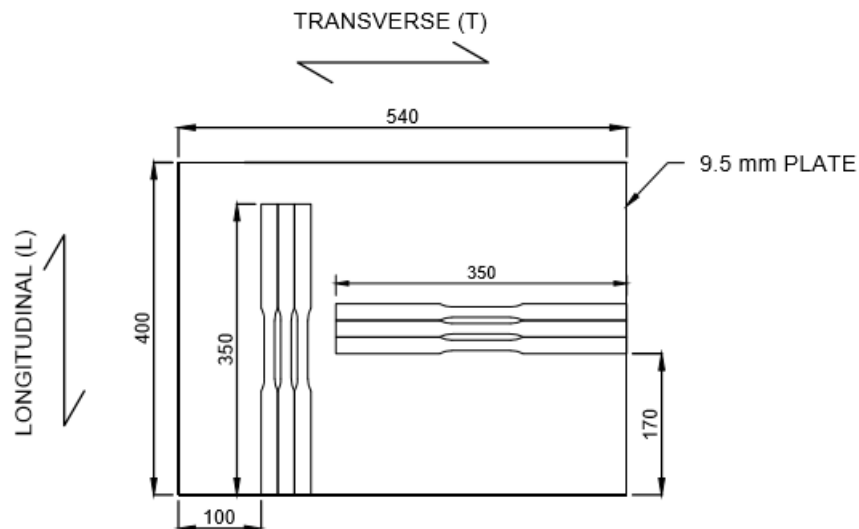

Figure 4-2: Tension coupon layout

Figure 4-3: Initial flaw in tension coupon L-3

Relevant material properties such as static yield stress, static ultimate stress, and elastic modulus are reported in Table 4-3. The mean static yield stress of 380 MPa is higher than the grade's nominal yield strength of 350 MPa; however, it is in line with the expected value. The elastic modulus and ultimate stress are also within the expected range.

Table 4-3: Tension coupon material properties

Coupon ID	Yield Stress (MPa)	Ultimate Stress (MPa)	Elastic Modulus (MPa)	Failure Strain (%)
L-1	375	470	203 170	38.9
L-2	371	448	197 819	37.6
T-1	385	450	203 196	35.3
T-2	387	450	199 280	35.9
T-3	385	450	201 003	34.1
Mean	**380**	**454**	**200 894**	**36.4**

As illustrated in Table 4-3, there was a slight difference in the yield stress in the longitudinal and transverse directions. The transverse coupons consistently gave a higher yield stress than those taken in the longitudinal direction. This indicates that a certain degree of anisotropy exists in the steel; however, the differences are not expected to affect connection behaviour.

4.2.3 Test Set-up

The experimental testing program was conducted in the I.F. Morrison structural engineering laboratory at the University of Alberta. A similar test set-up was used by Salem et al. (2016) and Thomas et al. (2014; 2016) in previous studies. The set-up allows for the

application of rotation, horizontal loading and vertical loading independently through the use of three separate actuators. A schematic illustration of the test set-up is shown in Figure 4-4. The loading beam is a W530×165 section and was chosen as it is compatible with the actuator connections and its web will not fail during the test. 20.6 mm (13/16 in.) diameter holes were drilled in the beam web at a centre-to-centre spacing of 40 mm to accommodate both the 230 mm (3B) and 310 mm (4B) deep plates and ensure the horizontal load is applied through the centre of the section. Additional design checks were performed to ensure that the beam web would not fail during any of the tests.
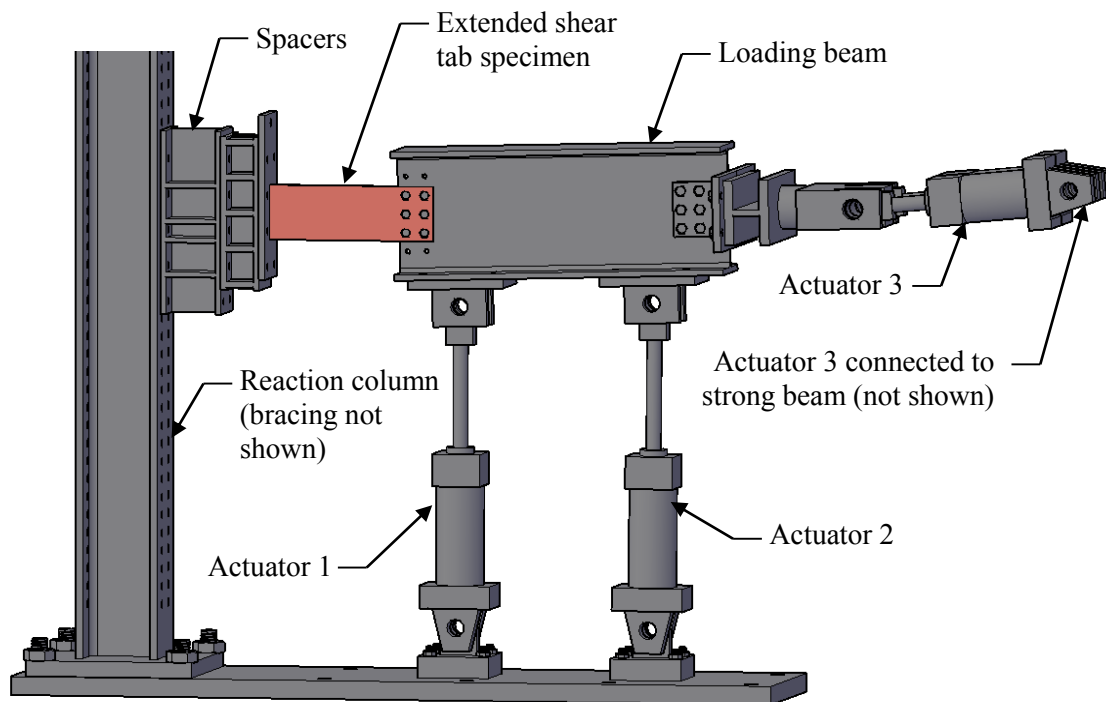
Figure 4-4: Experimental test set-up

As there were three different lengths of extended shear tab in this program, the reaction column was required to be placed in two different locations and the use of spacers was necessary. The reaction column was anchored to the strong floor using a base plate and four pre-stressed anchor rods that can only be placed every 610 mm (2 ft.), thus, two locations were required to satisfy the requirements of this test program. Additionally, the column was restrained against any in-plane displacements using a diagonal brace connected to a second reaction column (not shown in Figure 4-4). The 25 mm (1 in.) thick support plate was bolted

to either a spacer or the flange of the reaction column using eight 25 mm (1 in.) diameter pretensioned bolts so that no slip would occur at this location. The extended shear tab was bolted to the beam web using either six or eight 19 mm (3/4 in.) diameter ASTM A325 snug-tight bolts.

Actuators 1 and 2 were bolted to the loading beam using four 22 mm (7/8 in.) diameter pretensioned bolts each and anchored to the strong floor with the use of a custom steel base plate. Actuator 3 was bolted to a strong beam that was in turn bolted to the lab's shear walls using eight 25 mm (1 in.) diameter pretensioned bolts. The actuator was then connected to the loading beam using two side lap plates and a thick load transfer plate. The side lap plates are 12.7 mm (1/2 in.) thick and connect to the web with nine 22 mm (7/8 in.) diameter bolts.

Lateral bracing of the beam was provided near the connection to ensure that no out-of-plane displacement failure would occur in the loading beam. This was achieved by using Teflon® sheets attached to steel plates, which were then connected to two short columns on either side of the beam that were anchored to the strong floor. The Teflon® sheets were shimmed in order to lightly touch both the top and bottom flange of the loading beam and provide lateral support with minimal vertical restraint. A photograph of the completed test set-up is shown in Figure 4-5.
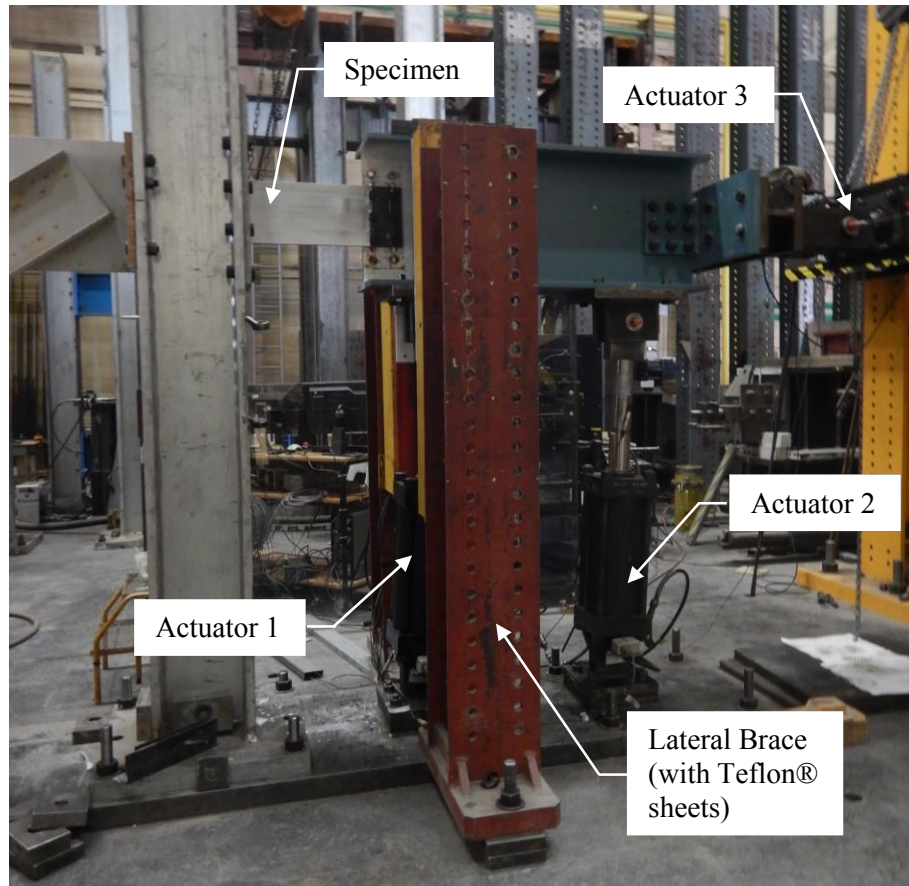
Figure 4-5: Completed experimental test set-up

4.2.4 Instrumentation

The behaviour of the connection was monitored using load cells, pressure transducers, cable transducers, clinometers, and linear variable differential transformers (LVDT). Data points were collected every second to ensure that any change in the connection was captured immediately. A camera was also used to capture stop motion footage of the test.

Load cells were mounted on each actuator and pressure transducers were used as a redundant load measurement. The ratio of the load as measured by each system was used to ensure that all instrumentation was working correctly. The extension of each actuator was measured using a cable transducer, and its rotation was measured with a clinometer. With the data recorded from these instruments, as well as initial measurements prior to testing, the total forces in the connection and the moment at the support could be calculated.

A clinometer was mounted to the web of the loading beam to measure beam rotation. The clinometer was calibrated and zeroed prior to each test. A redundant measure for the beam rotation was also calculated using the data from the clinometers and cable transducers on Actuators 1 and 2 and no discrepancies were observed.

Additional cable transducers were used to measure any vertical displacement at the support and the connection. The connection displacement was always taken at a point on the beam flange below the vertical line of bolts closest to the support. A LVDT was also mounted to the extended shear tab to measure any in-plane horizontal displacements during the test.

4.2.5   Test Procedure

The extended shear tab specimen was lifted into position using a chain hoist, and then bolted to the reaction column and the web of the loading beam. The plate was then whitewashed to highlight when and where yielding occurred during the test.

Loading was applied in stages, similar to the procedure described in Section 3.2.4 for the finite element parametric study. Actuator 2 was first used to apply the 0.03 radian rotation and Actuator 1 was used to keep the vertical load at approximately zero. For specimens with axial compression, the horizontal load was applied next using Actuator 3. Finally, actuator 1 was used to apply an upward vertical load to the connection. During this stage, the rotation and horizontal load were maintained. The vertical load was applied until failure of the connection occurred, which was characterized by an inability to accept any further load and a decrease in the load–displacement curve.

Safety measures were employed as a precaution for potential hazards identified prior to testing. The main hazard source for this testing program is sudden bolt failure that could turn the detached bolt into a projectile. Therefore, a Plexiglas® shield was placed between the test set-up and the hydraulic jack and data acquisition control systems. Additionally, caution tape was used to prevent anyone from accessing this area during testing.

4.3   Test Results and Discussion

Results from the six experimental tests are presented in Table 4-4. Similar to the results from the finite element analysis, the experimental load–displacement curves displayed two

distinct peaks. The first peak is caused by the formation of a plastic hinge at the support, and the subsequent softening of the system as load is shed towards the bolts. The ultimate peak is recorded as the highest vertical load observed during testing, which in the case of the highest axial load can be the same as the first peak. The ratio of the maximum moment at the weld toe to the reduced plastic moment calculated using Equation 3-1 and the bolt group eccentricity ratio at failure are also listed in the table.

Table 4-4: Results of experimental tests

Specimen ID	Capacity at First Peak (kN)	Ultimate Capacity (kN)	Maximum $M/M_{p(reduced)}$	e_b/e_g at Failure
3B-0	83.9	102.6	0.939	0.63
4B-0	119.2	159.1	0.797	0.65
3B-10	102.6	120.2	0.956	0.84
4B-10	141.2	175.6	0.884	0.81
3B-25	108.4	108.4	0.985	1.14
4B-25	185.7	185.7	0.938	0.98

4.3.1 Connection Capacity

The connection capacity was obtained using load–displacement curves that were generated for each test, and an example is shown in Figure 4-6 for test 4B-0. As illustrated, the first peak occurs early in the test and at a low level of vertical displacement; however, much more ductility is required to reach the ultimate capacity of the connection. The spikes in the curve are formed due to the incremental load application and how the 0.03 radian beam rotation was maintained using the hydraulic jacks.

The redistribution of load once a plastic hinge is formed at the support caused a decrease in the connection vertical load capacity in all six tests. In the tests with high axial compression, 3B-25 and 4B-25, this decrease caused the ultimate capacity to be reached at the first peak, as presented in Figure 4-7. Therefore, it is important to note that the capacity of extended shear tab connections will decrease during loading, which could affect other structural elements.
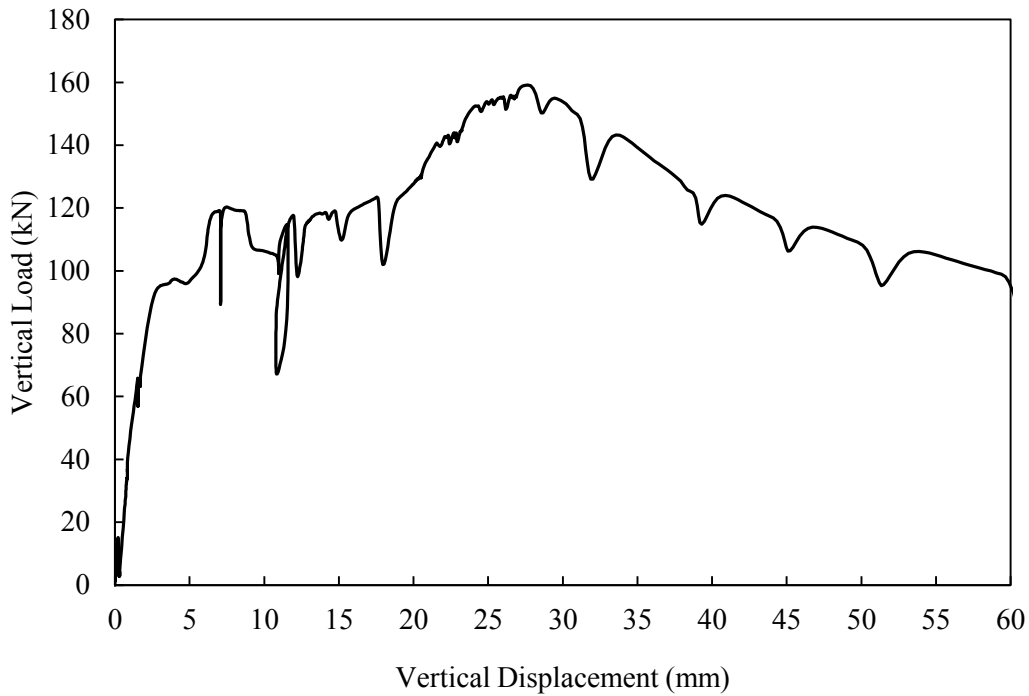
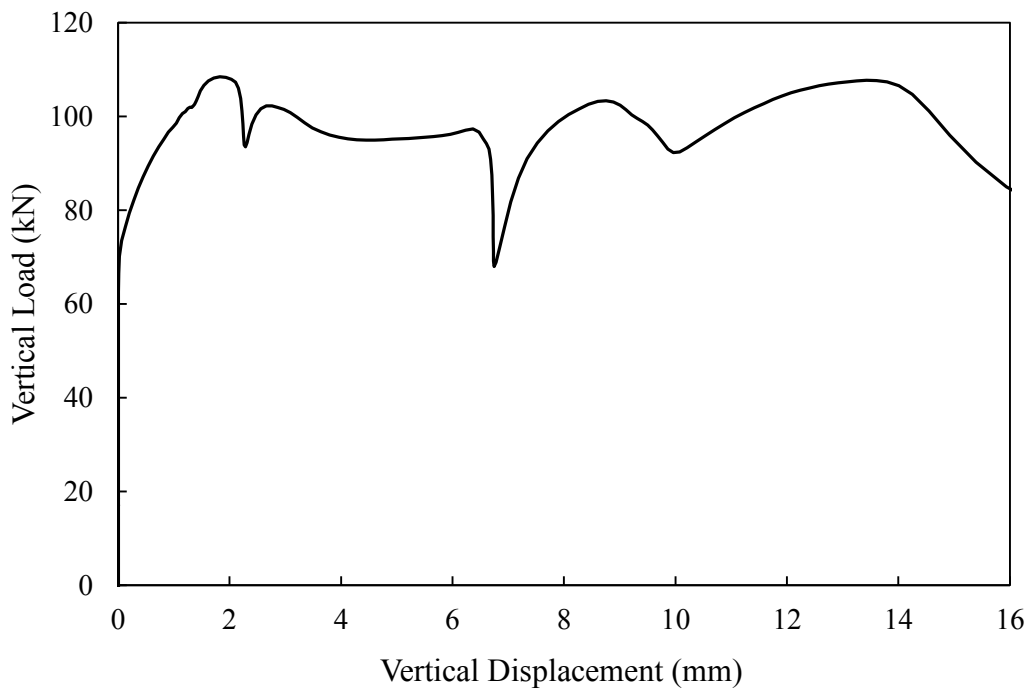Figure 4-6: Load–displacement response for 4B-0

Figure 4-7: Load–displacement response for 3B-25

The vertical displacement of the connection was measured at a point on the beam flange aligned with the vertical line of bolts closest to the support. The initial rotation of the beam caused the bottom flange to move downwards, resulting in a negative value of connection

vertical displacement prior to the application of vertical load. Since the test focused mainly on the behaviour of the extended shear tab connection under increasing shear load, the rotation can be deemed part of the initial set-up. As a result, the curves for all experimental tests were shifted to begin at zero vertical displacement. No curve was shifted more than 1.3 mm. Load–displacement curves for all experimental tests are included in Appendix C.

4.3.2 Bending Moment Distribution

In-plane bending moments at both the support and bolt line were obtained for each experimental test. The moment at the support, M_S, was calculated using the horizontal and vertical components of the load measured by each actuator and their respective moment arms. The moment at the centre of the bolt group, M_{BG}, was derived using statics, as illustrated by the free body diagram in Figure 4-8. It is common to assume that the shear load is acting at the centre of the bolt group, or at a distance equal to the geometric eccentricity, e_g, from the support. As such we can find the moment at the bolt line using Equation 4-1 and knowing that the bolt gauge used was 80 mm.
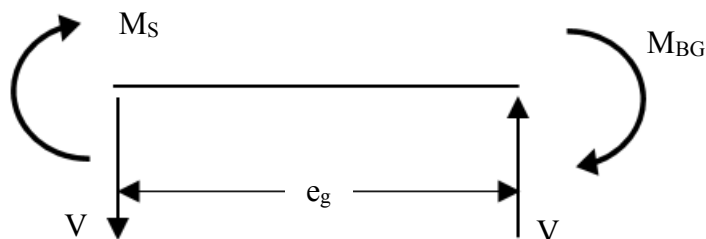
Figure 4-8: Simplified free body diagram

$$M_{BG}=V{\cdot}e_g - M_S \qquad\qquad 4\text{-}1$$

The bending moment, M_S, in Figure 4-8 is the moment at the weld toe; therefore, it is offset from the support plate by 8 mm. This is because the weld material not only increases the cross-sectional thickness, but also changes the material properties. The bending moment is normalized using the reduced plastic moment, Equation 3-1, to account for the effect of axial and shear stresses on the plate's moment capacity. This calculation utilizes the yield stress of the material obtained from the tension coupon tests. The moment at the bolt line is normalized in the same way, although the actual behaviour is much more complex. The entire system, which consists of the extended shear tab plate, the bolts, and the beam web,

contributes to resisting the moment at the bolt line. Therefore, using the reduced plastic moment of the gross cross-section gives a conservative estimate of moment utilization.

A graph showing the variation of the bending moment ratio at both the weld toe and the first vertical bolt line is presented in Figure 4-9, where a positive moment ratio corresponds to compression in the fibres above the neutral axis. This indicates that the plate was initially in single curvature; however, as loading progressed the plate switched into double curvature. Moment ratio–displacement curves for all specimens are included in Appendix C.
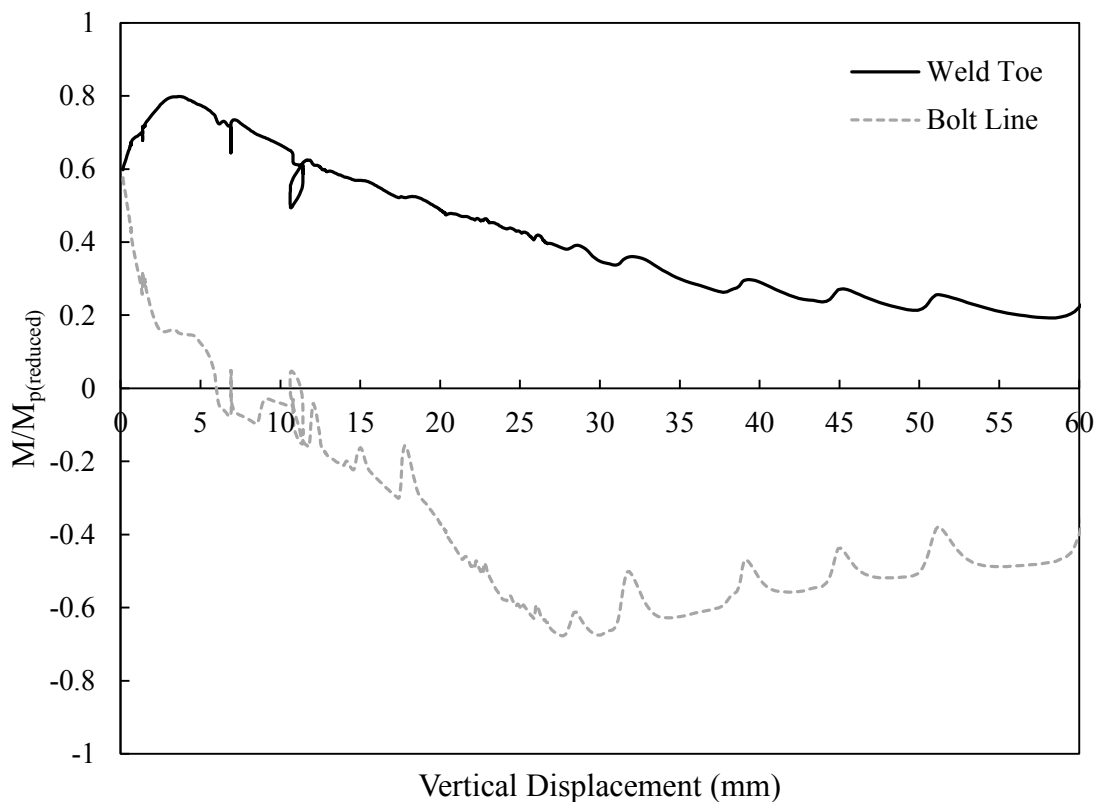
Figure 4-9: Bending moment ratio variation of specimen 4B-0

In all of the tests, the maximum bending moment ratio at the weld toe was greater than the maximum ratio calculated at the bolt line. This is consistent with the findings of the finite element parametric study, in which the critical length was always governed by plasticity at the support. Additionally, the same behaviour is observed in the bending moment and load–displacement curves. Initially, the capacity is heavily influenced by moment at the weld

toe. However, once load redistribution occurs, the moment at the bolt line mirrors the vertical load–displacement curve.

All of the bending moment ratios at the weld toe listed in Table 4-4 are less than 1.0, indicating that the plastic moment capacity of the section was not reached. As stated in Section 4.2.1, the test matrix was designed such that all 230 mm deep (3B) specimens should exceed their plastic capacity, as their tested length is shorter than their critical length. This was not the case for any of the 3B specimens that were tested; and implies that the critical length must then be shorter than the tested length. However, the ratio for 3B-25 is close to 1.0 and within the 3% error used during the finite element parametric study. This phenomenon is further discussed in Section 4.4.6. The 310 mm deep (4B) specimens behaved as expected and exhibited moment ratios at the weld toe less than 1.0. As such, we can conclude that the critical length of the 4B specimens is shorter than the tested length.

4.3.3 Shear Load Eccentricity

The bolt group shear load eccentricity is the distance from the centre of the bolt group to the point of inflection and its variation was monitored during each test. The bolt group shear load eccentricity (e_b) was calculated similarly to the method used by Salem et al. (2016), as follows:

$$e_b = e_g - \frac{M_S}{V} \qquad\qquad 4\text{-}2$$

where e_g is the geometric eccentricity, M_S is the moment at the weld toe, and V is the sum of the vertical load components measured for all actuators. Figure 4-10 shows that initially, the eccentricity ratio is negative, which indicates that the point of inflection was not along the plate, but in the loading beam span. The point of inflection then moved towards the support creating a positive eccentricity ratio. It gradually increased until the ultimate shear capacity was reached, and then the value remained approximately constant until failure. This plateau was only observed for the specimens tested without horizontal load; the eccentricity ratio for these other specimens increased until failure.

The eccentricity ratio at failure for each test is recorded in Table 4-4. It was observed that the eccentricity ratio at failure is not dependent on the depth of the section, but is heavily influenced by the addition and level of horizontal loading. As the compression increased,

so too did the eccentricity ratio at failure. Specimen 3B-25 has an eccentricity ratio of 1.14 at failure, which indicates that the point of inflection had progressed past the support.
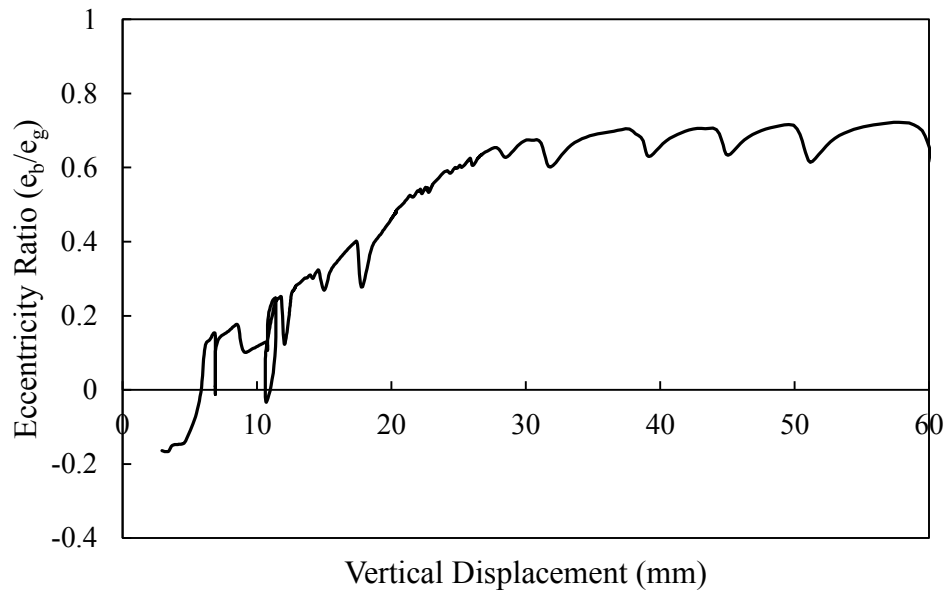

Figure 4-10: Eccentricity ratio variation for specimen 4B-0

4.3.4 Failure Modes

The extended shear tab connection was designed such that the bolts and the weld would not fail during the test. This allowed the specimen to undergo a stability failure, and as such, the only observed failure modes were out-of-plane deformations (OPD) and buckling. Out-of-plane deformations can be distinguished from buckling as they occur gradually as the vertical load is applied. Table 4-5 lists the critical failure mode for each experimental test.

Table 4-5: Failure modes of experimental tests

Specimen ID	Failure Mode
3B-0	OPD
4B-0	OPD
3B-10	Buckling
4B-10	Buckling
3B-25	Buckling
4B-25	Buckling

Out-of-plane deformations were observed in all six tests and began at low levels of vertical displacement. The displacement first occurred at the top of the plate, near the fixed support.

The displacement continued to increase as additional vertical load was applied, but then the behaviour differed depending on the level of compression.

4.3.4.1 Shear and Rotation Only

When no horizontal load is applied to the extended shear tab connection, the governing failure mode is out-of-plane deformation. This is evident in the load–displacement curve, Figure 4-6, as the post-peak behaviour shows a gradually decreasing slope, indicating that failure was not sudden. Figure 4-11 shows the deformed shape of specimen 4B-0 from different angles after the test. The whitewash flaked off as the material yielded, showing similar but opposite yield patterns near the bolts and support on the east side (a) and west side (b), respectively. The yielding initiated at the point of maximum out-of-plane displacement at either the top or bottom of the plate, and then moved towards the closest support. The last image, Figure 4-11(c) shows that the deformations resulted in a twist deformation of the plate.

(a)

(b)

(c)
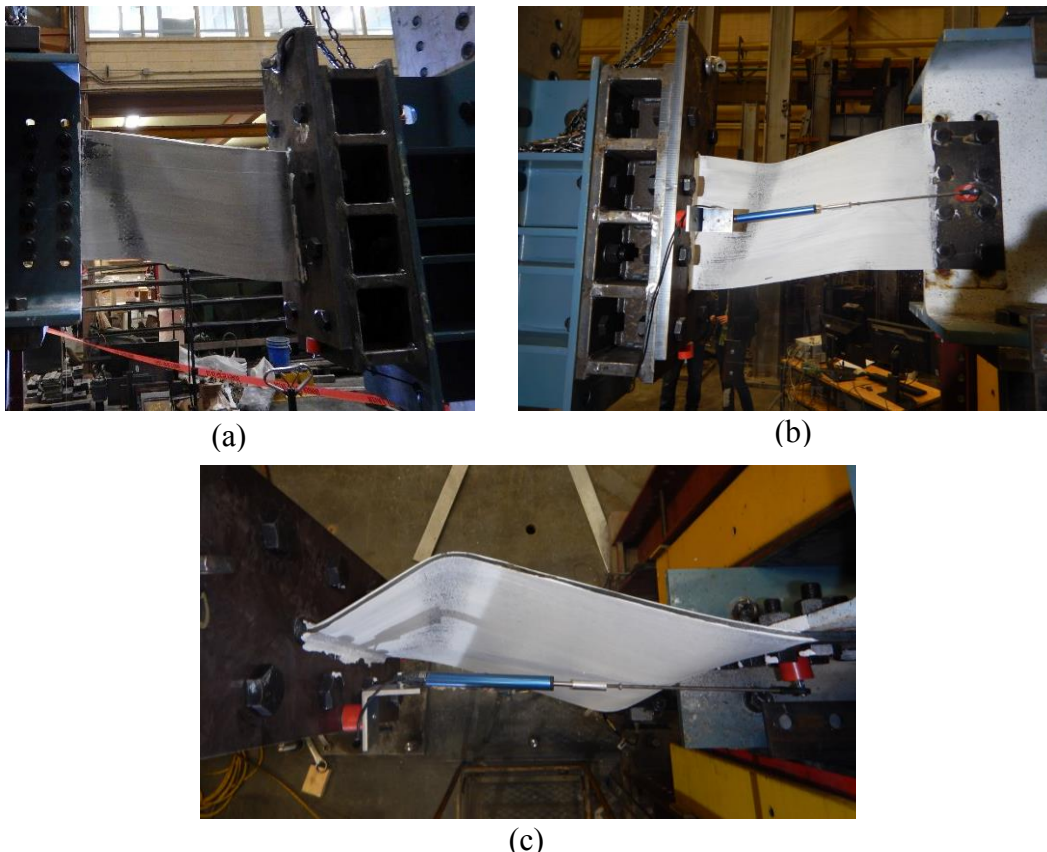
Figure 4-11: Deformed shape of specimen 4B-0, different views:
(a) East side; (b) West side; (c) Top

4.3.4.2 Effects of Axial Compression

Two levels of axial compression were applied to determine its effect on the stability behaviour of extended shear tab connections. The critical failure mode under the combined loading of rotation, shear and compression was buckling. This was characterized by both a decrease in shear capacity, and the inability of the connection to sustain the applied horizontal load. The failure was sudden and caused a large in-plane horizontal displacement of the plate.

The test specimens subjected to 10% of their nominal axial yielding capacity exhibited slightly different behaviour from those subjected to higher loads. Figure 4-12 shows a bottom view of specimen 3B-10 prior to failure. Some twist deformation is visible, and closely resembles the tests that were conducted with no horizontal load. Additionally, the yield pattern, highlighted by flaking of the whitewash, showed yielding near the bolts that was initiated due to out-of-plane displacement at the bottom of the plate. However, the presence of a horizontal compression load caused the plate to buckle and fold along the yield line closest to the support.

Due to the higher level of compression, specimens 3B-25 and 4B-25 did not experience any twist throughout the duration of the test. As previously stated, the plate experienced some out-of-plane displacement near the support early in the test. However, the addition of vertical loading caused the plate to buckle and fail at this location. The failure was sudden, and occurred at such low levels of vertical displacement that load distribution did not have time to occur; therefore, no yielding was observed near the bolt line. Photographs of different views of specimen 4B-25 are shown in Figure 4-13.
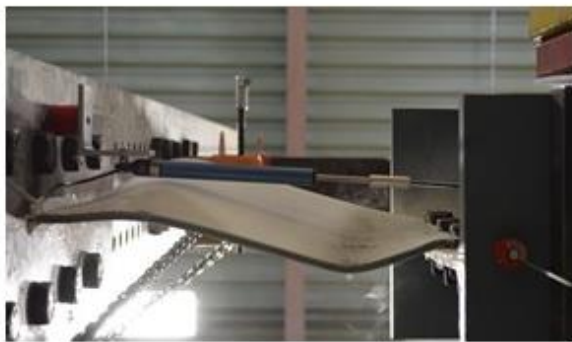
Figure 4-12: Deformed shape of specimen 3B-10, different views:
(a) Bottom view prior to failure; (b) West view after failure

Figure 4-13: Deformed shape of specimen 4B-25 after testing:
(a) East view; (b) Bottom view

4.4 Comparison of Experimental Results with FEA

The results of the full-scale experimental testing program were used to further validate the finite element model described in Chapter 3. The model had previously been validated with full-scale tests where the extended shear tab experienced a strength-governed failure, and was found to be capable of predicting this behaviour. To determine the effectiveness of the existing model in predicting a stability failure, a new analysis was conducted with the

geometry, material properties, and loading conditions of the full-scale tests. The following sections compare the results obtained experimentally in the laboratory, and those taken from an equivalent finite element analysis conducted in Abaqus.

Load–displacement curves, bending moment variation curves and deformed shapes are used to compare the results. These are the main indicators of behaviour, and provide both quantitative and qualitative comparisons.

4.4.1   Material Properties in Model

Engineering stress–strain curves were obtained for the tested plate based on five tension coupon tests, as described in Section 4.2.2. In order to use these results in Abaqus, an approximate static tri-linear curve was created, and is depicted in Figure 4-14. The first highlighted point on the curve was obtained by averaging the values of static yield stress and strain hardening strain; the second was similarly calculated with averaged ultimate static stress and ultimate strain. This curve was then converted to true stress–strain as it is the required format for input into the Abaqus program.
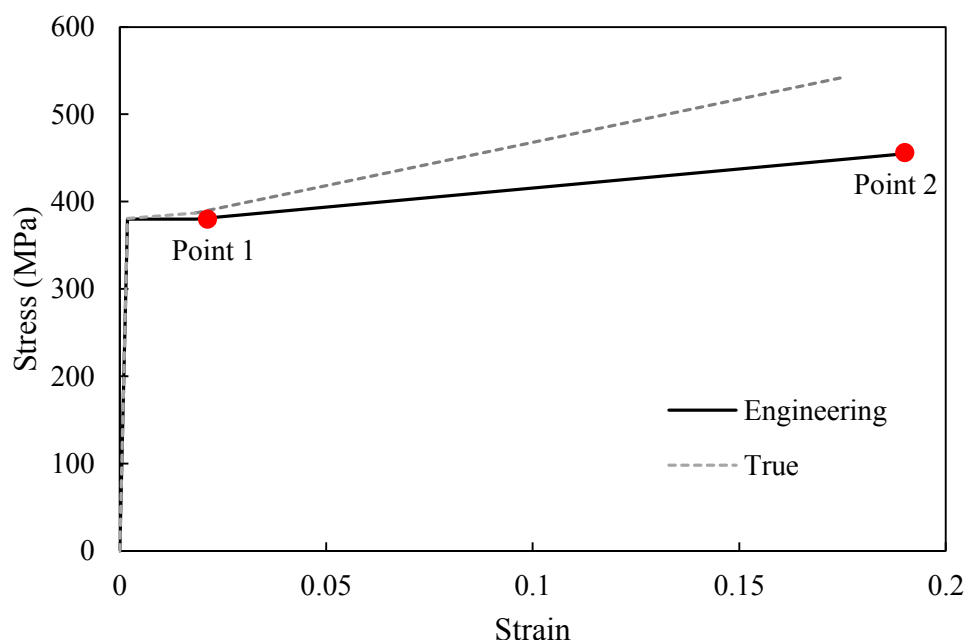
Figure 4-14: Tri-linear static stress–strain curves

4.4.2 Connection Capacity

Connection capacities for both the experimental and numerical tests were derived using load–displacement curves, and are listed in Table 4-6. Generally, the finite element analysis predicts a higher ultimate capacity than what was observed in the lab, and a slightly lower capacity at the first peak. The differences are more pronounced at higher levels of horizontal load, evidenced by the percent difference of 16.5% at the ultimate capacity for specimen 3B-25.

Table 4-6: Comparison of connection shear capacities

Specimen ID	Experimental Tests		Finite Element Analysis	
	Capacity at First Peak (kN)	Ultimate Capacity (kN)	Capacity at First Peak (kN)	Ultimate Capacity (kN)
3B-0	83.9	102.6	82.6	111.8
4B-0	119.2	159.1	121.6	172.5
3B-10	102.6	120.2	91.1	122.3
4B-10	141.2	175.6	136.0	190.2
3B-25	108.4	108.4	98.8	126.3
4B-25	185.7	185.7	151.6	181.6

Load–displacement curves comparing the models with the experimental test results are depicted in Figure 4-15 to Figure 4-20. The overall shape of the experimental and finite element load–displacement curves is very similar. Both curves exhibit an initial peak at a low level of displacement, and a subsequent decrease due to load redistribution. The ultimate peak also occurs at approximately the same vertical displacement, with the exception of tests 3B-0 and 4B-25.

It is evident that the stiffness is adequately captured by the numerical model in the initial elastic portion, as the slopes are almost parallel. Again, the exception to this is specimen 4B-25, shown in Figure 4-20, where the experimental test has a much softer slope in the elastic portion. As this behaviour is very different from the other specimens, which closely matched the finite element curves, further investigation was carried out. The stop motion video footage was reviewed, and showed that the reaction column moved in-plane during the application of the horizontal load, and this was reinforced using data from the LVDT.

Once the vertical load application began, the reaction column moved out-of-plane and twisted, creating a more flexible support condition. Therefore, it was concluded that the 4B-25 experimental test is not representative of an extended shear tab connection with a fixed boundary condition.
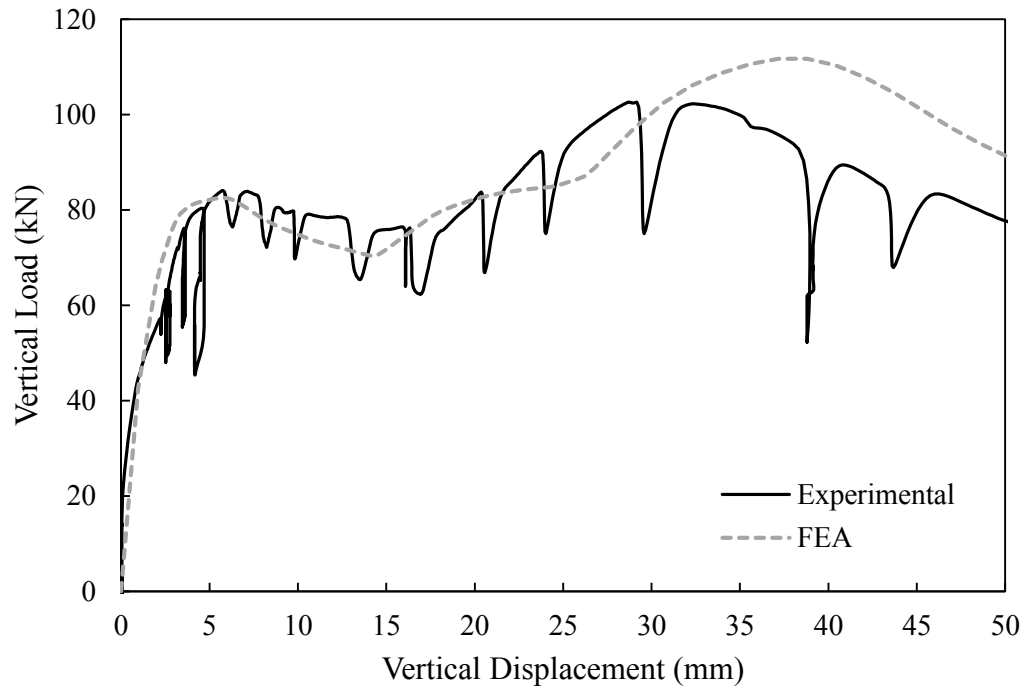

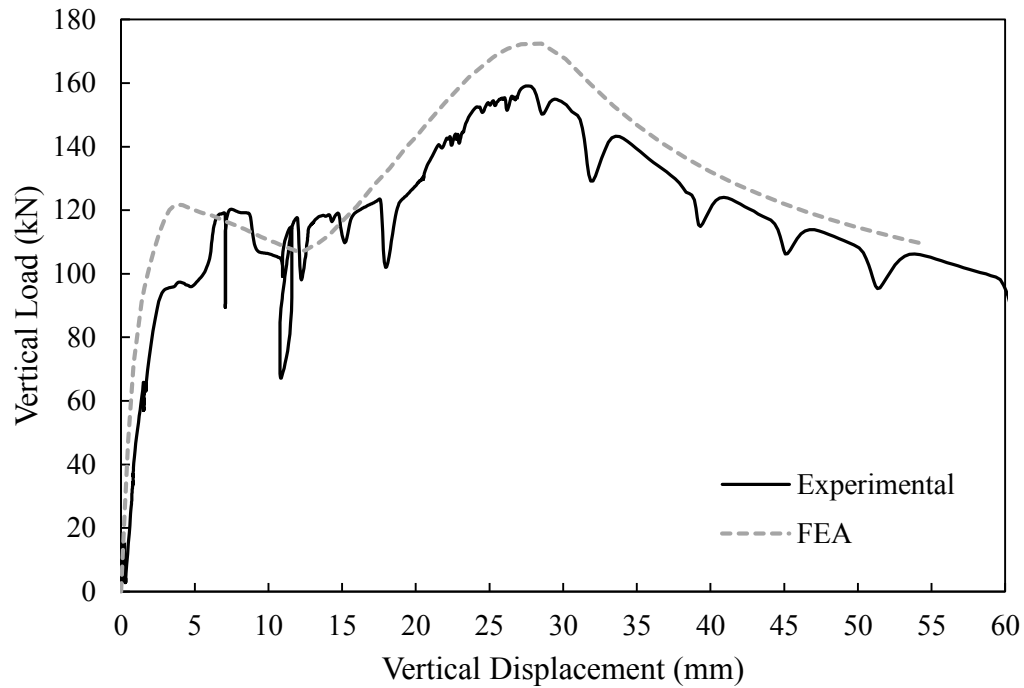Figure 4-15: Comparison of numerical and experimental test results for specimen 3B-0

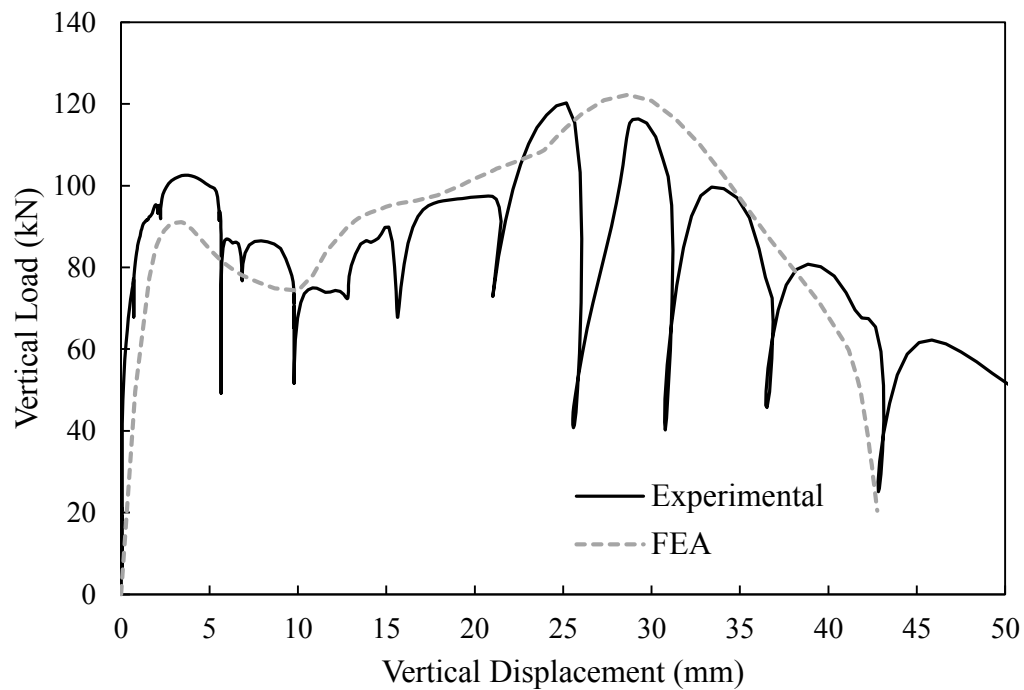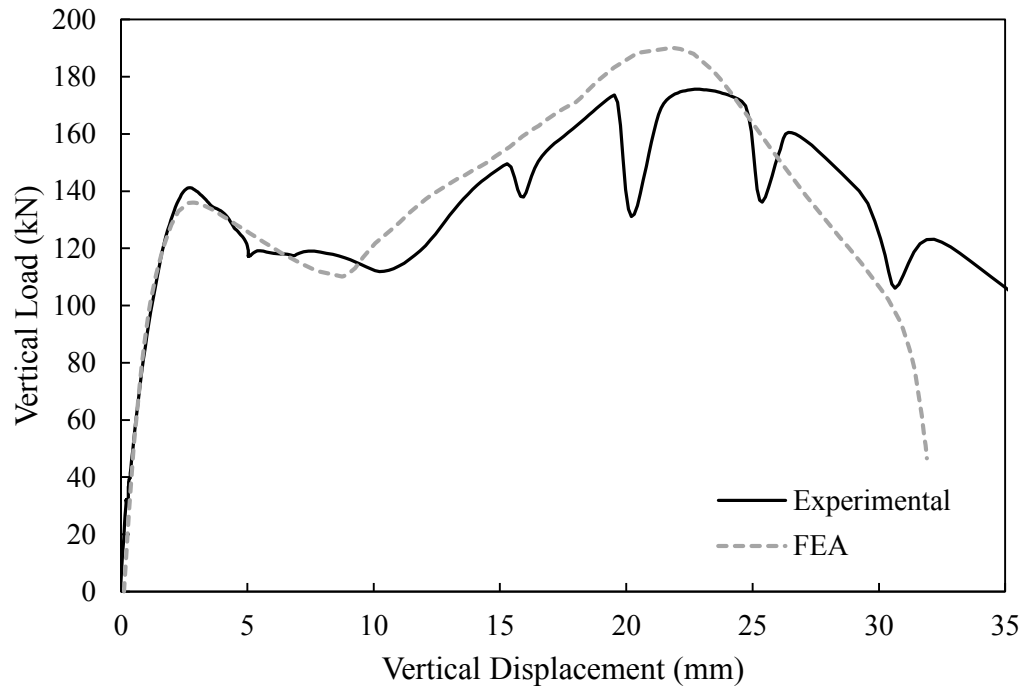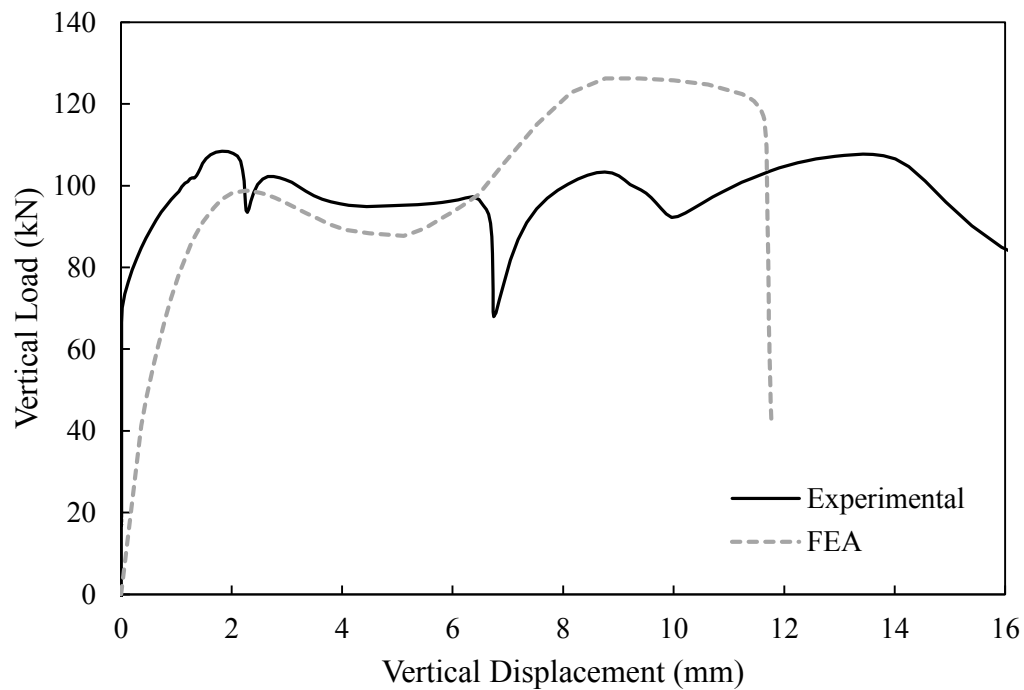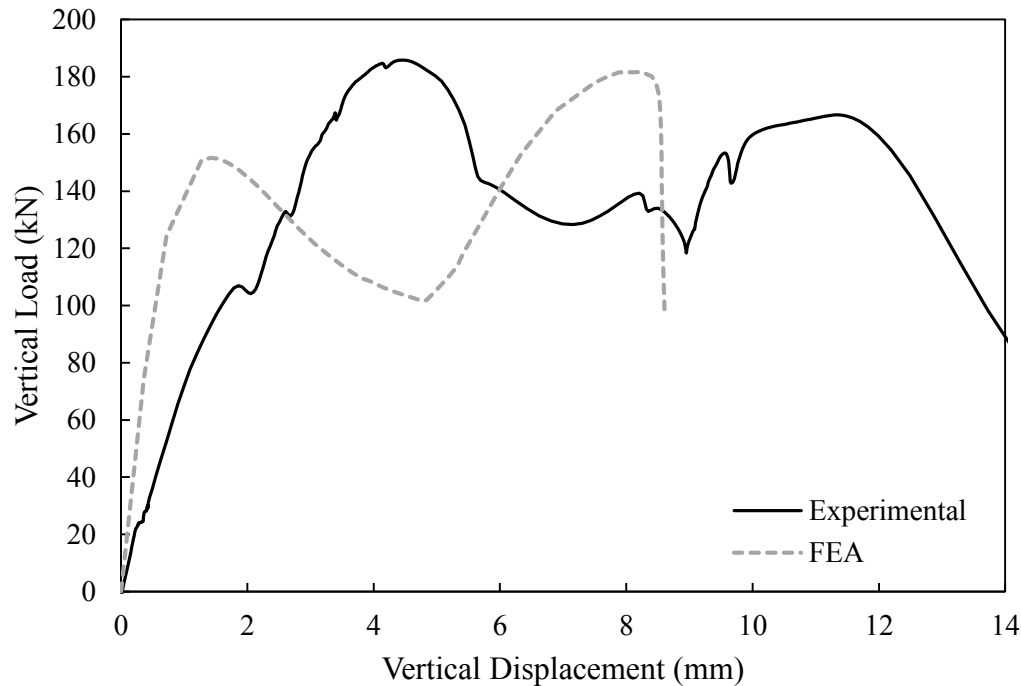Figure 4-16: Comparison of numerical and experimental test results for specimen 4B-0

Figure 4-17: Comparison of numerical and experimental test results for specimen 3B-10

Figure 4-18: Comparison of numerical and experimental tests results for specimen 4B-10

Figure 4-19: Comparison of numerical and experimental test results for specimen 3B-25

Figure 4-20: Comparison of numerical and experimental test results for specimen 4B-25

4.4.3 Bending Moment Distribution

The maximum bending moment ratios at the weld toe from the finite element models are compared to those of the experimental results in Table 4-7. The finite element analysis produced a higher bending moment ratio at the weld toe for all specimens, with the exception of 4B-25. This reinforces the earlier conclusion that the experimental test for this specimen was not representative of the conditions of this study; since the support was more flexible, it contributed to resisting the moment at this location. Generally, the percent error decreases with the addition of horizontal load, as more of the plastic capacity is utilized to resist the axial compression. There is a large discrepancy between the bending moment ratios for the 3B-0, 4B-0, and 3B-10 specimens, and the cause of this will be discussed in Section 4.4.6.

Figure 4-21 presents a comparison between the bending moment ratio at both the weld toe and bolt line for specimen 4B-10. There is good correlation at the weld toe, and the post-peak curves have a similar slope. At the bolt line, the shape of the finite element and experimental curves resemble one another, but the peak moment at the bolt line is

under-predicted by the model. This relationship is representative of all other test comparisons, and these graphs are included in Appendix D.

Table 4-7: Comparison of peak $M/M_{p(reduced)}$ at the weld toe

Specimen ID	Experimental Tests	Finite Element	% Error
3B-0	0.939	1.061	13.0 %
4B-0	0.797	0.899	12.8 %
3B-10	0.956	1.036	8.4 %
4B-10	0.884	0.893	1.0 %
3B-25	0.985	1.003	1.8 %
4B-25	0.938	0.900	4.1 %
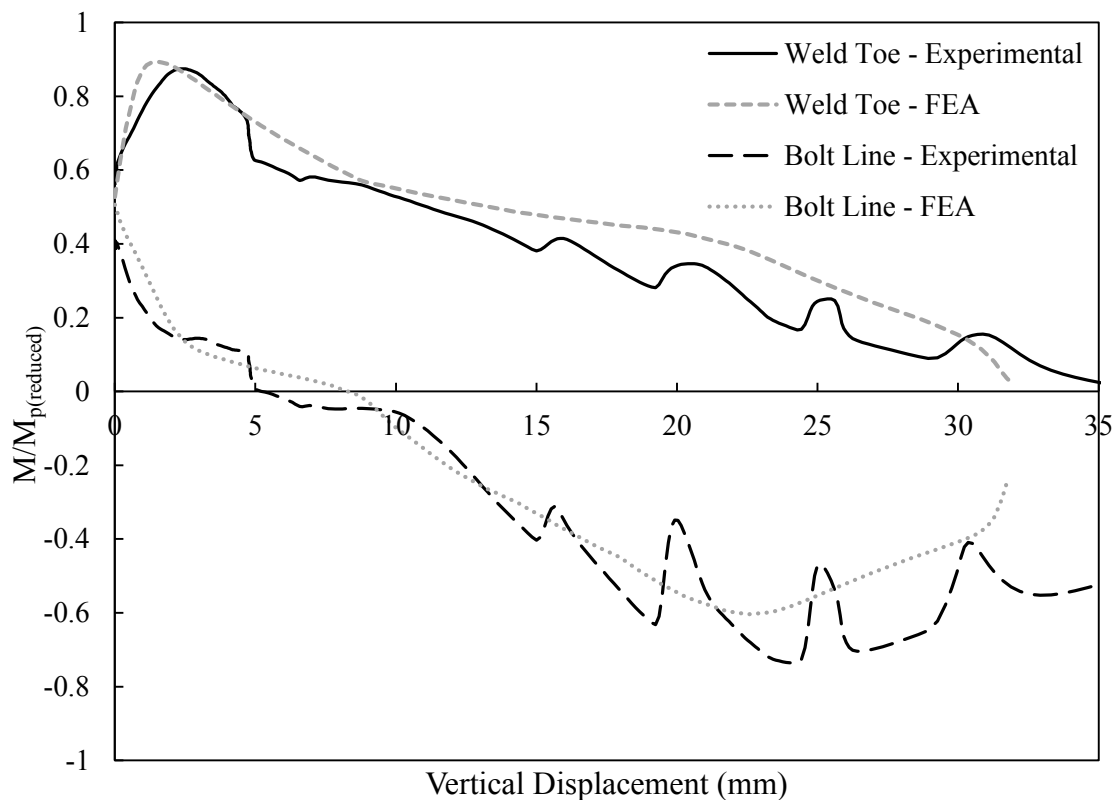
Figure 4-21: Bending moment variation of specimen 4B-10

The bending moment at the bolt line, for the entire section, was extracted from the finite element model using the procedure described in Section 3.4.3. As an additional comparison, the moment was also calculated using Equation 4-1, and the moment curves

produced from both methods are depicted in Figure 4-22. The curves are almost coincident, and as Equation 4-1 is derived based on statics, this gives added confidence in the model.
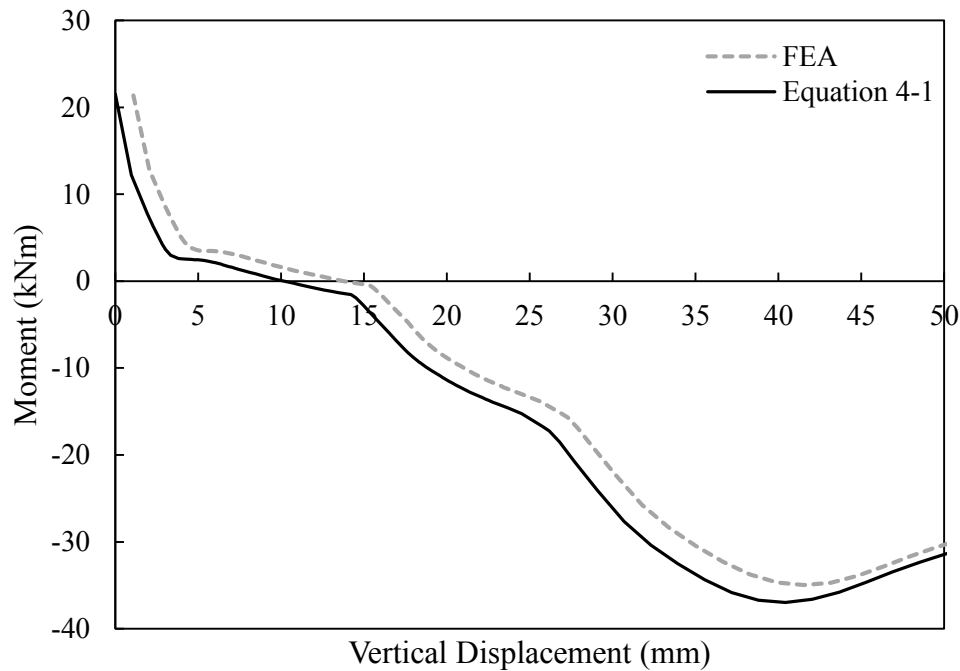
Figure 4-22: Comparison of calculation methods for the bending moment at the bolt line

4.4.4 Shear Load Eccentricity

The value of the bolt group shear load eccentricity obtained numerically at failure was compared to that from the experimental tests to examine how adept the model is at predicting this important design parameter. Table 4-8 lists the eccentricity ratios at failure for both the experimental and finite element tests. The finite element analysis consistently under-predicts the eccentricity ratio at failure, and shows little effect due to the addition of axial compression. This is expected, as the finite element analysis predicts a higher shear capacity and a higher value of bending moment at the support as compared to the experimental tests. Due to the form of Equation 4-2, this results in a lower eccentricity ratio, since the geometric eccentricity is constant.

Table 4-8: Bolt group shear load eccentricity ratio at failure

Specimen ID	Experimental Tests	Finite Element
3B-0	0.63	0.56
4B-0	0.65	0.55
3B-10	0.84	0.63
4B-10	0.81	0.62
3B-25	1.14	0.56
4B-25	0.98	0.64

4.4.5 Failure Modes and Deformed Shape

In addition to the quantitative comparisons presented, a qualitative comparison was also made. The failure mode of the modelled specimens was determined as per Section 3.4.4 and produced matching results to the experimental test. The specimens tested under shear and rotation only, failed due to excessive out-of-plane deformations, whereas the addition of a horizontal compression load caused a sudden buckling failure. The deformed shapes were compared and different views and specimens are presented in Figure 4-23. Yielding patterns in the finite element model were visualized using the equivalent plastic strain (PEEQ in Abaqus) distribution. It is evident that the finite element model was able to accurately replicate the deformed shape, as well as the yielding patterns.

A top view of specimen 3B-0 is shown in Figure 4-24. Although, the deformed shape is the same, the displacements occurred in opposite directions. This highlights the uncertainties of predicting stability failures.
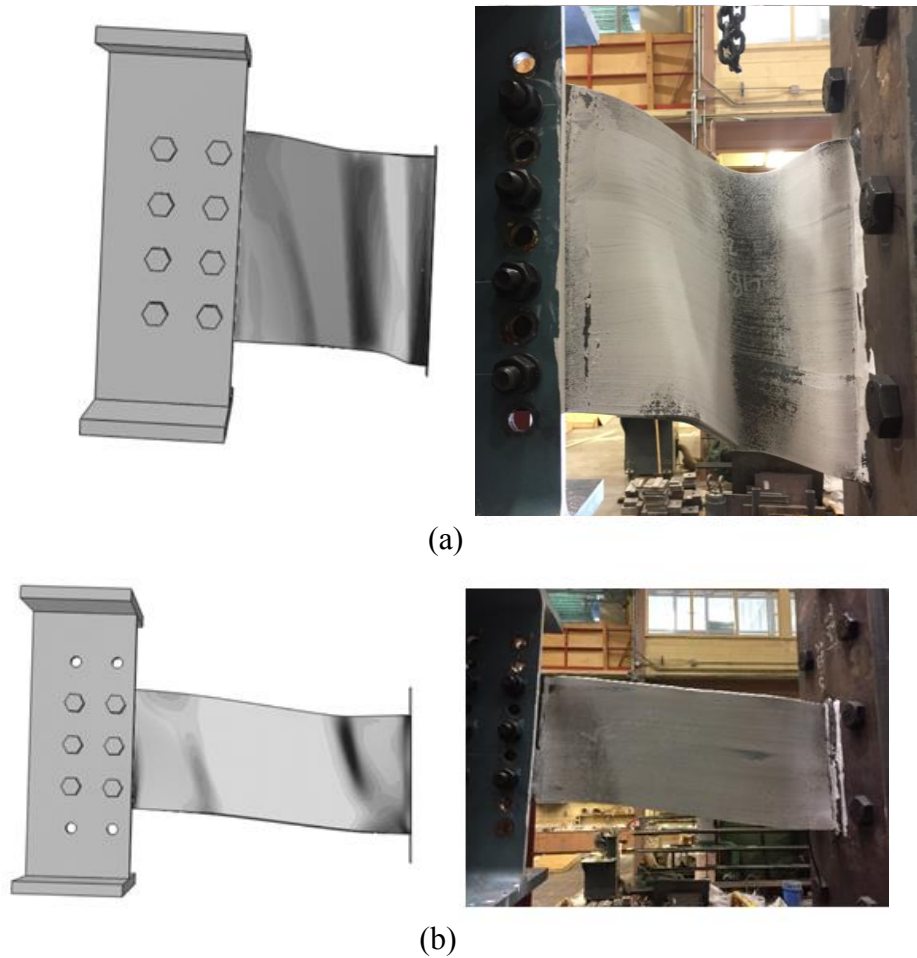
(a)

(b)

Figure 4-23: Qualitative comparison of numerical and experimental test specimens:
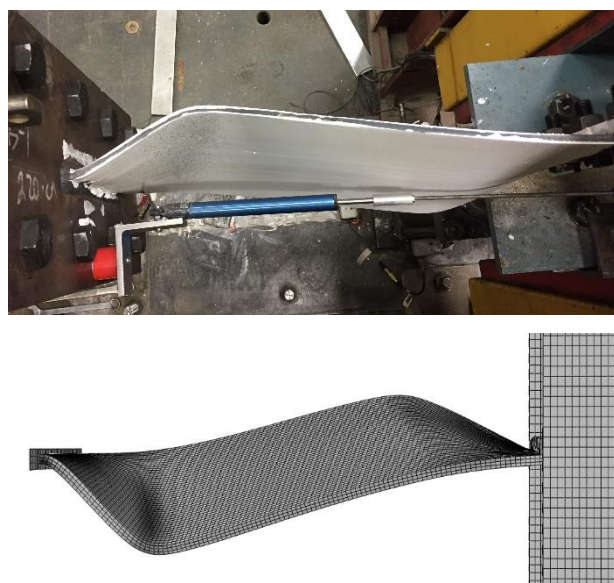(a) Specimen 4B-10; (b) Specimen 3B-0

Figure 4-24: Top view of specimen 3B-0

4.4.6 Initial Imperfections

In part to investigate the reason for the numerical models over-predicting the support moment ratios at the first peak in the vertical load–displacement response, an analysis was carried out to determine the sensitivity of extended shear tab connections to initial imperfections. Two types of imperfection were observed during the laboratory testing program: an initial misalignment of the column, and an initial skew caused by the extended shear tab not being welded perpendicular to the support plate. The misalignment imperfection is an issue that could arise during construction. In the set-up, the reaction column was placed approximately 5 mm too far east, as per Figure 4-25. This caused the plate to bear on the web of the loading beam and induced initial stresses in the plate. This imperfection only affected the 3B-0 and 4B-0 specimens as the set-up was modified for the shorter plates. The second imperfection was measured in the laboratory by using a carpenter's square, flush with the support plate, as illustrated in Figure 4-26. The maximum angle of skew observed was approximately 0.6 degrees in specimen 3B-10.
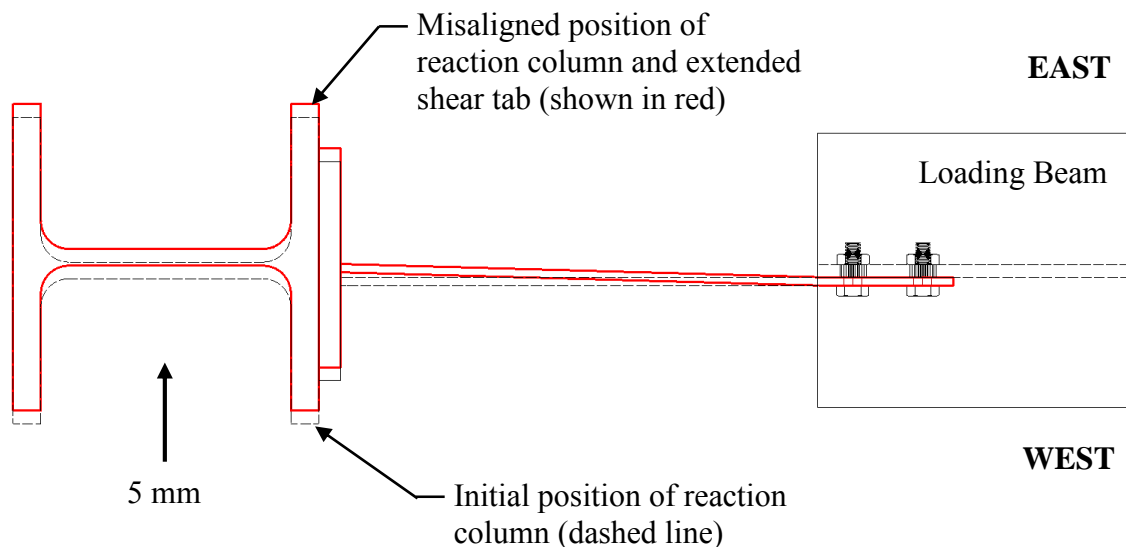

Figure 4-25: Schematic view of initial misalignment (3B-0 and 4B-0)

Figure 4-26: Initial skew of extended shear tab specimen (4B-0)

The misalignment imperfection was added to the finite element model for specimens 3B-0 and 4B-0, as this is consistent with the conditions during testing. Since the second imperfection was observed on multiple specimens, only the 3B-10 model was modified to save on computational effort. A comparison of the results is presented in Table 4-9.

Table 4-9: Comparison of results with initial imperfections

Specimen ID	Capacity at First Peak (kN)		Ultimate Capacity (kN)		Maximum $M/M_{p(reduced)}$	
	Exp.	FEA	Exp.	FEA	Exp.	FEA
3B-0[*]	83.9	80.0	102.6	102.9	0.939	1.030
4B-0[*]	119.2	120.5	159.1	160.7	0.797	0.923
3B-10[†]	102.6	88.2	120.2	118.9	0.956	0.995

[*] Misalignment imperfection
[†] Skew imperfection

The inclusion of the initial imperfections reduces the capacity at the first peak only slightly, but allows the finite element model to predict the ultimate capacity with high accuracy. This is shown in the load–displacement curves in Figure 4-28 to Figure 4-29. The graph also includes a curve for the geometrically perfect finite element model to show the improvement that was attained with the addition of initial imperfections. The improvement was most apparent for specimen 3B-0, where the percent error on the ultimate capacity decreased from 8.97% to 0.29%. Specimens 4B-0 and 3B-10 were similarly reduced to have approximately a 1.0% error on the ultimate shear capacity.

The initial imperfections also had the effect of reducing the bending moment ratio at the weld toe for specimens 3B-0 and 3B-10. The percent error decreased from 13.0% and 8.4% to 9.7% and 4.1%, respectively, and the moment ratio for specimen 3B-10 was reduced to less than 1.0. Therefore, it can be concluded that the reason the shallow, 3B, specimens in the experimental testing program did not reach a bending moment ratio of 1.0 at the weld toe, is mainly due to initial imperfections. The changes in both ultimate capacity and bending moment ratio indicate that extended shear tab connections are sensitive to initial imperfections. As these imperfections reduce the moment ratio, they also have an effect on the critical length for any given geometry and this is discussed in Chapter 5.
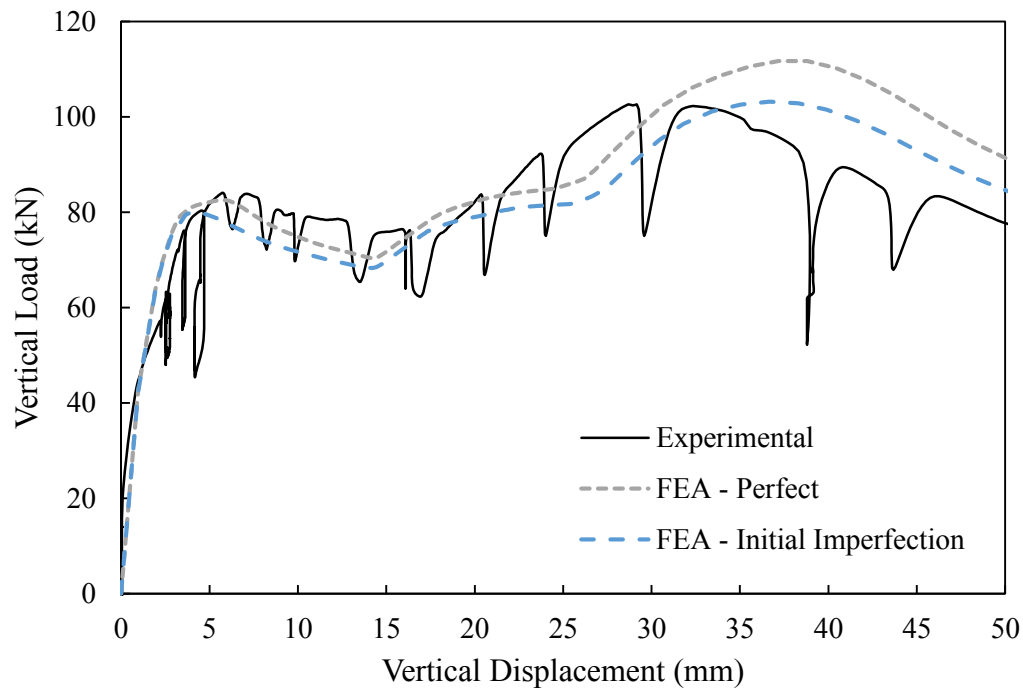
Figure 4-27: Influence of initial misalignment for specimen 3B-0
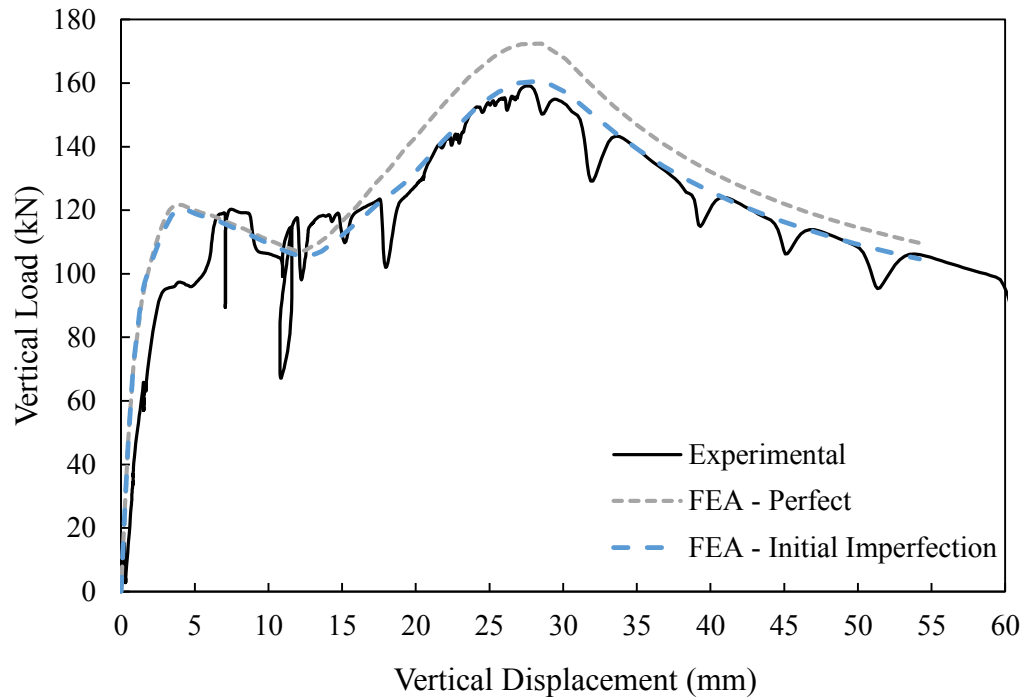
Figure 4-28: Influence of initial misalignment for specimen 4B-0
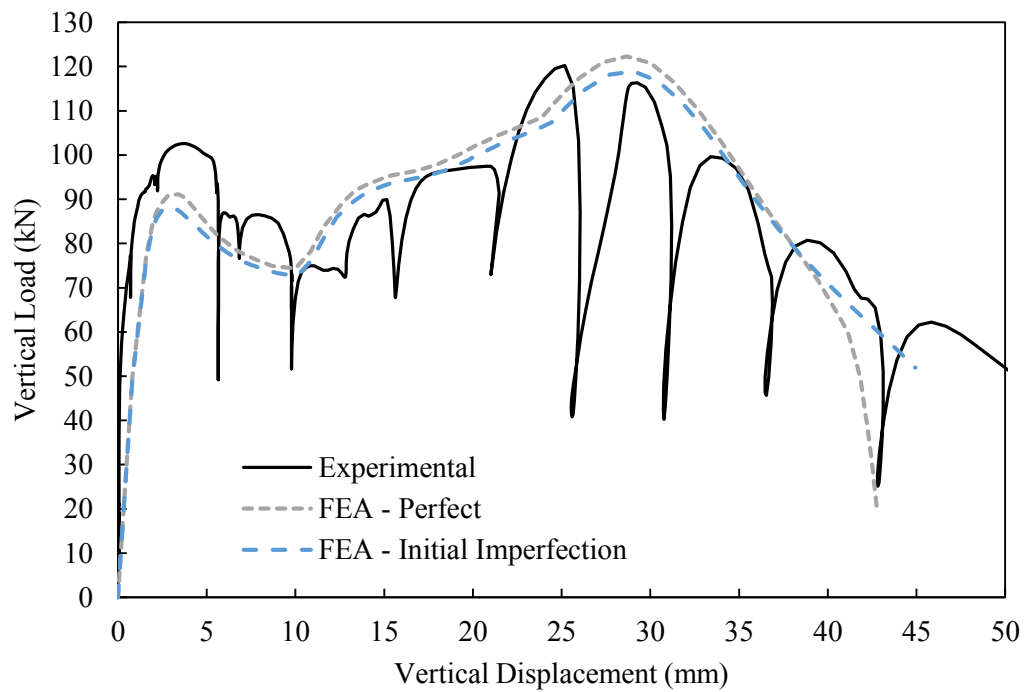
Figure 4-29: Influence of initial misalignment for specimen 3B-10

4.5 Summary

A full-scale experimental testing program was conducted on six extended shear tab specimens that varied in plate depth, plate length, and level of axial compression. The plates were tested using an existing set-up that was modified to accommodate the longer plate lengths tested in this study. The plates were subjected to a combination of rotation, horizontal loading, and vertical loading.

Load–displacement and bending moment ratio–displacement curves were produced for each test, and used to determine the capacity and failure mode of the connection. The curves for all tests exhibited two peaks; however, the second peak did not always correspond to the ultimate capacity. The bending moment for all tests never exceeded the plate plastic moment capacity, but was governed by bending at the weld toe. The tests with no applied horizontal compression load failed due to excessive out-of-plane deformations, whereas the specimens with horizontal load buckled.

The full-scale tests were compared to finite element models having the same measured material properties and geometry. The comparison showed that the finite element model consistently over-predicted both the ultimate capacity and bending moment of the specimen. However, it was able to correctly predict the deformed shape and failure modes observed in the laboratory. The inclusion of initial imperfections improved the accuracy of the finite element model. This indicates that extended shear tab connections, and thus their critical length, are sensitive to these common fabrication and erection imperfections.

CHAPTER 5: DISCUSSION AND DESIGN RECOMMENDATIONS

5.1 Introduction

A comprehensive finite element parametric study was completed in order to determine the effect of stability on extended shear tab connections, and the results are presented in Chapter 3. The critical length was obtained for extended shear tab plates with different geometries and levels of axial compression. This chapter discusses the critical length as an important limit, and quantifies the effect of axial compression and initial imperfections. Additionally, a design philosophy regarding the connection shear capacity is presented and discussed with respect to current design methods. Finally, design recommendations for obtaining the critical length of extended shear tab connections are proposed.

5.2 Discussion

5.2.1 Critical Length

The critical length represents the limit between a strength and a stability governed failure. Extended shear tab plates with lengths shorter than this limit will be able to reach their full cross-sectional plastic capacity prior to failure. Therefore, the design recommendations presented in previous studies by Thomas et al. (2014; 2016) and Salem et al. (2016) would be applicable. However, extended shear tabs that exceed the critical length are unable to reach their plastic moment capacity, and so their behaviour is not well understood. As such, the critical length is an important parameter in the design of extended shear tab connections.

The critical length was obtained as described in Section 3.4.3 for 26 models with varying plate depth, plate thickness and level of axial compression. As previously stated, the critical length was taken as the length where the combination of stresses resulted in a value of Neal's equation (Equation 2-5) close to 1.0, at either the support or first vertical bolt line. In this study, the critical length was always governed by plasticity at the support, due to its high rotational stiffness.

In order to develop an equation to predict the critical length for different geometries, the failure mode of the connections was investigated. As described in Section 3.4.4, extended

shear tab connections that were analyzed with no applied horizontal load failed due to excessive out-of-plane deformations, which are similar to those displayed during classic lateral–torsional buckling. The critical moment causing lateral–torsional buckling of extended shear tab plates, similar to that for main structural flexural members with C_w taken as zero, is as follows:

$$M_{cr} = \frac{\omega_2 \pi}{L_b} \sqrt{EI_y GJ} \qquad \text{5-1}$$

where ω_2 is a coefficient to account for the moment gradient along the plate, L_b is the unbraced length—measured from the support to the first vertical bolt line—E is the elastic modulus, I_y is the weak-axis moment of inertia of the plate, G is the elastic shear modulus, and J is the St. Venant torsional constant. As the critical length represents the length of plate that is able to reach its full plastic cross-sectional capacity at the support, Equation 5-1 was equated with the plastic moment capacity of the plate, M_p, given in Equation 5-2. Additionally, the ω_2 coefficient was calculated using the actual moment distribution obtained from Abaqus and Equation 5-3.

$$M_p = \frac{F_y t d^2}{4} \qquad \text{5-2}$$

$$\omega_2 = 1.75 + 1.05\kappa + 0.3\kappa^2 \leq 2.5 \qquad \text{5-3}$$

In the equations, F_y is the minimum specified yield stress, t is the plate thickness, d is the plate depth, and κ is the ratio of the smaller end moment to the larger, taken as positive for double curvature and negative for single curvature (CSA 2014). Since the critical length is governed by reaching full plasticity at the support early in the analysis, κ is calculated using the moments at this level of vertical displacement, shown by the red line in Figure 5-1.
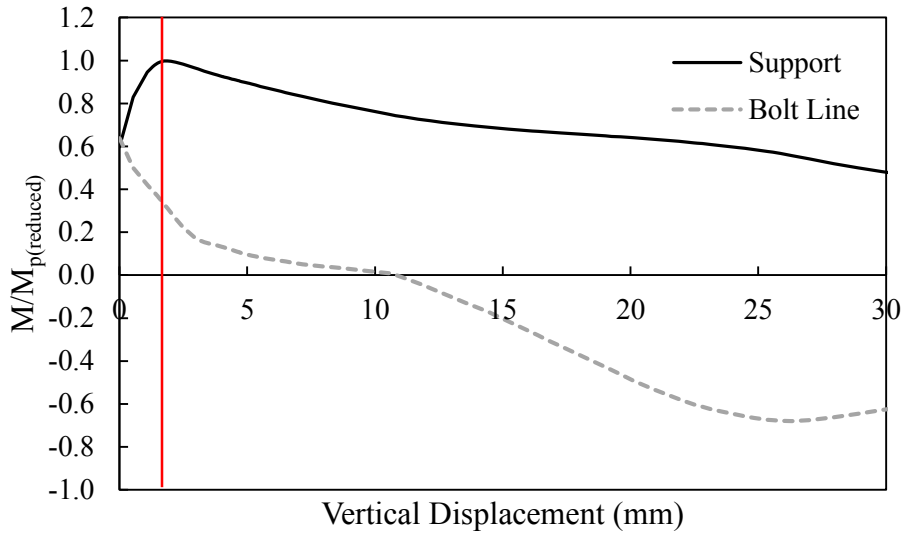
Figure 5-1: Bending moments used in κ calculation for specimen 4B-10-0

The classic lateral–torsional buckling equation is derived assuming that both ends are simply supported about the vertical axis (and torsionally, but any effect of warping is in this case negligible); however, in this study the support boundary condition was fixed against all translations and rotations. End restraint has been shown to significantly affect the lateral–torsional buckling strength, and an effective length concept was proposed by Galambos (1968) to account for various end conditions. For a member with both ends fixed, Galambos (1968) recommends an effective length factor of 0.5, and when one end is simply supported and the other is fixed, this factor becomes 0.7. As previously mentioned, the support in this study was fixed, but the exact fixity of the bolted end condition was not quantified. As such, it was assumed to act as partially fixed, and an effective length factor of 0.65 was chosen. The critical length for extended shear tabs can thus be calculated using Equation 5-4. The equation was used to predict the critical length for all finite element tests with no applied horizontal load, and the analysis-to-predicted ratio is presented in Table 5-1. Included are two additional models with a depth of 390 mm (five horizontal bolt lines) that were analyzed to expand the available data for this discussion.

$$L_{cr} = \frac{\omega_2 \pi}{0.65 M_p} \sqrt{EI_y GJ} \qquad\qquad 5\text{-}4$$

Table 5-1: Critical length predictions

Specimen ID	ω_2	Critical Length, L_{cr} (mm)		Analysis-to-Predicted Ratio
		Analysis (FEA)	Prediction (Equation 5-4)	
2B-6-0	1.786	535	499	1.072
2B-10-0	1.867	1385	1167	1.187
3B-6-0	1.441	285	263	1.086
3B-10-0	1.661	685	677	1.012
3B-13-0	1.777	1435	1295	1.108
4B-6-0	1.322	185	179	1.035
4B-10-0	1.504	485	455	1.066
4B-13-0	1.708	985	923	1.067
5B-10-0	1.411	335	339	0.987
5B-13-0	1.572	685	676	1.014
			Mean	**1.063**
			COV	**0.054**

The mean analysis-to-predicted ratio of 1.063 with a small coefficient of variation indicates that Equation 5-4 is capable of predicting the critical length for extended shear tabs subjected to rotation and shear loading. The critical length equation represents an upper limit on when strength based design methods can be used.

The shortcoming of this equation is that an analytical or experimental moment distribution is required to obtain the value of ω_2. Further investigation revealed that the moment gradient at this level of vertical displacement is bounded approximately by the two cases illustrated in Figure 5-2. In both cases, the moment at the support is larger and has a value close to the plastic moment capacity. Case 1 shows the moment gradient when the moment at the first vertical bolt line is at its minimum value of zero; this is commonly observed in shallow, thick plates. Case 2 applies to deep, thin plates, and represents the maximum moment observed at the first vertical bolt line at this level of vertical displacement.
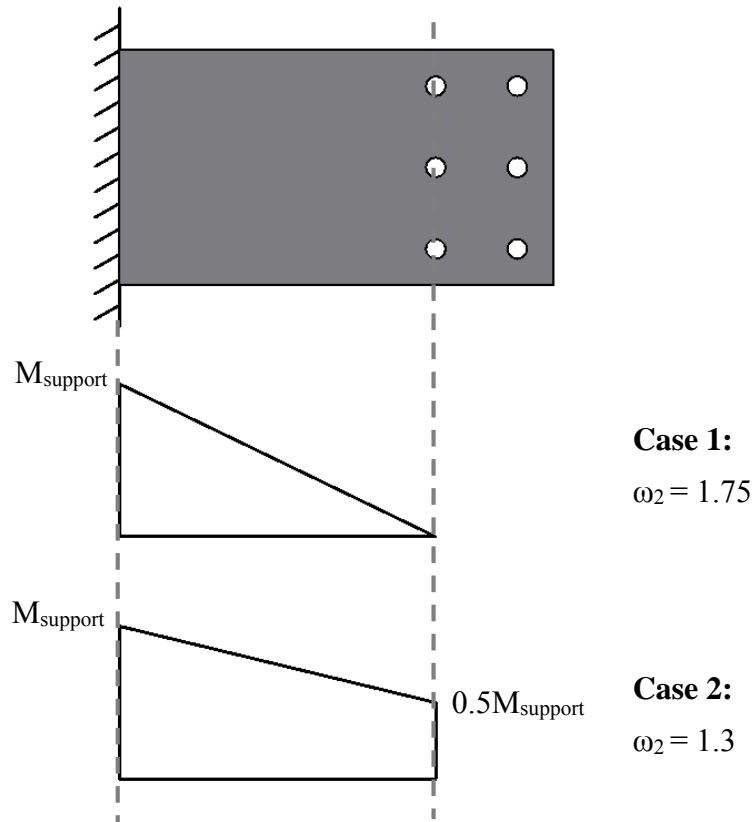
Figure 5-2: Bending moment gradient along plate

As seen in Table 51, the value of ω_2 varies with both plate depth and thickness, and Figure 5-3 shows that this is a linear relationship with minimal deviation. The graph further supports the above conclusions, but also shows that values of ω_2 greater than 1.75 were observed. In these cases, the moment at the first vertical bolt line was small and of the opposite sign to that at the support, and it is conservative to neglect it. This relationship was used to develop Equation 5-5, which gives an estimate of the value of ω_2 when the experimental distribution is unknown. This empirical calculation of ω_2 only slightly impacts the effectiveness of the critical length prediction (Equation 5-4), and results in a mean analysis-to-predicted ratio of 1.072 with a coefficient of variation of 0.076. While Equation 5-5 could be non-conservative for large values of d/t, thicknesses less than the minimum included in this study are rare. However, further confirmation is warranted for extended shear tabs greater than five bolts deep.

$$\omega_2: \ 1.3 \leq 2.1 - 0.017\left(\frac{d}{t}\right) \leq 1.75 \hspace{3cm} \text{5-5}$$
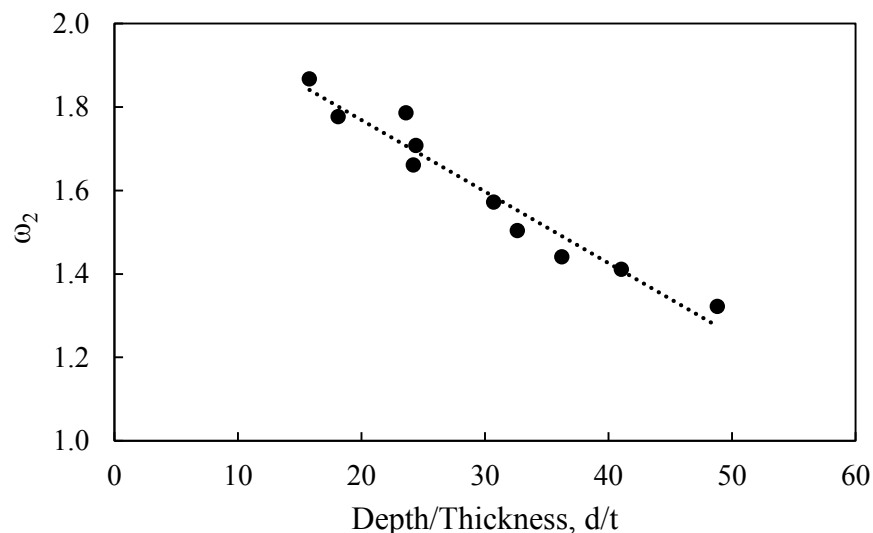
Figure 5-3: Variation of ω_2 with plate-depth-to-thickness ratio

5.2.1.1 Effect of Boundary Condition

Extended shear tab connections can have a range of in-plane rotational boundary conditions depending on their application. To determine if the critical length is affected by the stiffness of the boundary condition, finite element tests conducted by Salem et al. (2016) were analyzed. Extended shear tab connections with a flexible support, which was characterized by a 700×180×11 mm plate fixed only at its perimeter, were investigated (Salem et al. 2016) and three specimens underwent a shear tab plate failure (rather than in the bolts or the weld). These tests were used to determine the effect of support stiffness on the critical length, as the failure mode was identical.

The decreased stiffness of a rotationally flexible support mainly affects the moment gradient along the plate, i.e., the ω_2 coefficient. Similar to the cases with a stiff support, the moment gradients along plates near their critical length were analyzed at a vertical displacement corresponding to the first peak on the load–displacement curve. At this low displacement, the plate is always in single curvature and the value of ω_2 is as presented in Figure 5-4. The relationship between ω_2 and the ratio of depth-to-thickness remained linear; however, the flexible boundary condition produced a smaller slope. As the depth-to-thickness ratio increases from the minimum value in the study, connections with a flexible support have an increasingly larger ω_2 coefficient as compared to a plate with identical geometry and a fixed support. Based on the form of Equation 5-4, this indicates that the

critical length of extended shear tab plates with a flexible support will be greater than those with a fixed support and Equation 5-5 is conservative.
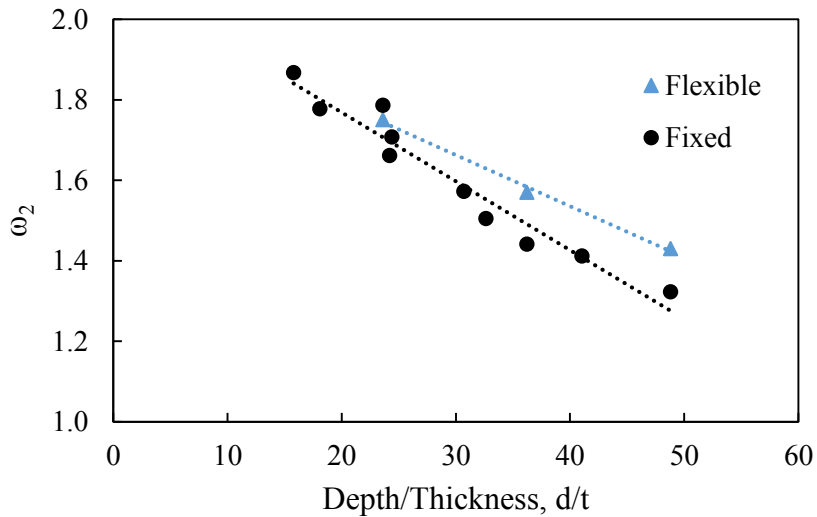
Figure 5-4: Comparison of ω_2 for fixed and flexible boundary conditions

With a flexible boundary condition, a relatively low moment is resisted at the support; this causes a significant shear load eccentricity on the bolt group (Salem et al. 2016). Therefore, the behaviour of the connection tends to be governed by plate strength at the bolt line rather than at the support. As described in Section 3.4.1, the peak moment at the first vertical bolt line occurs at the same vertical displacement as the ultimate shear capacity. The moment gradient was also investigated at this level of vertical displacement, and it was determined that in all cases the plate is in double curvature and the ω_2 coefficient is equal to 2.5 (Equation 5-3). This value is greater than those presented in Figure 5-4, and thus Equation 5-5 is again conservative for determining the critical length of extended shear tab connections with flexible supports.

5.2.1.2 Effect of Axial Compression

Discussion in the previous sections focused on predicting the critical length for extended shear tab connections with no axial loading. Equation 5-4 was developed due to the similarity between lateral–torsional buckling and the observed failure mode of out-of-plane deformations. As part of the parametric study, 18 models were analyzed with an applied horizontal compression load of either 10% or 25% of the plate nominal axial yielding

capacity. These tests also experienced stability failures and, therefore, for simplicity the same critical length equation was used and the axial compression was accounted for using a reduction factor.

To determine the form of this factor, the critical length was predicted as per Equation 5-4, with ω_2 determined using Equation 5-3 with moments obtained from Abaqus, and the analysis-to-predicted ratios were calculated. Figure 5-5 illustrates the relationship between this ratio and the depth-to-thickness ratio of each plate. As expected, the tests with no horizontal load are clustered around 1.0; however, the tests with horizontal compression loading show a linearly increasing trend. These relationships were used to develop Equations 5-6 and 5-7 to account for the presence of axial compression in a simple way when calculating the critical length.
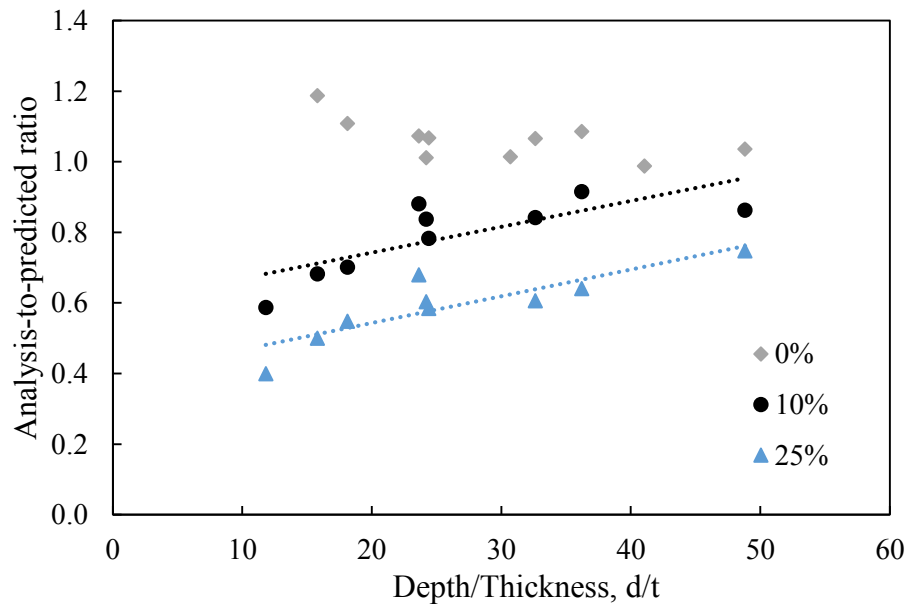
Figure 5-5: Analysis-to-predicted ratio using Equation 5-4 for models with compression

For 10% nominal axial compression: $\psi_{Axial(10\%)} = 0.0073\left(\dfrac{d}{t}\right) + 0.595$ 5-6

For 25% nominal axial compression: $\psi_{Axial(25\%)} = 0.0076\left(\dfrac{d}{t}\right) + 0.391$ 5-7

The original equation to predict critical length, Equation 5-4, was multiplied by the factor [ψ] from Equation 5-6 or 5-7 for models with an applied horizontal load of 10% or 25%,

respectively, of the plate nominal axial yielding capacity. The coefficient ω_2 is calculated based on Equation 5-3 and the analytical moment gradient at the level of vertical displacement corresponding to formation of a plastic hinge at the support. The predicted critical length was then compared to the value obtained from the numerical analysis, and the results are presented in Table 5-2. The average analysis-to-predicted ratio is 1.000, with a coefficient of variation equal to 0.090. The ratios for the shallow, 150 mm deep (2B) specimens have the largest deviation from 1.0, indicating that the efficacy of the equation increases with depth.

Table 5-2: Critical length predictions with axial compression

Specimen ID	ω_2	Critical Length, L_{cr} (mm)		Analysis-to-Predicted Ratio
		Analysis	Prediction	
2B-6-10	1.667	410	357	1.148
2B-6-25	1.501	285	239	1.191
2B-10-10	1.666	710	740	0.960
2B-10-25	1.553	485	496	0.978
2B-13-10	1.732	1135	1318	0.861
2B-13-25	1.703	760	915	0.831
3B-6-10	1.409	235	221	1.065
3B-6-25	1.371	160	166	0.961
3B-10-10	1.568	535	493	1.084
3B-10-25	1.464	360	343	1.049
3B-13-10	1.635	835	867	0.964
3B-13-25	1.527	610	588	1.037
4B-6-10	1.372	160	177	0.907
4B-6-25	1.336	135	138	0.981
4B-10-10	1.512	385	381	1.010
4B-10-25	1.419	260	274	0.948
4B-13-10	1.619	685	677	1.012
4B-13-25	1.457	460	454	1.013
			Mean	**1.000**
			COV	**0.090**

A similar investigation as for the case without axial load was carried out to determine a method of calculating the ω_2 coefficient for connections with axial compression, without any test data. The coefficient was observed to be dependent on the depth-to-thickness ratio, as before, but also the level of axial compression. Figure 5-6 shows that there is an approximately linear relationship between the variables, where the trend line becomes slightly shallower at higher levels of horizontal compression. Due to this phenomenon, two different equations, Equations 5-8 and 5-9, were derived to calculate the ω_2 coefficient at each tested level of horizontal load. It should be noted that the moment gradient coefficient is still bounded by minimum and maximum values of 1.3 and 1.75, respectively. Using this in place of the analytical moment gradient resulted in an average analysis-to-predicted ratio of 1.002, with a coefficient of variation of 0.088. Comparing these to the values in Table 5-2, it was concluded that the ω_2 equations are able to accurately represent the actual moment gradient with a similar accuracy.
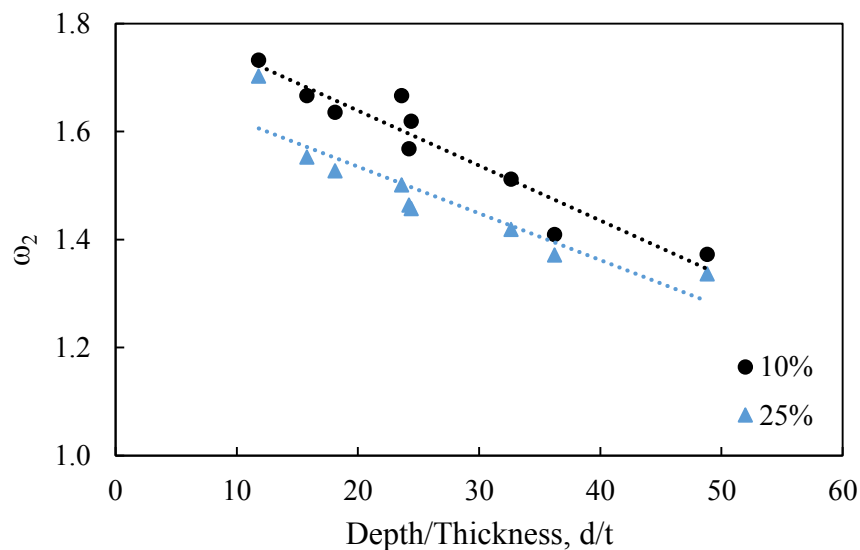
Figure 5-6: Variation of ω_2 with plate-depth-to-thickness ratio at each tested level of horizontal load

For 10% nominal axial compression: $\omega_{2(10\%)} = 1.84 - 0.01\left(\dfrac{d}{t}\right)$ 5-8

For 25% nominal axial compression: $\omega_{2(25\%)} = 1.71 - 0.0086\left(\dfrac{d}{t}\right)$ 5-9

To eliminate the need for individual equations at each level of horizontal load, the influence of this parameter on the ω_2 coefficient was investigated. This would improve the design procedure in terms of simplicity, and eliminate any ambiguity at levels of axial compression that were not directly investigated. It was determined that the horizontal load had less of an effect than the plate depth and thickness and so the variable, x, that best described this behaviour is:

$$x = \left(\frac{d}{t}\right)\left(\frac{P}{P_y}\right)^{0.3} \qquad\qquad 5\text{-}10$$

where P is the applied horizontal compressive load, and P_y is the plate nominal axial yielding capacity. Figure 5-7 plots this variable against the moment gradient coefficient derived using moments obtained from Abaqus, and shows that the data is condensed around a linear trend line. The slope of this line was used to derive Equation 5-11 to calculate the ω_2 coefficient in the presence of axial compression. The average analysis-to-predicted ratio using Equation 5-11 is 1.000 with a coefficient of variation of 0.089. Therefore, it was concluded that this method provides an equally accurate method of calculating the moment gradient coefficient.

$$\omega_2: \ 1.3 \leq 1.78 - 0.016\left(\frac{d}{t}\right)\left(\frac{P}{P_y}\right)^{0.3} \leq 1.75 \qquad\qquad 5\text{-}11$$
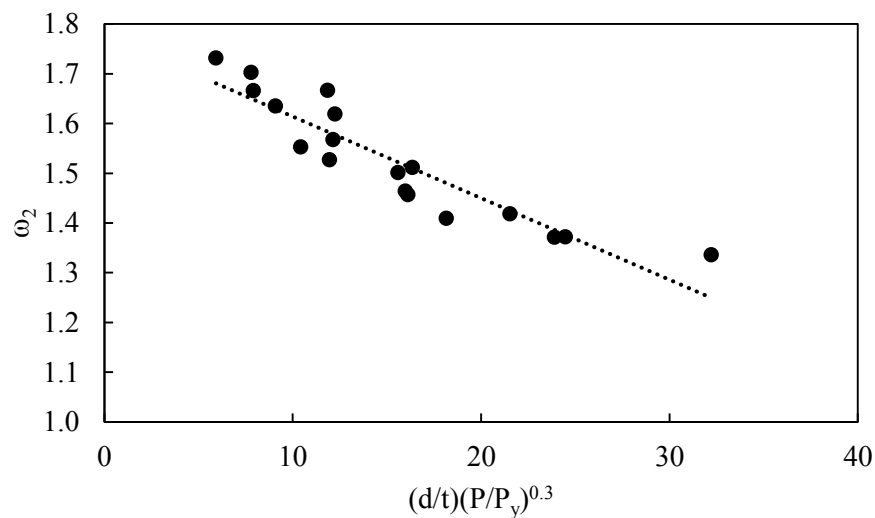
Figure 5-7: Variation of ω_2 with plate depth, thickness and axial compression

5.2.1.3 Initial Imperfections

In Chapter 4, it was noted that extended shear tab connections are sensitive to initial imperfections. Therefore, an investigation was carried out to quantify the effects of an initial misalignment on the critical length. The misalignment imperfection was chosen as it represents a common potential issue during erection of beams with extended shear tab connections. The original model was modified to include an initial misalignment of 5 mm in order to be consistent with the study in Section 4.4.6. The length was then reduced until the combination of stresses at the support resulted in a value of Neal's equation (Equation 2-5) of approximately 1.0. Again, an error on the length of ±3% was accepted, and the new critical lengths for cases without axial load are presented in Table 5-3. The percent reduction between the two critical lengths is reported. It is observed that the imperfection has a larger influence on the critical length for shallow, thick plates. The bending moment ratio for model 4B-6-0 was not altered enough by the imperfection to change the critical length value. This indicates that certain geometries exist where the stress distribution is less susceptible to erection misalignments.

Table 5-3: Critical lengths with misalignment imperfection

Specimen ID	Critical Length, L_{cr} (mm)		% Reduction
	Perfect	With Imperfection	
2B-6-0	535	475	11.2
2B-10-0	1385	1185	14.4
3B-6-0	285	250	12.3
3B-10-0	685	600	12.4
3B-13-0	1435	1285	10.5
4B-6-0	185	185	0
4B-10-0	485	470	3.1
4B-13-0	985	900	8.6

Figure 5-8 was created to develop a factor capable of reducing the critical length prediction for the presence of initial misalignment imperfections. The ratio between the critical length with and without imperfections was calculated and plotted against the depth-to-thickness ratio, which was observed again to be the most influential variable. A fairly linear trend

line was observed, with the imperfections reducing the critical length by a maximum value of approximately 15% for plates with a low depth-to-thickness ratio, and no reduction was needed for those with a high ratio. The trend line resulted in Equation 5-12, representing a reduction factor on the critical length calculated by Equation 5-4.

$$\psi_{II} = 0.0034 \left(\frac{d}{t}\right) + 0.817 \qquad\qquad 5\text{-}12$$
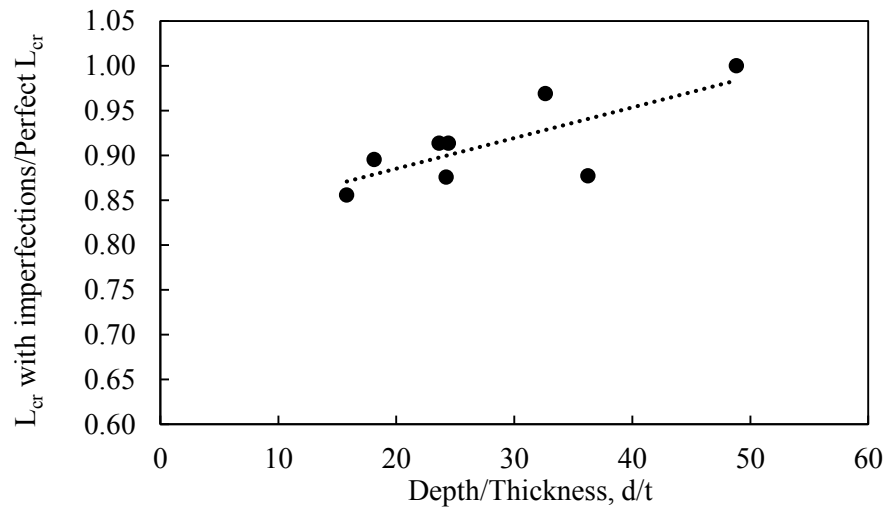
Figure 5-8: Impact of misalignment imperfection with the plate depth and thickness

The predicted critical lengths, accounting for the presence of an initial misalignment imperfection, are listed in Table 5-4. The mean analysis-to-predicted ratio is 1.086 with a coefficient of variation of 0.079. The critical length is under-predicted by the largest amount for the models with the longest lengths, 2B-10-0, 3B-13-0, and 4B-13-0, which means that the imperfection factor is reducing the critical length by more than necessary. This is because the factor is applied as a percentage of the perfect critical length; therefore, a larger initial length results in a larger reduction. However, the factor provides a good overall prediction for the models in this study.

To determine the effect of an initial misalignment imperfection on extended shear tab connections with axial compression, three models were analyzed. New critical lengths were found for the 2B-13-25, 3B-10-25, and 3B-13-25 models, as these depth-to-thickness ratios were seen to be the most affected by imperfections. In all three cases, the bending moment ratio was reduced by less than 1.3%, which is within the ±3% error that was deemed acceptable on the critical length. This could be due to the order of load application, where

the entire horizontal compression load is applied prior to any vertical loading, as well as the form of Neal's equation (Equation 2-5). The majority of the plate's cross-sectional strength is utilized in resisting the bending moment and horizontal load. Once the vertical load is applied, the imperfection causes a small reduction in the resisted shear and moment. This reduction is smaller for models with axial compression because the axial load already causes out-of-plane displacements in the geometrically perfect model, similar to those created by an initial misalignment, suggesting that their effect has already been accounted for. Therefore, it was determined that extended shear tab connections are not sensitive to misalignment imperfections at high levels of axial compression.

Table 5-4: Predicted critical lengths with misalignment imperfection

Specimen ID	Critical Length (mm)		Analysis-to-Predicted Ratio
	Analysis	Predicted	
2B-6-0	475	426	1.116
2B-10-0	1185	953	1.244
3B-6-0	250	254	0.984
3B-10-0	600	619	0.969
3B-13-0	1285	1147	1.120
4B-6-0	185	173	1.071
4B-10-0	470	434	1.084
4B-13-0	900	820	1.098
		Mean	**1.086**
		COV	**0.079**

5.2.2 Shear Capacity

In this section, a philosophy regarding the shear capacity and ductility requirements of extended shear tabs is discussed. This is necessary because a double-peak phenomenon was often observed in the vertical load–displacement curves for plates at the critical length. Additionally, the shear capacities obtained in this study are compared with those obtained by checking the limit state of buckling according to the provisions of both the 14th and 15th editions of the *Steel Construction Manual* (AISC 2011; 2017).

5.2.2.1 Design Philosophy

An example vertical load–displacement curve is provided in Figure 5-9 for the 3B-10-0 model, and all other vertical load–displacement curves are included in Appendix A. Generally, extended shear tab connections are designed to reach their ultimate capacity; however, once the length of the plate is increased, this capacity occurs at very large levels of vertical connection displacement. The magnitude of this displacement varies among models, and can be far from practical for most applications. For example, the ultimate capacity for the 3B-10-0 model occurs at approximately 40 mm of vertical displacement; however, the 2B-10-0 model reaches its ultimate capacity at 95 mm of vertical displacement. Therefore, the designer must ensure that the connection has sufficient ductility to reach the ultimate shear capacity. Also, a small decrease in shear capacity is observed after the first peak, due to load redistribution, and should be accounted for in the design and detailing of the connection.
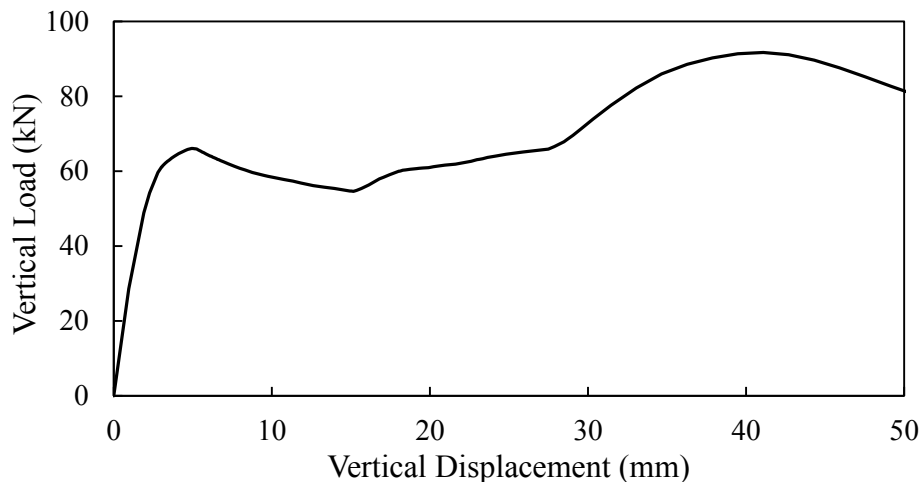
Figure 5-9: Load–displacement response for model 3B-10-0

Conversely, the extended shear tab connection may be designed based on the shear capacity observed at the first peak in the load–displacement curve. Based on 26 models at the critical length in the parametric study, the capacity at the first peak has a mean value of 81% of the corresponding ultimate capacity. This value is dependent on the failure mode; connections that failed due to buckling have a higher average, because the horizontal compression caused failure to occur much sooner, whereas those that failed from out-of-plane deformations were able to reach a higher ultimate capacity. As described in Chapter 3, the

first peak is reached at a much lower vertical connection displacement; therefore, the designer is able to reduce ductility requirements if a lower shear capacity is acceptable.

5.2.2.2 Comparison with Current Design Methods

The design methods for checking stability of extended shear tab connections in the 14th and 15th editions of the *Steel Construction Manual* (AISC 2011; 2017) were evaluated and compared to the capacities obtained from the parametric study. As discussed in Chapter 2, the AISC methods do not account for the application of axial load in the capacity predictions; therefore, they are compared only to the models analyzed without axial compression.

The 14th edition (AISC 2011) uses a slenderness parameter to reduce the yield strength available to resist the shear load, F_{cr}. The shear capacity is then calculated using the following formula:

$$V_n = \frac{F_{cr}Z_x}{e_g} \qquad \text{5-13}$$

where V_n is the nominal shear strength, F_{cr} is the available buckling stress, Z_x is the plastic section modulus, and e_g is the geometric eccentricity. The plastic section modulus is used here since the plastic moment capacity is reached in all models. The shear capacity is predicted using Equations 2-9 to 2-13 and the analysis-to-predicted ratios are listed in Table 5-5.

Table 5-5: Analysis-to-predicted ratios for the 14th edition AISC design method

Specimen ID	Predicted Shear Capacity (kN)	Analysis-to-Predicted Ratios	
		Capacity at First Peak	Ultimate Capacity
2B-6-0	22.9	1.16	1.33
2B-10-0	14.4	1.12	1.39
3B-6-0	82.3	1.01	1.80
3B-10-0	63.3	1.04	1.45
3B-13-0	43.8	1.08	1.30
4B-6-0	219.5	1.05	1.6
4B-10-0	142.6	1.10	1.63
4B-13-0	108.3	1.06	1.35
5B-10-0	307.8	1.11	1.67
5B-13-0	223.4	1.08	1.46
	Mean	**1.08**	**1.50**
	COV	**0.04**	**0.11**

Based on the analysis-to-predicted ratios, it can be concluded that the 14th edition AISC method under-predicts the capacity at both the first peak and the ultimate capacity. However, the predicted capacity at the first peak is much closer to the analysis results and has a smaller coefficient of variation. Finally, the resisting shear was calculated using Equation 2-14 and was found to be less than the shear capacity in all cases; therefore, all models would require stiffeners (stabilizer plates) as per this design method.

A different approach is used in the 15th edition *Steel Construction Manual* (AISC 2017) design method, and it is described in Section 2.3.2. The moment gradient is accounted for using Equation 2-17, which was empirically developed for double-coped beams. In all cases, the nominal predicted flexural strength, M_n, was taken as the plastic moment capacity as per Equation 2-18, and the associated analysis-to-predicted ratios are listed in Table 5-6.

Table 5-6: Analysis-to-predicted ratios for the 15th edition AISC design method

Specimen ID	Predicted Moment Capacity, M_n (kNm)	Predicted Shear Capacity (kN)	Analysis-to-Predicted Ratios	
			Capacity at First Peak	Ultimate Capacity
2B-6-0	13.8	23.9	1.11	1.27
2B-10-0	20.6	14.4	1.12	1.39
3B-6-0	32.3	99.5	0.84	1.49
3B-10-0	48.4	66.7	0.99	1.37
3B-13-0	64.7	43.8	1.08	1.30
4B-6-0	58.7	261.0	0.88	1.36
4B-10-0	87.9	167.4	0.93	1.39
4B-13-0	117.5	114.6	1.00	1.28
5B-10-0	139.1	370.9	0.92	1.38
5B-13-0	185.9	256.4	0.95	1.27
		Mean	**0.98**	**1.35**
		COV	**0.10**	**0.05**

The mean analysis-to-predicted ratio at the first peak is 0.98 with a coefficient of 0.10, indicating that the shear capacity is well predicted. This is expected since the plastic moment is reached at this location, and used to calculate the predicted shear capacity. Similar to Equation 5-13, the full geometric eccentricity, e_g, is used to calculate the predicted shear capacity (for both the first peak and ultimate). This has been proven to be over-conservative and describes why the ultimate shear capacity is under-predicted for all models. The 15th edition S*teel Construction Manual* (AISC 2017) states that "alternative considerations of the design eccentricity are acceptable when justified by rational analysis". Thomas et al. (2014) recommend using an effective eccentricity equal to 75% of the geometric eccentricity to determine the ultimate shear capacity, and Table 5-7 lists the associated predicted ultimate shear capacities. Using the AISC 15th edition methodology with this reduced eccentricity, the mean analysis-to-predicted ratio is 1.01 with a coefficient of variation equal to 0.05, indicating that this effective eccentricity accurately captures the true moment distribution.

Table 5-7: Predicted ultimate shear capacity using the effective eccentricity

Specimen ID	Predicted Ultimate Shear Capacity (kN)	Analysis-to-Predicted Ratio
2B-6-0	31.9	0.95
2B-10-0	19.3	1.04
3B-6-0	132.6	1.12
3B-10-0	89.0	1.03
3B-13-0	58.5	0.98
4B-6-0	348.1	1.02
4B-10-0	223.2	1.04
4B-13-0	152.8	0.96
5B-10-0	494.5	1.04
5B-13-0	341.9	0.95
Mean		**1.01**
COV		**0.05**

5.3 Design Recommendations

Design recommendations for calculating the critical length of extended shear tab connections are proposed in this section. The equations and their derivations were discussed in Section 5.2.1. For extended shear tab connections that are subjected to rotation and shear loading only and excluding any imperfections, Equations 5-4 and 5-5 are recommended for calculating the critical length.

When an axial compressive load is applied, a factor is required to reduce the critical length. Axial zones have been identified based on the levels of axial compression that were considered in this study and the critical length equations are as follows:

Axial compression $\leq 10\%$: $\qquad L_{cr} = \psi_{Axial(10\%)} \dfrac{\omega_{2(10\%)}\pi}{0.65M_p} \sqrt{EI_yGJ}$ $\qquad$ 5-14

$10\% <$ Axial compression $\leq 25\%$: $\quad L_{cr} = \psi_{Axial(25\%)} \dfrac{\omega_{2(25\%)}\pi}{0.65M_p} \sqrt{EI_yGJ}$ $\qquad$ 5-15

where $\psi_{Axial(10\%)}$ and $\psi_{Axial(25\%)}$ are given by Equations 5-6 and 5-7, respectively. Axial loads in excess of 25% of the plate nominal axial yielding capacity are considered unusual and have not been investigated in this study; further research is required to address such cases.

The moment gradient coefficient ω_2 is calculated using Equation 5-8 for any level of axial compression less than or equal to 10%, and using Equation 5-9 for an axial compressive load between 10% and 25% of the plate nominal axial yielding capacity. Alternatively, Equation 5-11 provides a unified value as a function the axial load P.

In order to account for the effect of initial imperfections on the critical length, an additional reduction factor was developed for cases without axial load and is given by Equation 5-12. It was determined that imperfections have a greater effect on the critical length of extended shear tabs tested without axial compression, but it is recommended that the imperfection reduction factor also be applied to Equations 5-14 and 5-15 when axial compression is present, thus providing a conservative prediction of the critical length. For simplicity, a maximum reduction of 0.85 was observed and can be used in place of Equation 5-12.

5.4 Summary

The critical length is an important parameter in the design of extended shear tabs, as it represents the limit between a strength and a stability governed failure. An equation was developed to predict the critical length for plates, both with and without the application of an axial compressive load. The equation is based on the classic lateral–torsional buckling formulation, and includes an effective length factor to account for the fixity of the boundary conditions. The moment gradient at key levels of vertical connection displacement was discussed, and equations to calculate this coefficient in the absence of experimental or analytical results were recommended. Additionally, the effect of imperfections on the critical length was investigated, and a reduction factor to account for this was proposed.

The double-peak behaviour of the vertical load–displacement curves and its impact on connection design was discussed. The connection may be designed for the ultimate shear capacity as long as sufficient measures are in place to ensure that the required ductility is achieved. Conversely, the capacity at the first peak averaged approximately 81% of the ultimate shear capacity in the cases studied, and it occurred at a much lower level of vertical displacement. This allows the connection to be designed with a much smaller ductility requirement.

CHAPTER 6: CONCLUSIONS AND RECOMMENDATIONS

6.1 Summary

Extended shear tab connections are used to transfer shear loads in steel structures and are used extensively due to their low cost and contributions to ease of frame erection. As the plate is longer than in a conventional shear tab configuration, the need to cope the supported beam is eliminated. However, the increased length changes the behaviour of the connection and introduces instability concerns. Additionally, as structures become more complex, so too does the demand on these connections. Designers are increasingly requiring that extended shear tabs resist axial loads, in addition to shear and bending, which introduces more uncertainty with respect to plate stability.

Recent studies conducted at the University of Alberta investigated the strength of extended shear tab connections under combined loading, using both full-scale experimental tests and finite element modelling. These testing programs showed that the plates were able to reach their plastic moment capacity and, therefore, the strength was not hindered by instability. This study aims to determine at what plate length do stability issues arise and govern the behaviour of the connection.

A two-part research program was conducted that consists of a parametric study using the finite element analysis software Abaqus, and a full-scale experimental testing program. In both the numerical and experimental programs, the connection was tested under combined rotation, and horizontal and vertical loading. The parameters investigated in the study were: plate depth, plate thickness, and level of axial compression. A fixed support condition was used for all models and the critical length at the boundary between a strength and stability failure was obtained. The connection behaviour was evaluated using load–displacement curves, bending moment–displacement curves, and the plate deformed shape. Neal's interaction equation (Equation 2-5) was evaluated at both the support and the first vertical bolt line to determine whether the cross-sectional plastic moment capacity had been reached.

The results of the parametric study were used to create a matrix for the full-scale testing program. Six extended shear tab specimens were tested using an existing set-up that was

modified to meet the requirements of this program and accommodate the three different tested lengths. The connections were tested in an inverted manner, therefore with an upwards vertical displacement, to facilitate set-up in the laboratory. Three plates were expected to reach or exceed their plastic moment capacity, as their tested length was shorter than the critical length, while three were not. The results of the full-scale tests were then compared to data extracted from identical finite element models. Two initial imperfections were observed during the experimental program: misalignment of the shear tab plate and loading beam web, and plate skew resulting from the shear tab not being welded perpendicular to the support plate. The effect of these imperfections was investigated and quantified using a numerical analysis.

Finally, the findings from the parametric study and full-scale tests were used to develop an equation to predict the critical length of extended shear tabs. Factors were also empirically created to account for the influence of horizontal loading and initial imperfections. The shear capacity at the critical length was discussed, and compared to capacities predicted by both the 14th and 15th editions of the *Steel Construction Manual* (AISC 2011; 2017). The use of an effective eccentricity as opposed to the full geometric eccentricity, as proposed by Thomas et al. (2014), was also investigated.

6.2 Conclusions

The following conclusions are drawn from this research:

- The critical length is defined as the limit between a strength and stability governed failure. It corresponds to the length of plate where the interaction of bending, shear, and axial stresses reaches a value of Neal's equation of approximately 1.0 at the support. It was found that the critical length is typically long, and can be significantly longer than would be considered practical. Therefore, in many common cases the stability limit state does not need to be checked.

- Extended shear tab connections with a fixed support always reach their cross-sectional plastic moment capacity at the support prior to the bolt line. Therefore, the critical length is governed by plasticity at this location. Once a plastic hinge is formed at the support, load is shed towards the bolt line causing a double-peak in

the load–displacement response of the connection. Connections subjected to high horizontal loads can buckle prior to load redistribution and the formation of the second peak.

- The critical length is dependent on the depth and thickness of the plate. As plate thickness increases, the critical length becomes longer; however, as the plate gets deeper, the critical length is shorter.

- The shear capacity of extended shear tab connections is closely related to the critical length. Longer plates will have lower shear capacities, as the increased length causes a larger moment at the support for the same vertical load.

- Two failure modes were identified for extended shear tab connections at the critical length: out-of-plane deformations (ductile) and buckling (non-ductile). Buckling only occurred in plates with an applied horizontal compression load.

- The finite element model accurately predicted the behaviour and failure mode observed in the experimental tests; however, it over-predicted both the ultimate capacity and bending moment.

- Extended shear tab connections are sensitive to initial imperfections; they reduce both the ultimate shear capacity and bending moment ratio at the support. An initial misalignment imperfection can reduce the critical length by up to 15% as compared to perfect alignment. The effect of initial imperfections on the critical length decreases with increasing horizontal load.

- An equation to predict the critical length of extended shear tab connections was proposed. It is based on the lateral–torsional buckling equation and includes an effective length factor to account for out-of-plane rotational end restraint. Factors to reduce the critical length in the presence of horizontal compression load and initial imperfections were also proposed.

- Due to the double-peak nature of the load–displacement response, extended shear tab connections may be designed for either the capacity at the first peak or the ultimate capacity. The designer must ensure that the plate has sufficient ductility to reach the chosen capacity. The capacity at the first peak was a mean of 81% of the ultimate capacity for the cases considered, but occurred at a much smaller vertical displacement.

6.3   Recommendations for Further Research

This study has contributed to understanding the effect of instability on extended shear tab connections through the use of both numerical analysis and experimental testing. However, further investigation of the following topics would be beneficial in understanding the complex behaviour of this connection:

- To limit the size of the parametric study test matrix, only three plate depths, with a maximum of 310 mm, were investigated. Investigation of deeper plates is recommended, as the critical length decreased as the depth increased.

- The experimental program in this study tested only six extended shear tab specimens that bounded the critical length. An experimental testing program of specimens at or near the critical length is recommended to confirm the critical lengths obtained from the numerical analysis, and increase experimental data of long extended shear tab plates.

- The critical length represents the limit of when current, strength-governed design methods may be used to design extended shear tab plates. Further study is needed of the behaviour of plates that are longer than this critical length and are therefore governed by instability failure.

- Further investigation into the influence of initial imperfections on the stability behaviour of extended shear tab connections is required. Only the effect of an initial misalignment imperfection was investigated in relation to the critical length; therefore, consideration of other imperfection types would be beneficial. Additionally, it was observed that the depth and thickness of the plate impacted the reduction in critical length due to imperfection, and so investigating additional geometric parameters could improve knowledge regarding this behaviour.

REFERENCES

Abou-Zidan, A., and Liu, Y. (2015). "Numerical study of unstiffened extended shear tab connections." *J. Const. Steel Res.*, 107, 70–80.

AISC. (1994). *Steel Construction Manual LRFD, 2nd Edition*. American Institute of Steel Construction, Chicago, IL.

AISC. (2005). *Steel Construction Manual, 13th Edition*. American Institute of Steel Construction, Chicago, IL.

AISC. (2011). *Steel Construction Manual, 14th Edition*. American Institute of Steel Construction, Chicago, IL.

AISC. (2016). "Specification for Structural Steel Buildings." *ANSI/AISC 360-16*, American Institute of Steel Construction, Chicago, IL.

AISC. (2017). *Steel Construction Manual, 15th Edition*. American Institute of Steel Construction, Chicago, IL.

Astaneh, A., Call, S. M., and Mcmullin, K. M. (1989). "Design of Single Plate Shear Connections." *AISC Eng. J.*, 26(1), 21–32.

ASTM. (2014). *A370-14: Standard Test Methods and Definitions for Mechanical Testing of Steel Products*. ASTM International, West Conshohocken, PA.

CISC. (2016). *Handbook of Steel Construction, 11th Edition*. Canadian Institute of Steel Construction, Markham, ON.

CSA. (2014). *S16-14 Design of Steel Structures*. Canadian Standards Association, Mississauga, ON.

Dassault Systèmes. (2014). "Abaqus Analysis User's Guide" *Version 6.14*, Dassault Systèmes Simulia Corp, Providence, RI.

Dowswell, B. (2016). "Stability of Rectangular Connection Elements." *AISC Eng. J.*, 53(4), 171–201.

Dowswell, B. O., and Whyte, R. (2014). "Local Stability of Double-Coped Beams." *AISC Eng. J.,* 51(1), 43–52.

Galambos, T. V. (1968). "*Structural Members and Frames*." Prentice-Hall Inc., Englewood Cliffs, NJ.

Johnston, G., Driver, R. G., and Callele, L. (2015). "Strength and Behaviour of Double-coped Steel Beams Under Combined Loads." *Rep. No. 306,* University of Alberta, Edmonton, AB.

Marosi, M., Aronco, M. D., Tremblay, R., and Rogers, C. A. (2011). "Multi-row Bolted Beam to Column Shear Tab Connections." *Eurosteel*, 6th European Conference on Steel and Composite Structures, Budapest, Hungary, 555–560.

Metzger, K. A. B. (2006). "Experimental Verification of a New Single Plate Shear Connection Design Model". M.Sc. thesis. Virginia Polytechnic Institute and State University, Blacksburg, VA.

Mirzaei, A. (2014). "Steel Shear Tab Connections Subjected to Combined Shear and Axial Forces." Ph.D thesis. McGill University, Montreal, QC.

Muir, L. S., and Hewitt, C. M. (2009). "Design of Unstiffened Extended Single-Plate Shear Connections." *AISC Eng. J.*, 46(2), 67–80.

Neal, B. G. (1961). "The Effect of Shear and Normal Forces on the Fully Plastic Moment of a Beam of Rectangular Cross Section." *J. App. Mech.,* 28(2), 269–274.

Rahman, A., Mahamid, M., Amro, A., and Ghorbanpoor, A. (2007). "The Analyses of Extended Shear Tab Steel Connections Part I : Unstiffened Connections." *AISC Eng. J.*, 44(2), 117–132.

Salem, P., Driver, R. G., and Callele, L. (2016). "Unified Design Criteria for Steel Cantilever Plate Connection Elements." *Rep. No. 308,* University of Alberta, Edmonton, AB.

Sherman, D. R., and Ghorbanpoor, A. (2002). "Final Report: Design of Extended Shear Tabs." American Institute of Steel Construction, University of Wisconsin-Milwaukee.

Thomas, K., Driver, R. G., Callele, L., and Oosterhof, S. (2014). "Design and Behaviour of Extended Shear Tabs under Combined Loads." *Rep. No. 305,* University of Alberta, Edmonton, AB.

Thomas, K., Driver, R. G., Oosterhof, S. A., and Callele, L. (2016). "Full-scale Tests of Stabilized and Unstabilized Extended Single-plate Connections." *Structures*, 10, 49–58.

Thornton, W. A., and Fortney, P. J. (2011). "On the Need for Stiffeners for and the Effect of Lap Eccentricity on Extended Single-Plate Connections." *AISC Eng. J.*, 48(2), 117–125.

Appendix A: Finite Element Analysis Response Curves
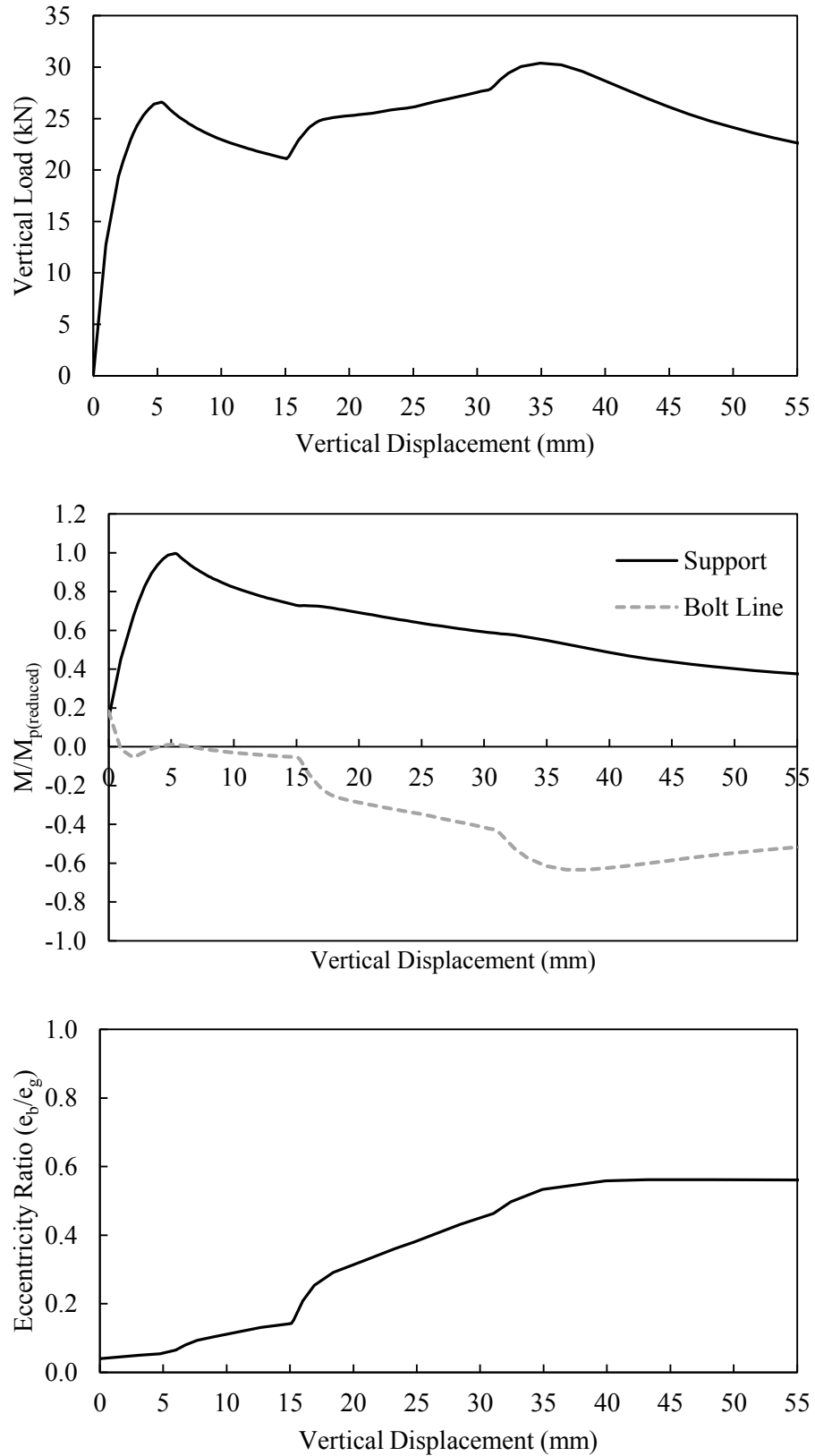
Figure A-1: Model 2B-6-0
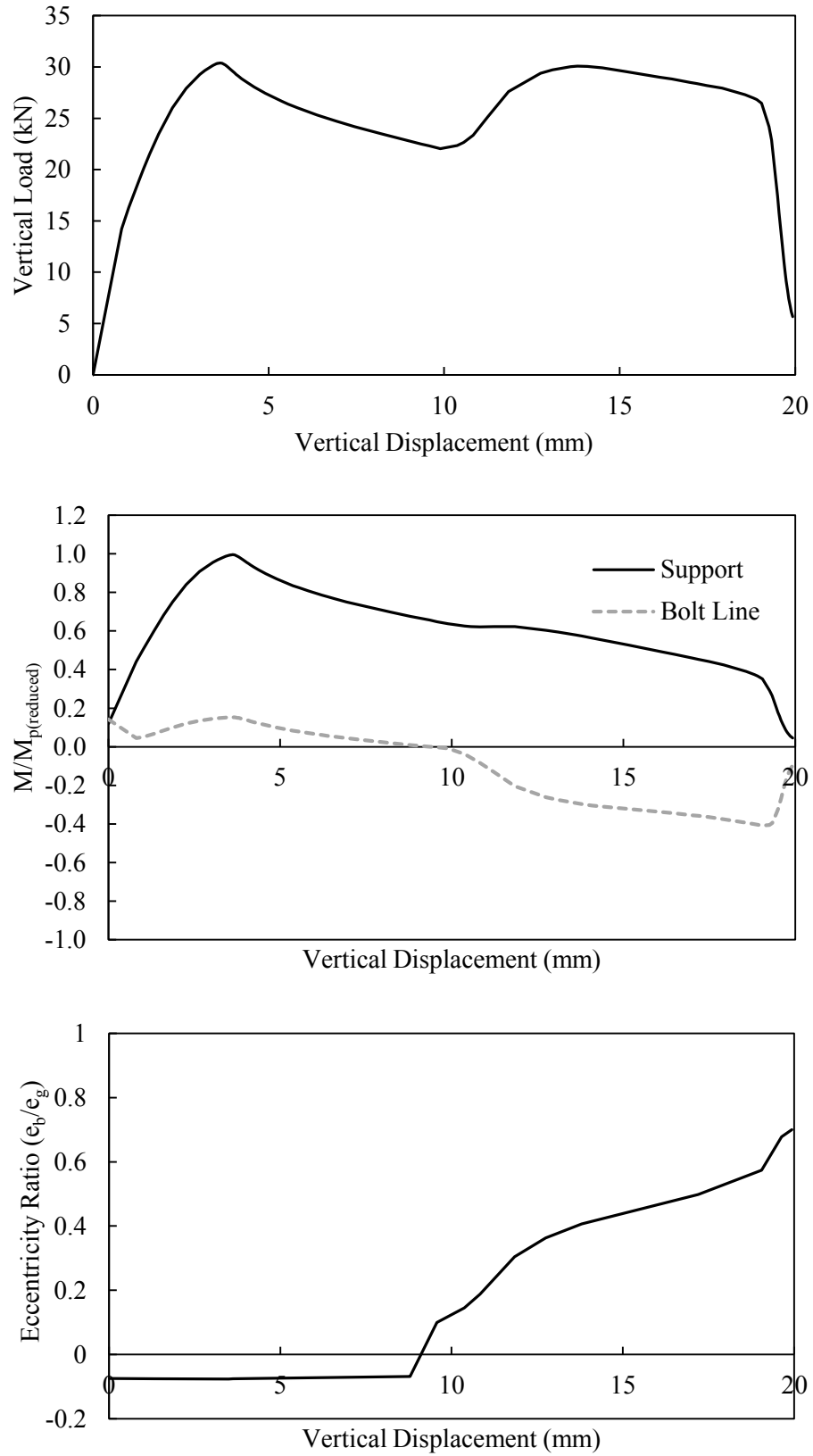
Figure A-2: Model 2B-6-10
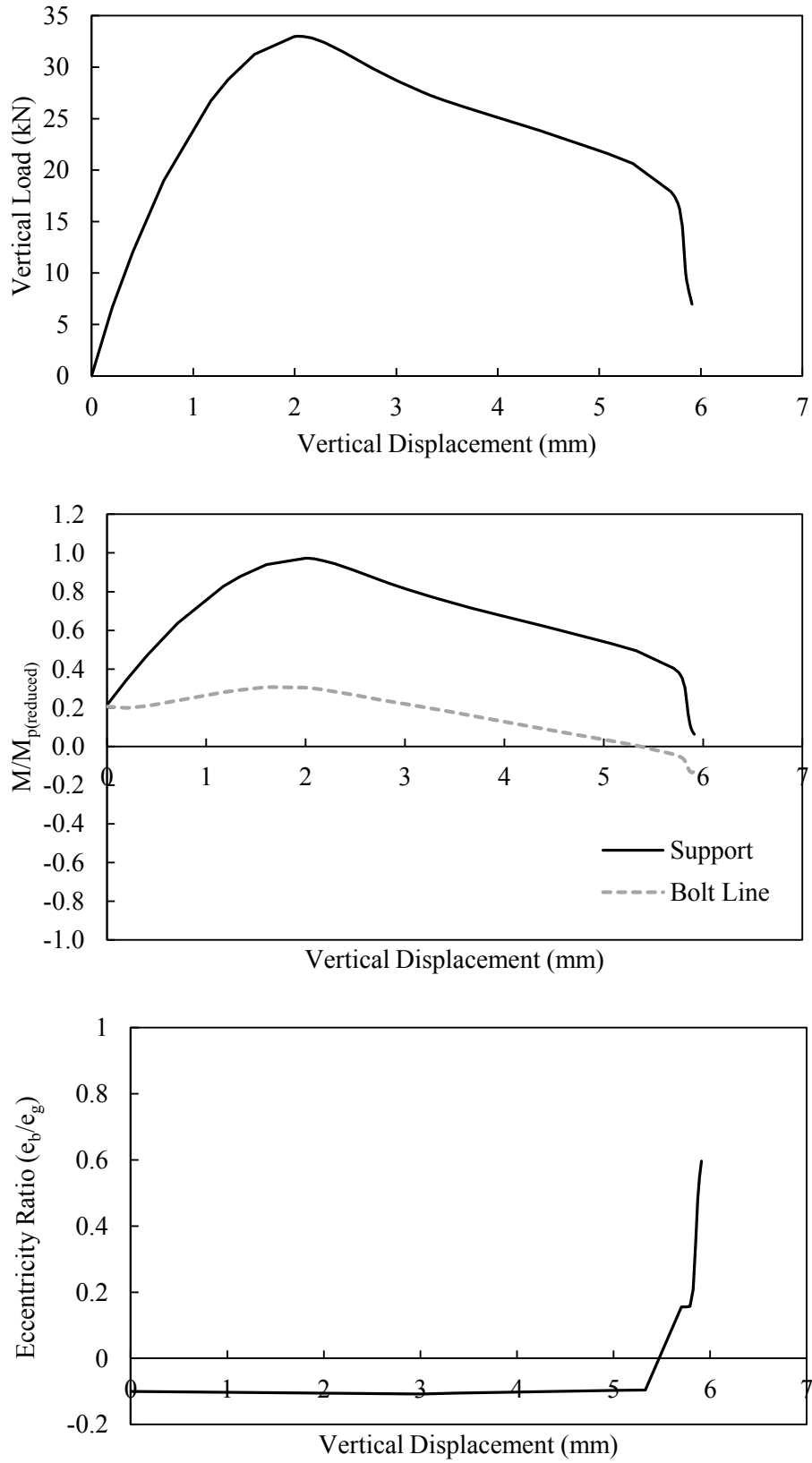
Figure A-3: Model 2B-6-25
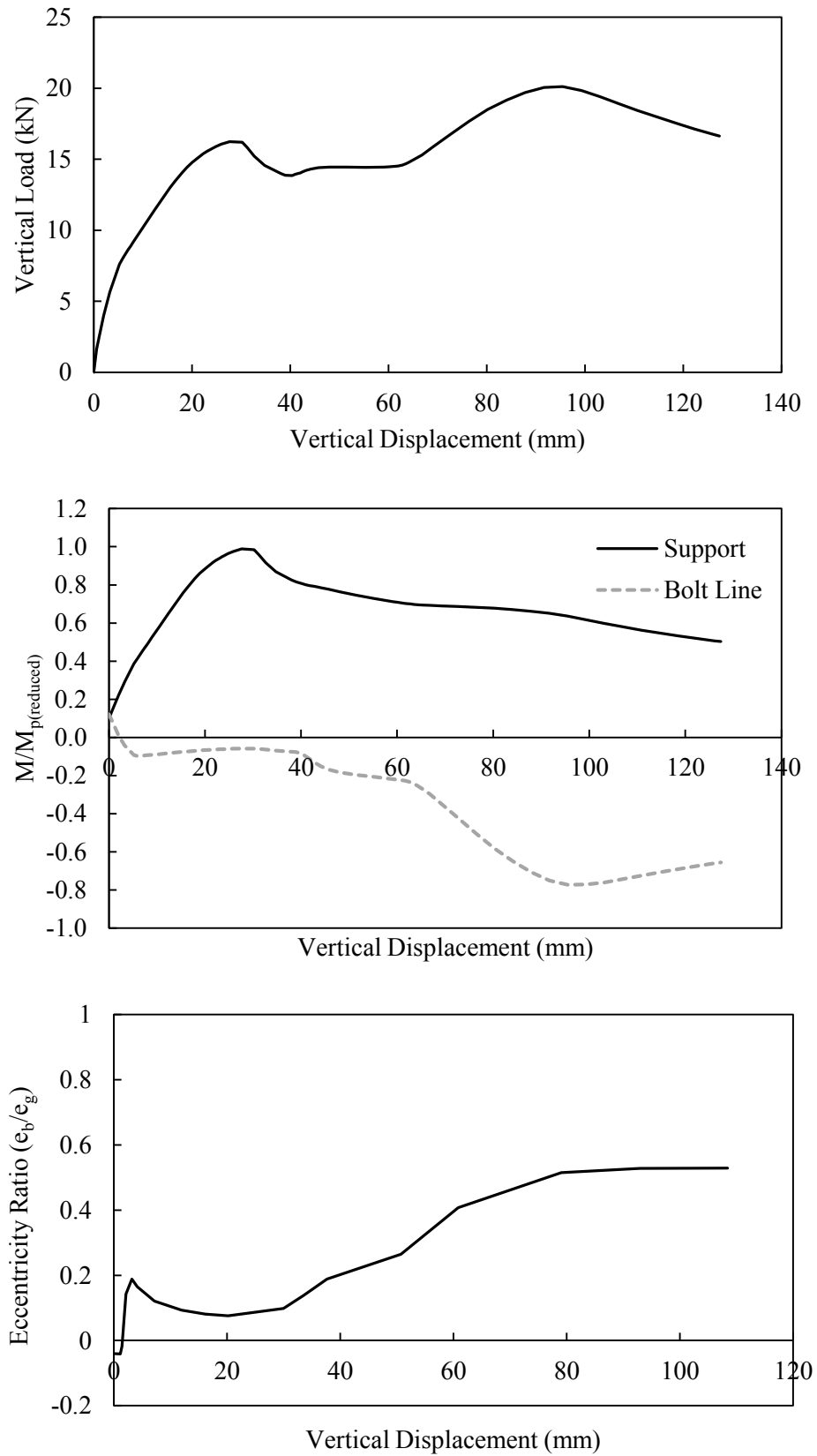
Figure A-4: Model 2B-10-0
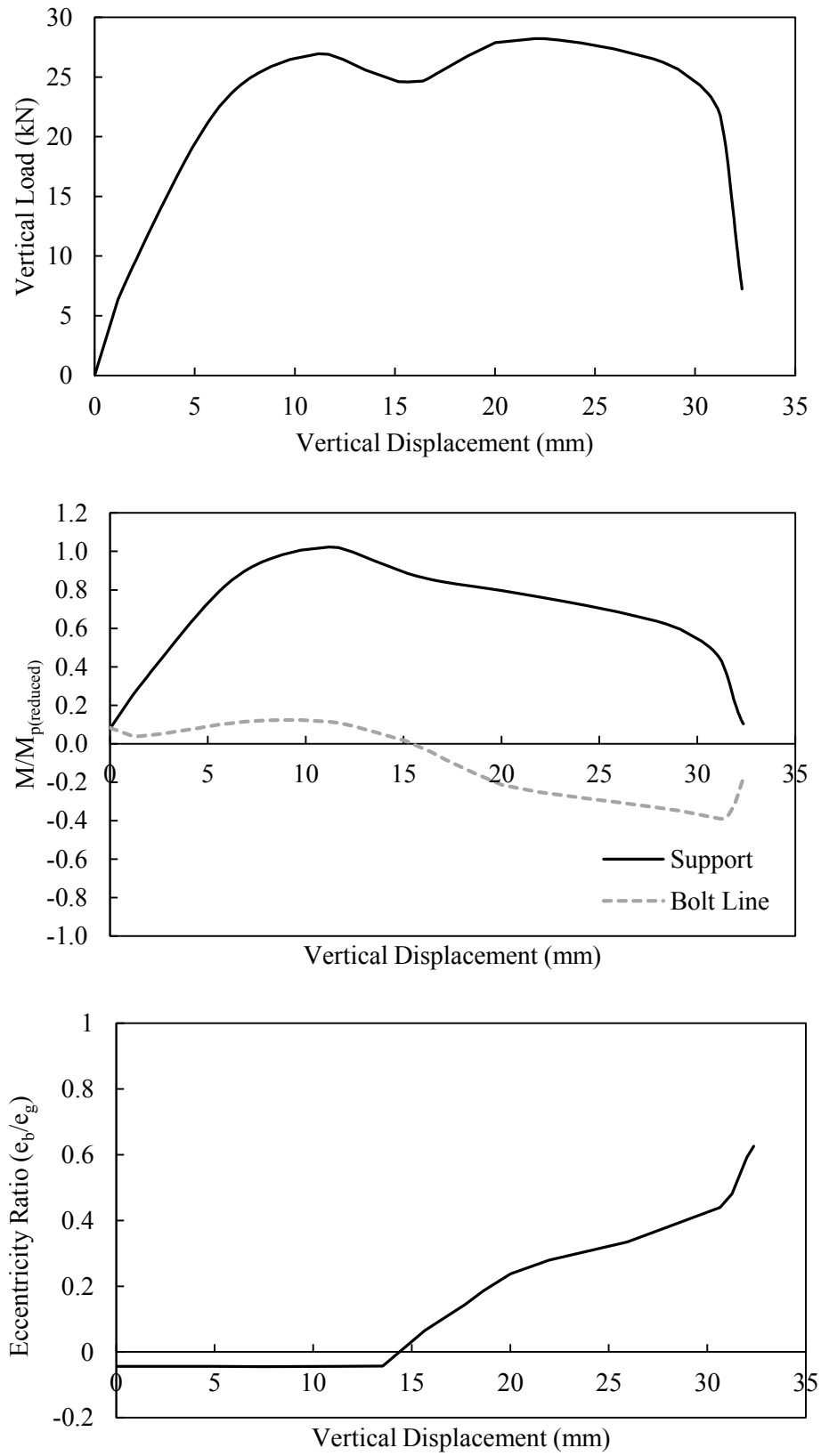
Figure A-5: Model 2B-10-10
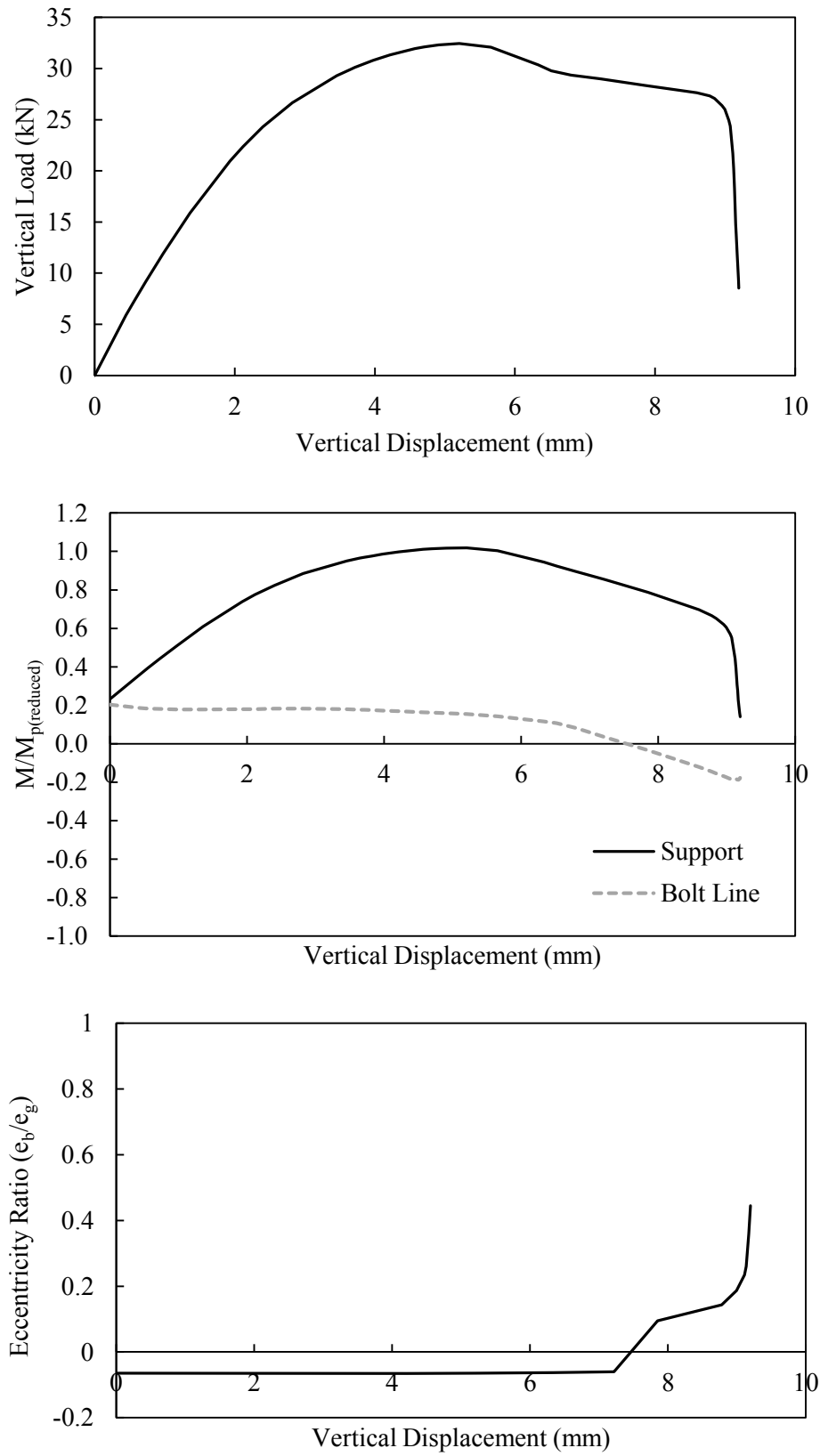
Figure A-6: Model 2B-10-25
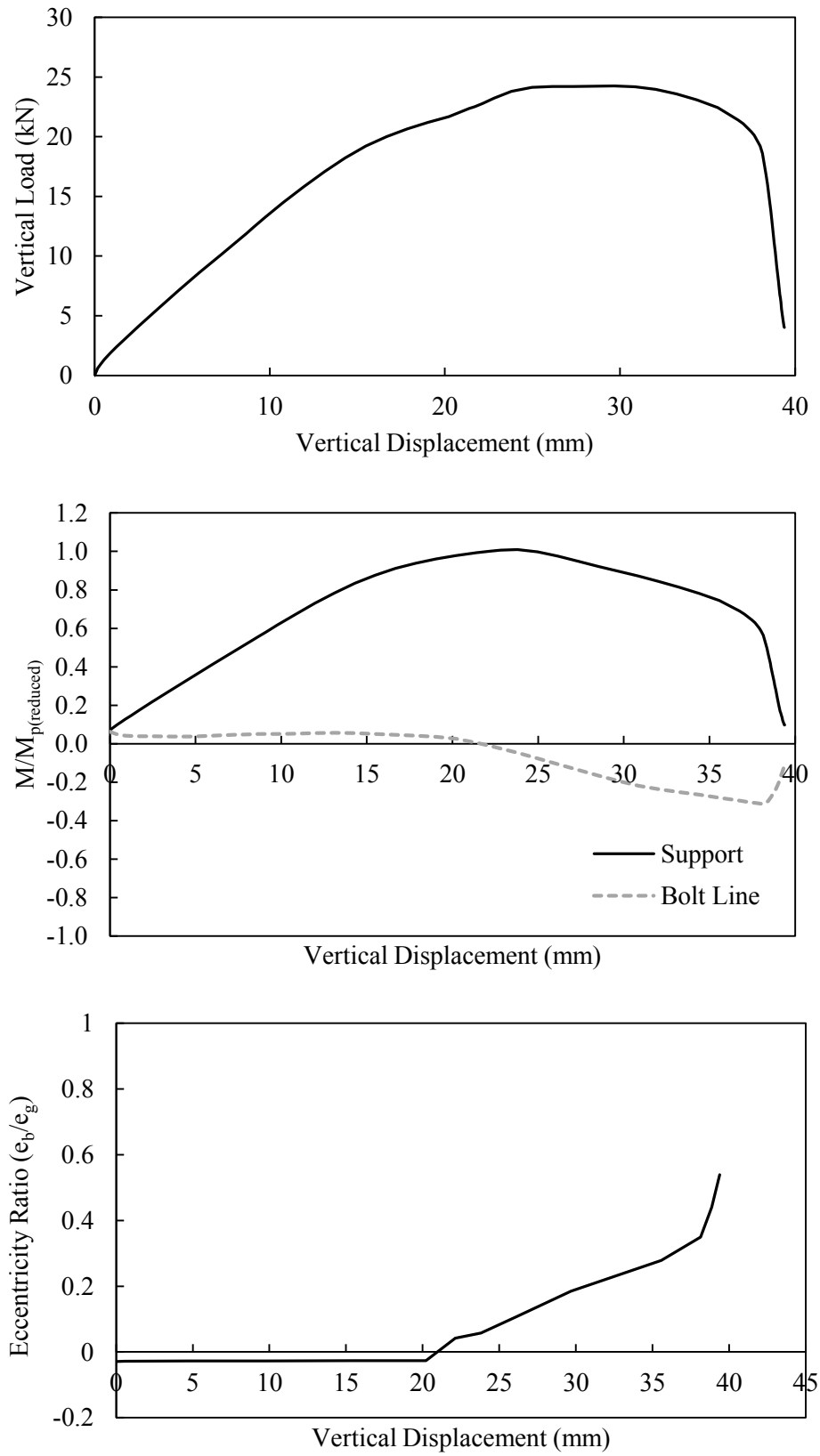
Figure A-7: Model 2B-13-10
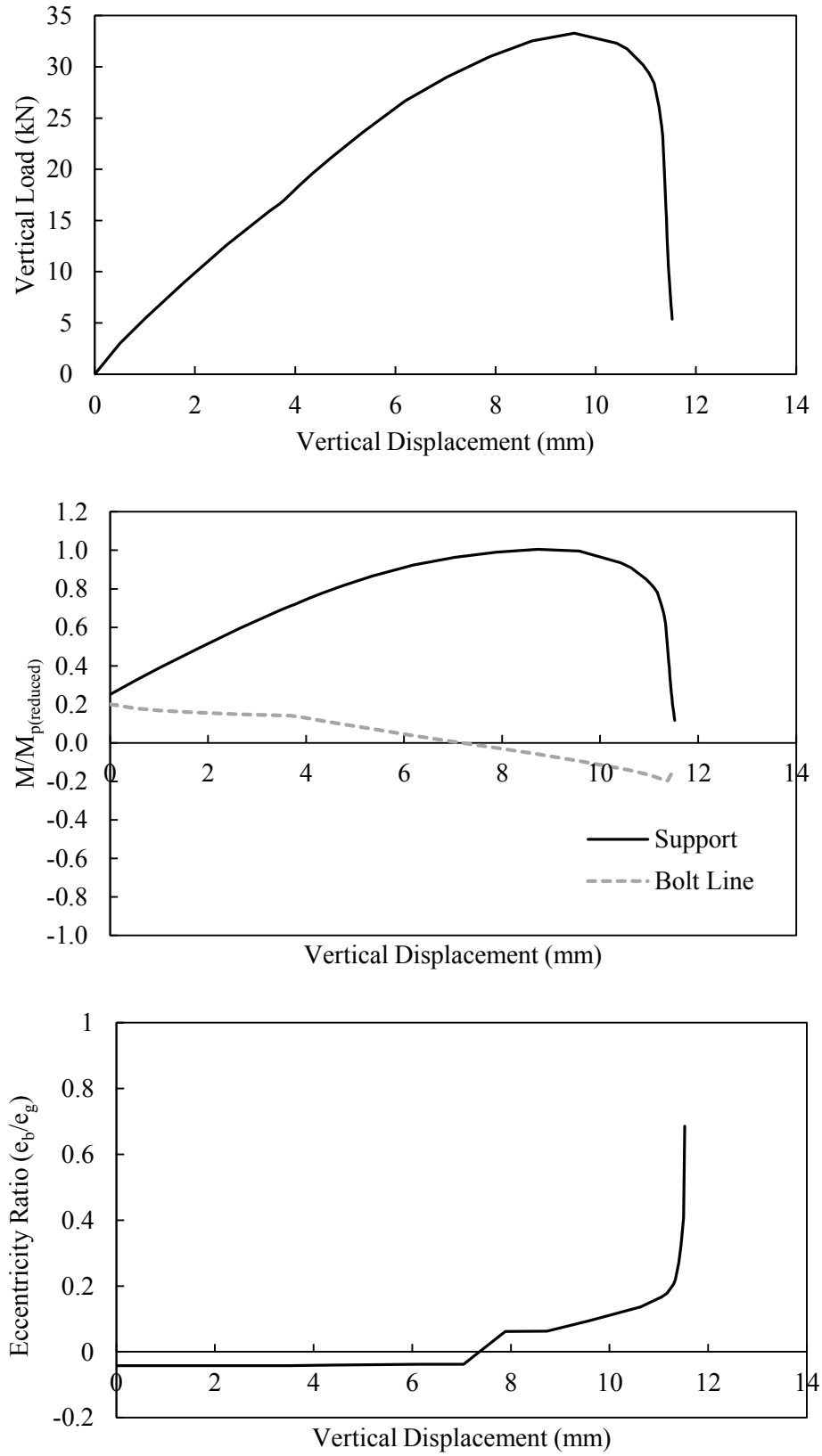
Figure A-8: Model 2B-13-25
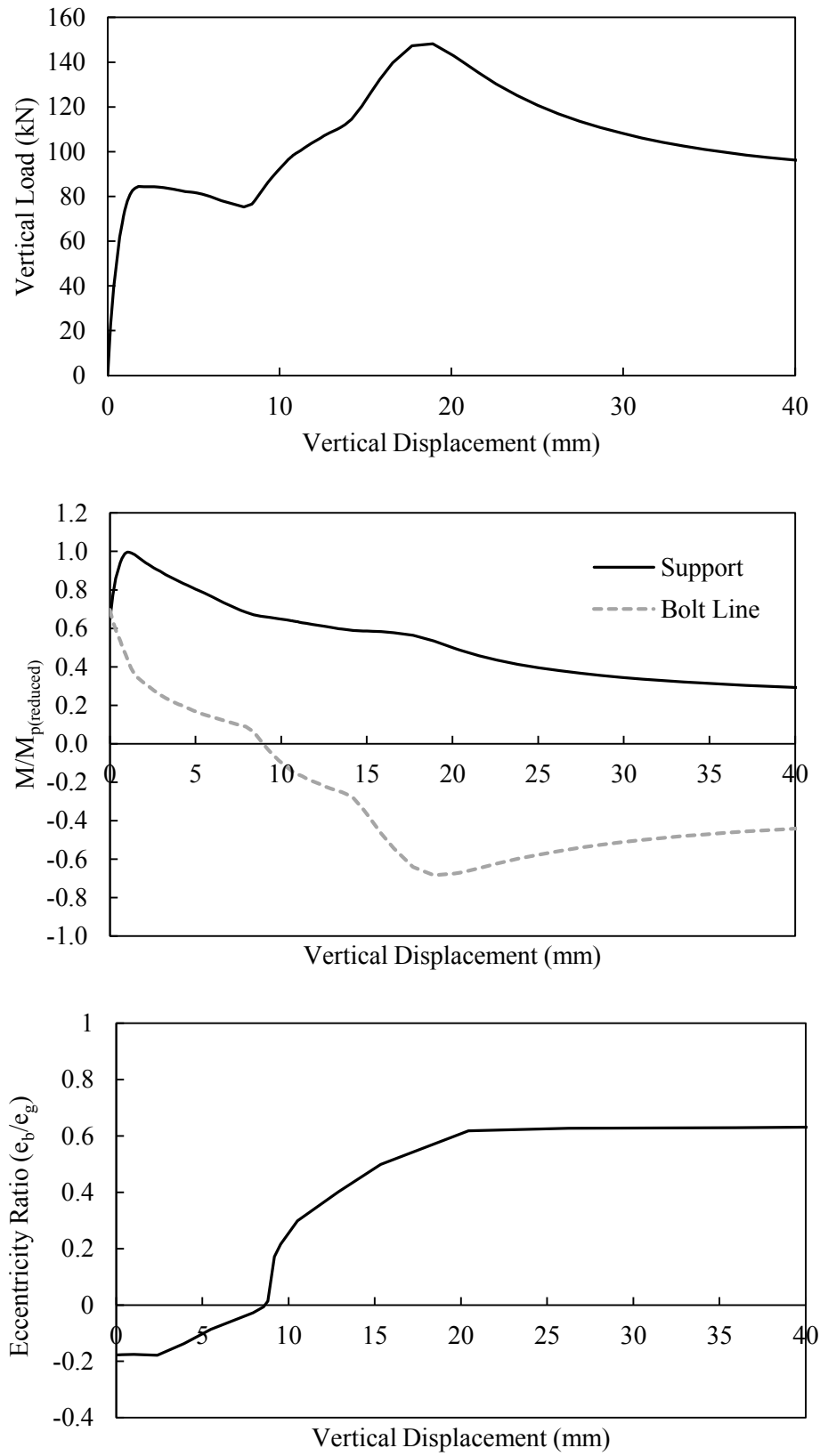
Figure A-9: Model 3B-6-0
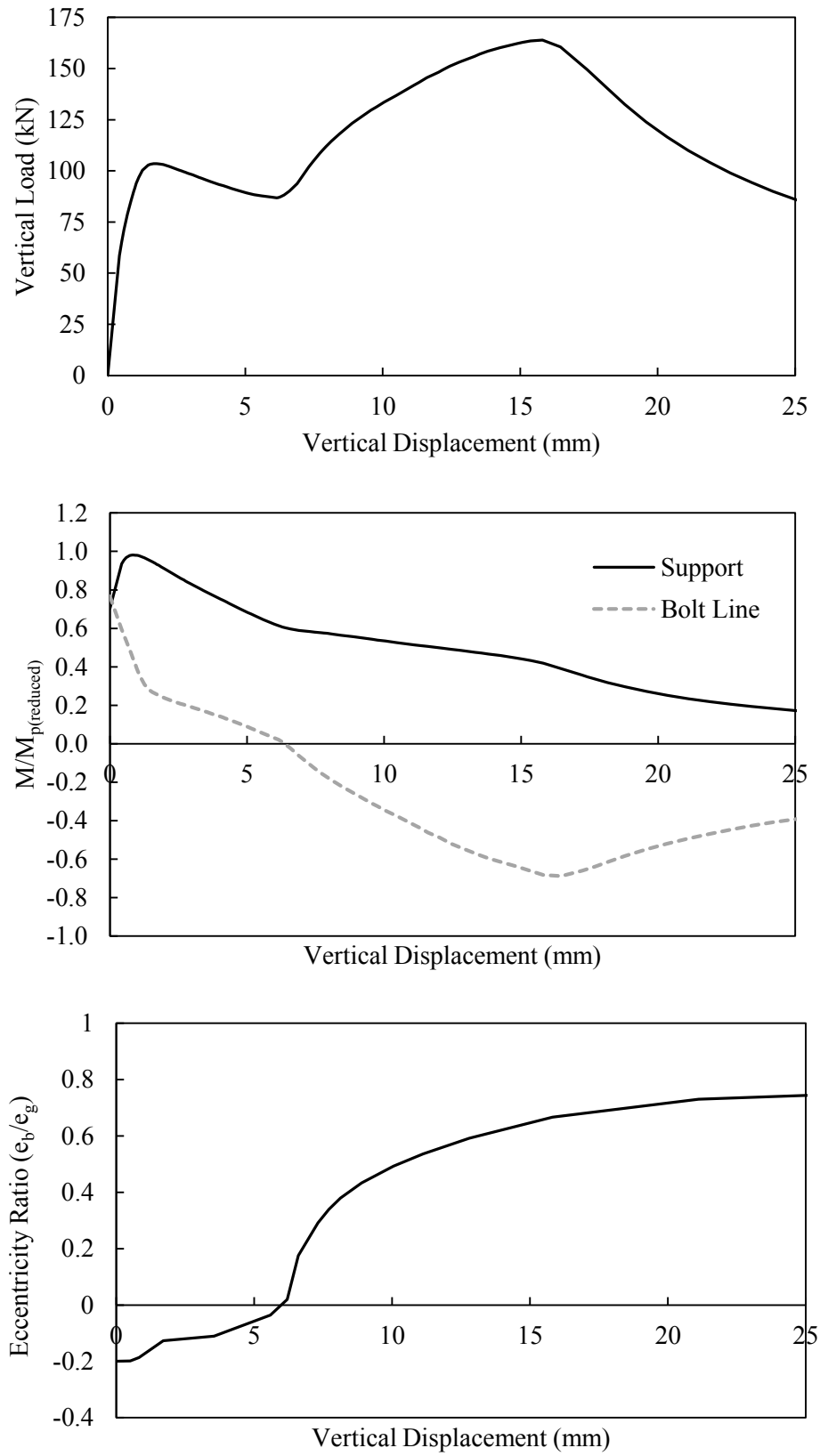
Figure A-10: Model 3B-6-10
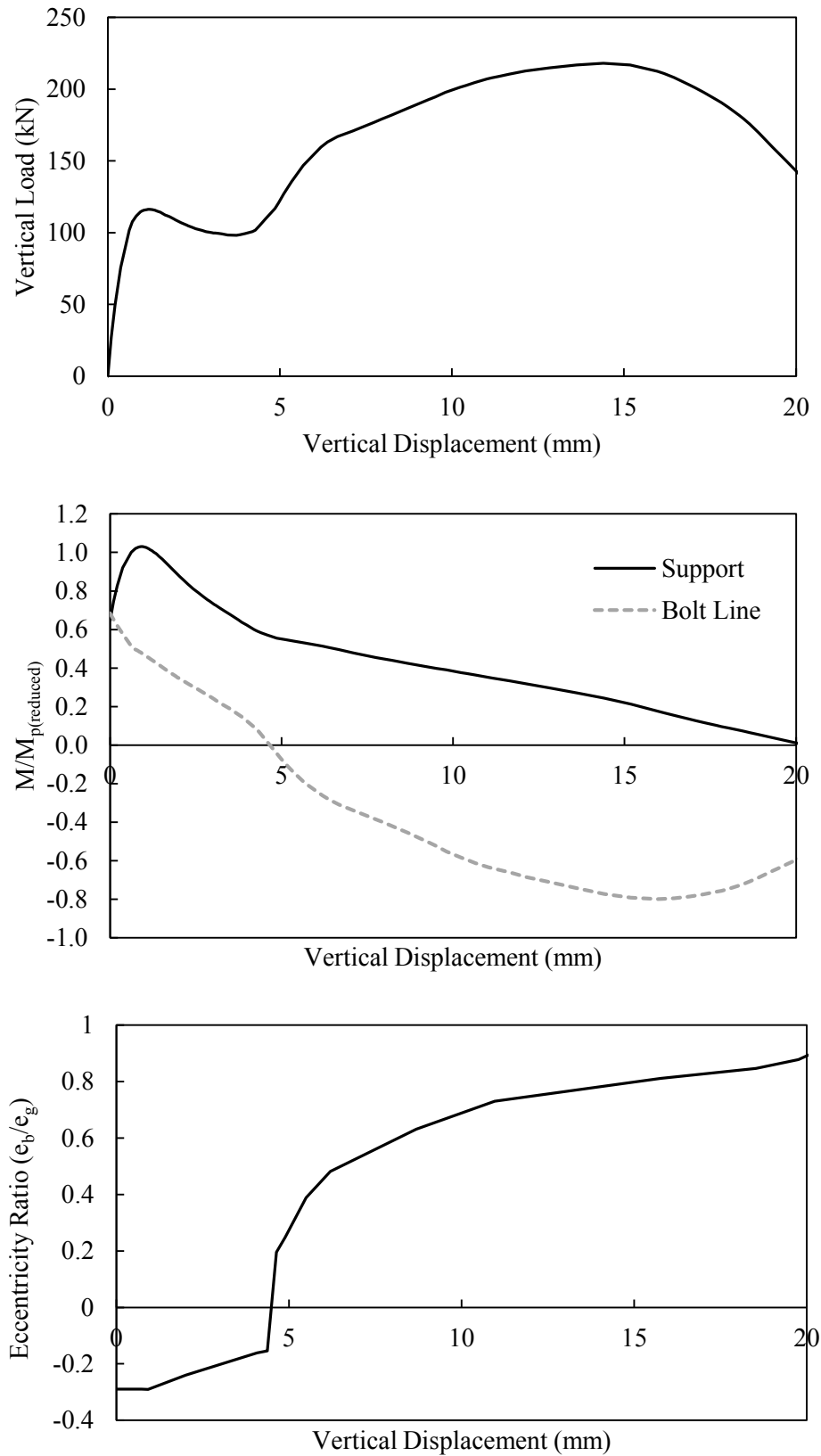
Figure A-11: Model 3B-6-25
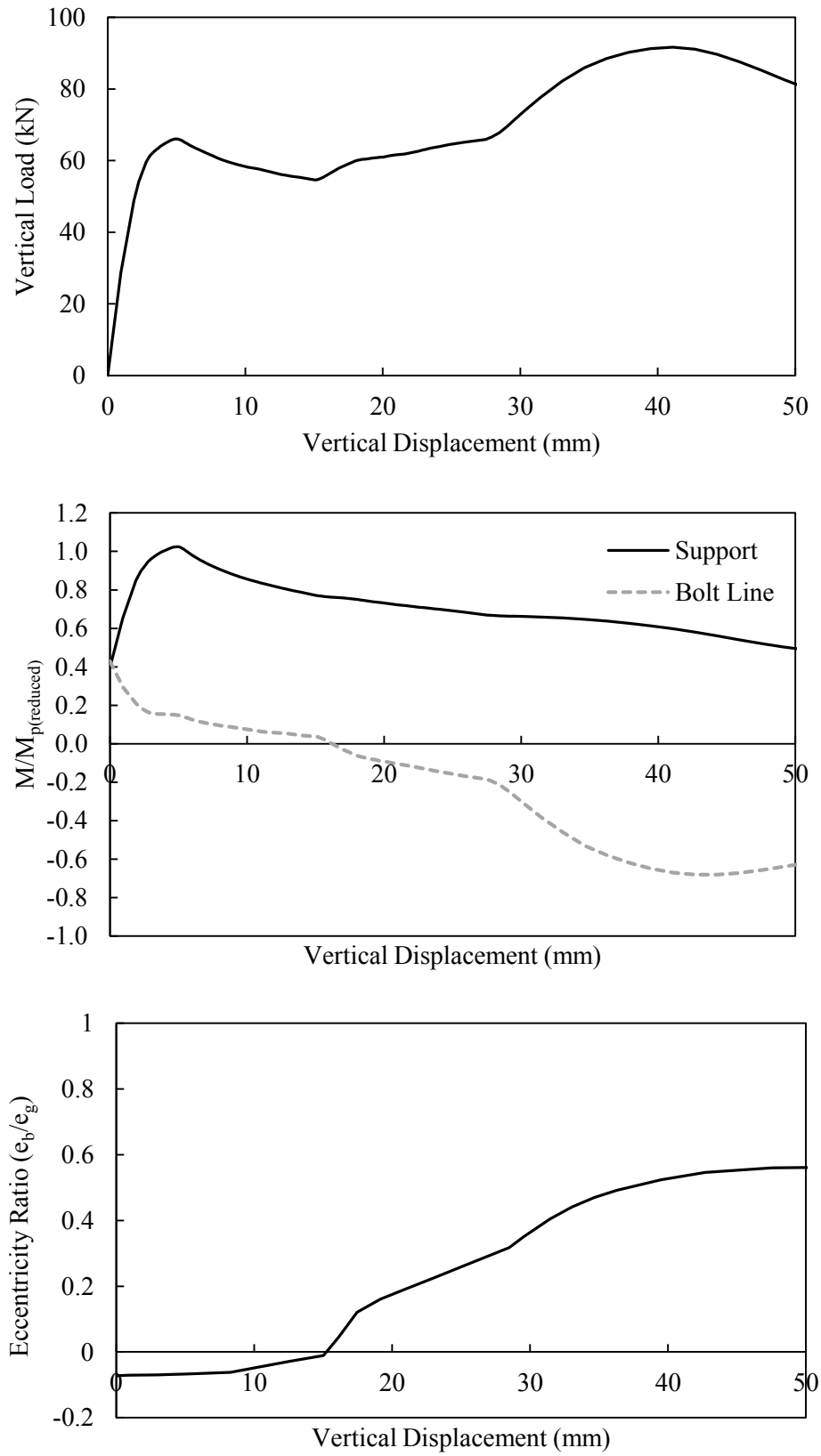
Figure A-12: Model 3B-10-0
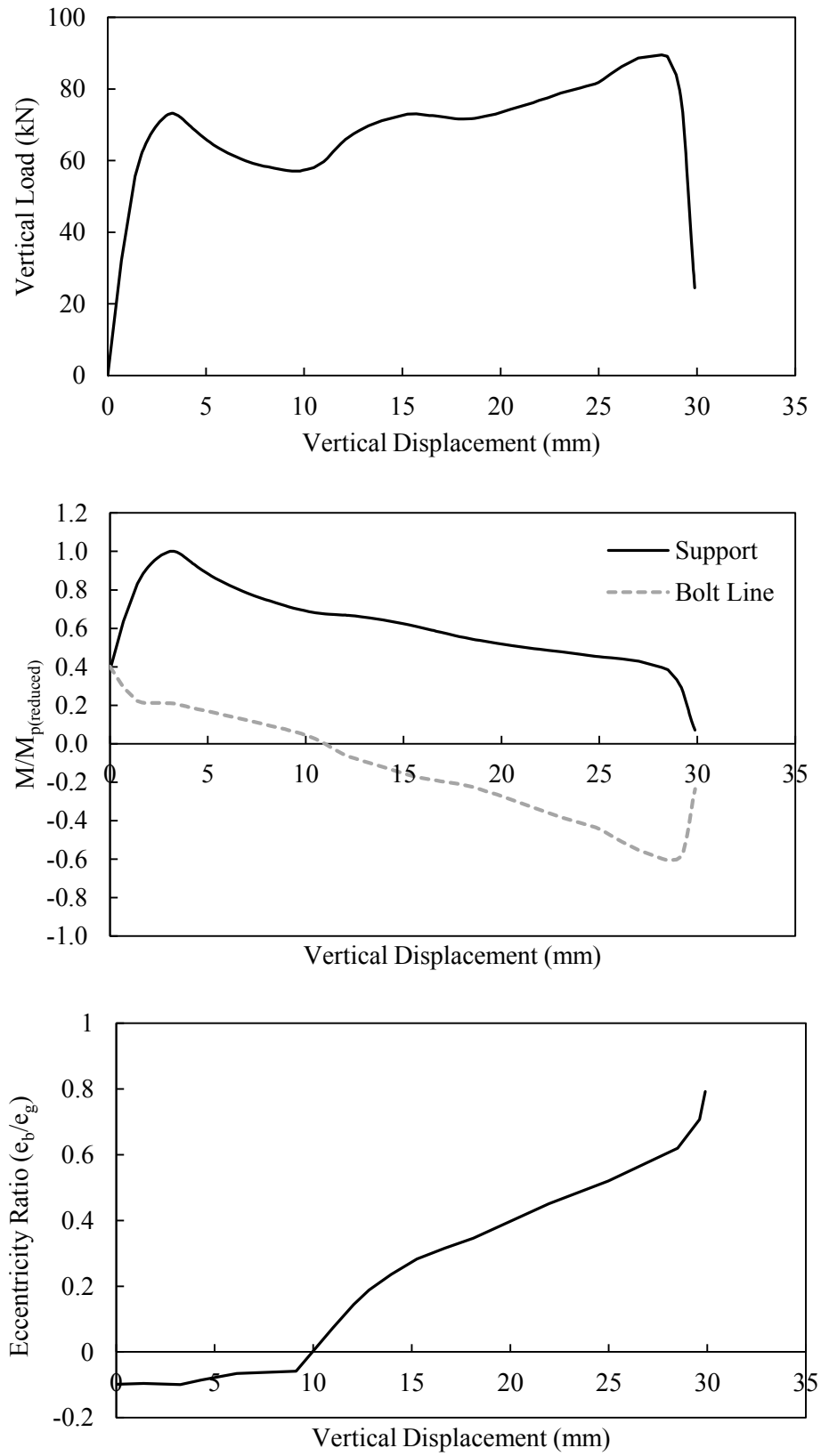
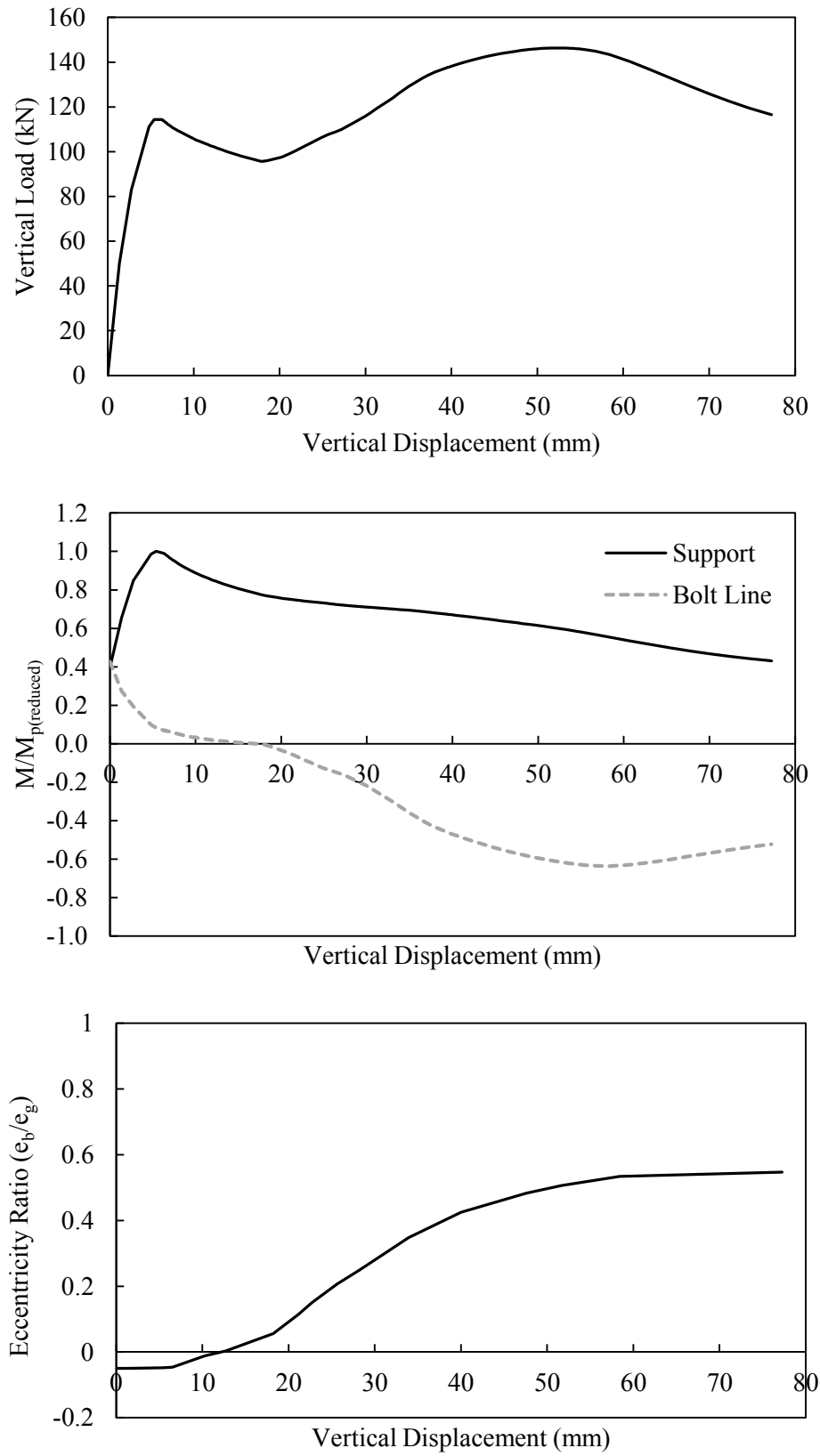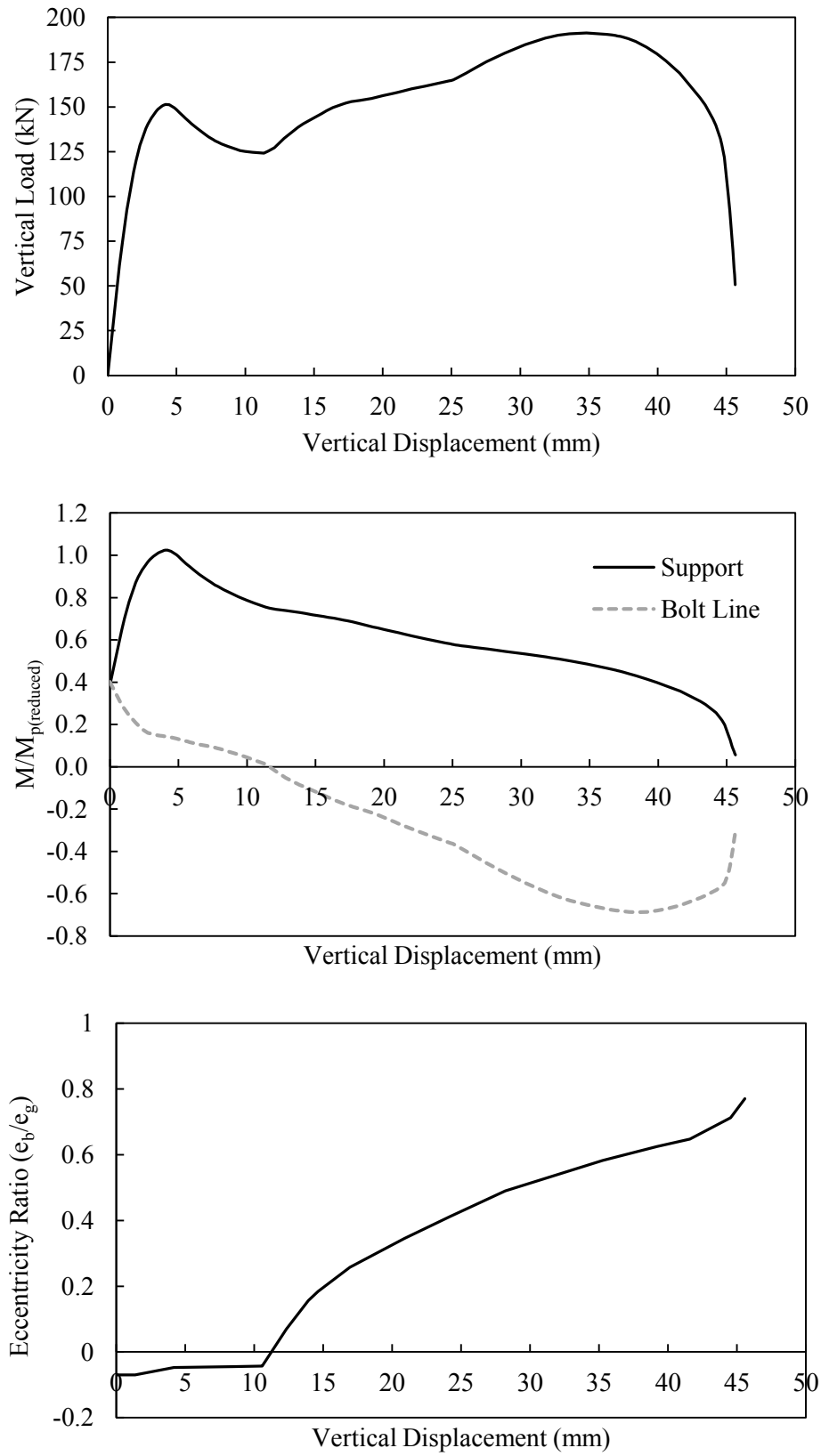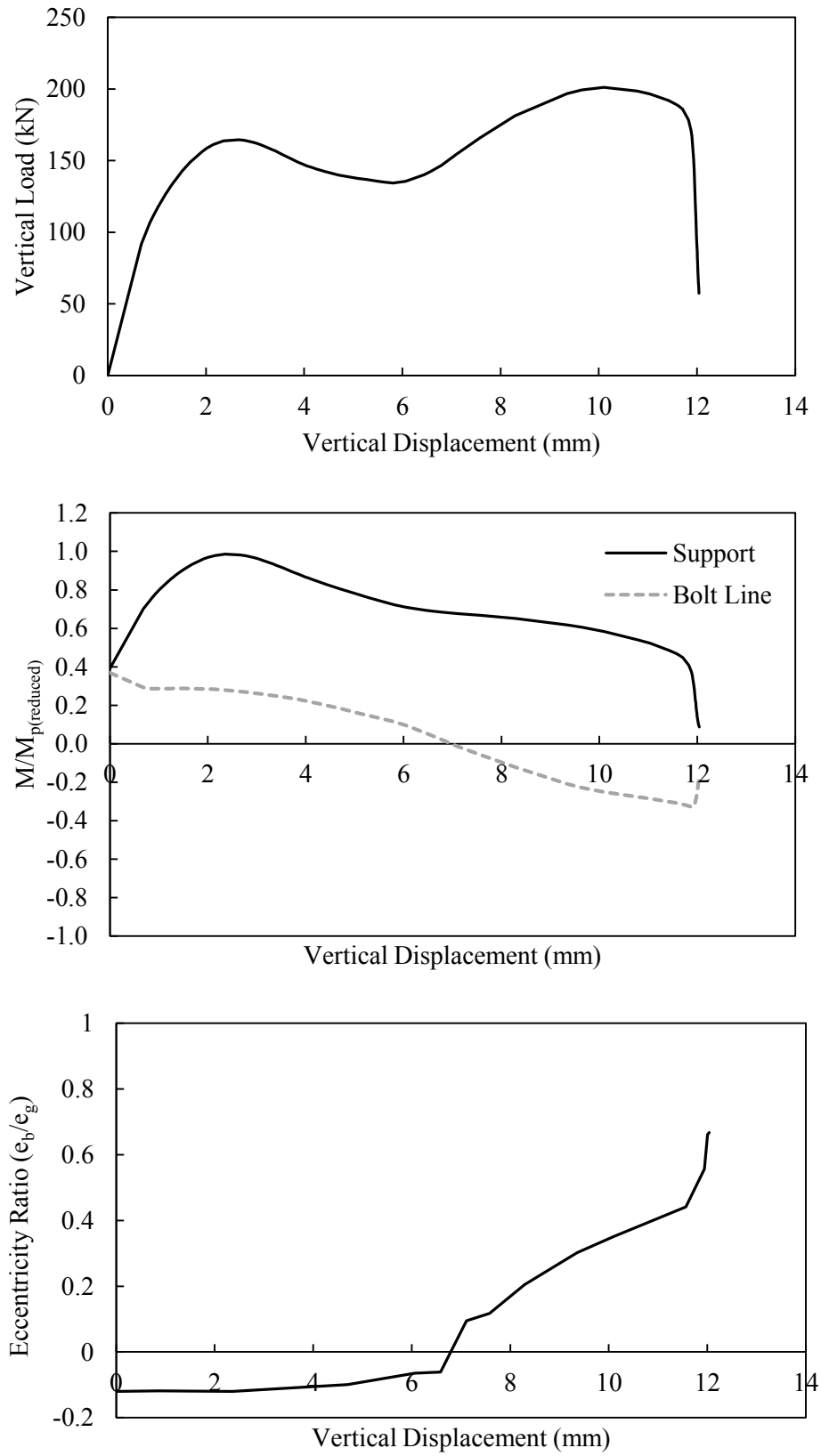Figure A-13: Model 3B-10-10
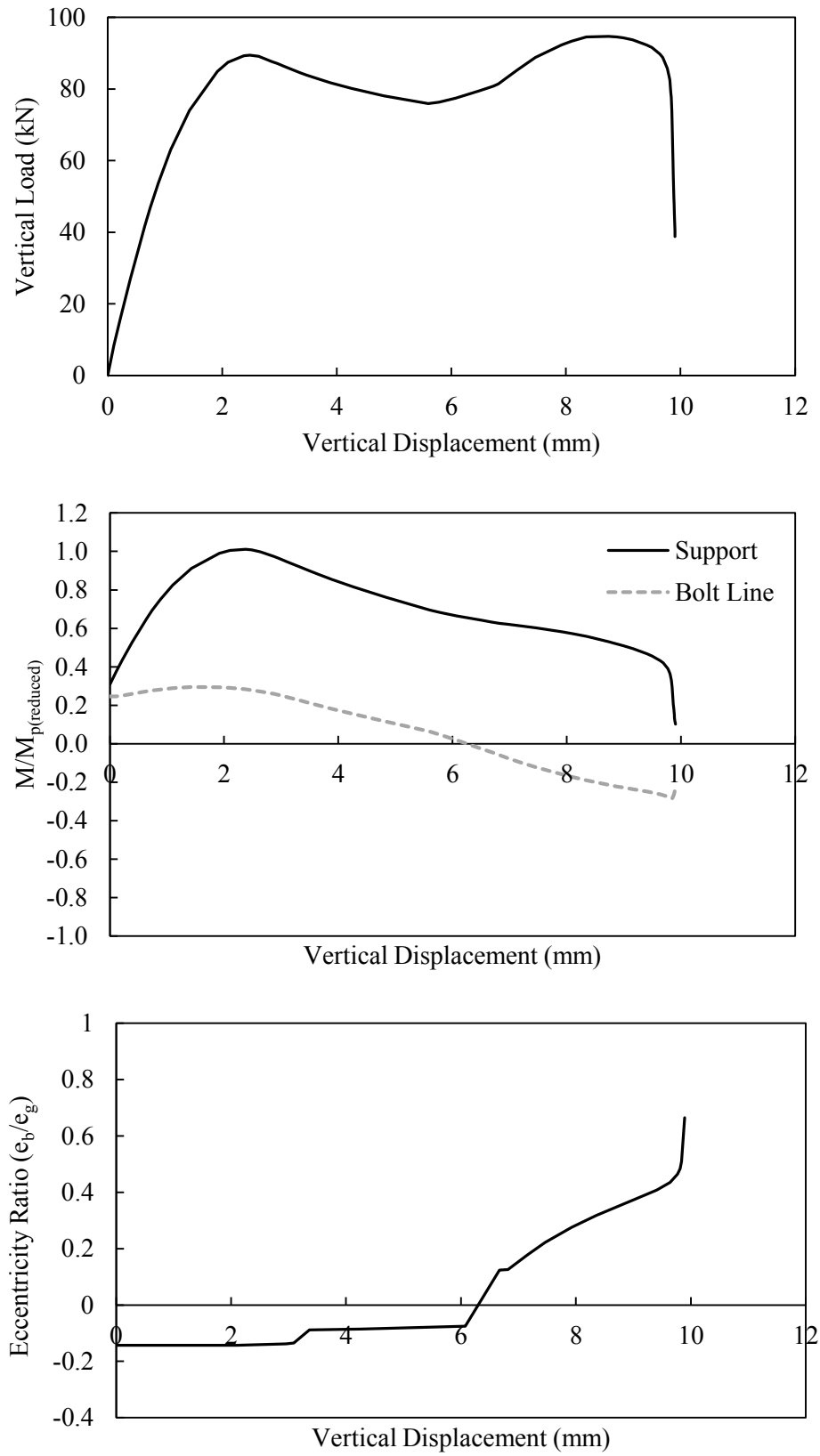
Figure A-14: Model 3B-10-25
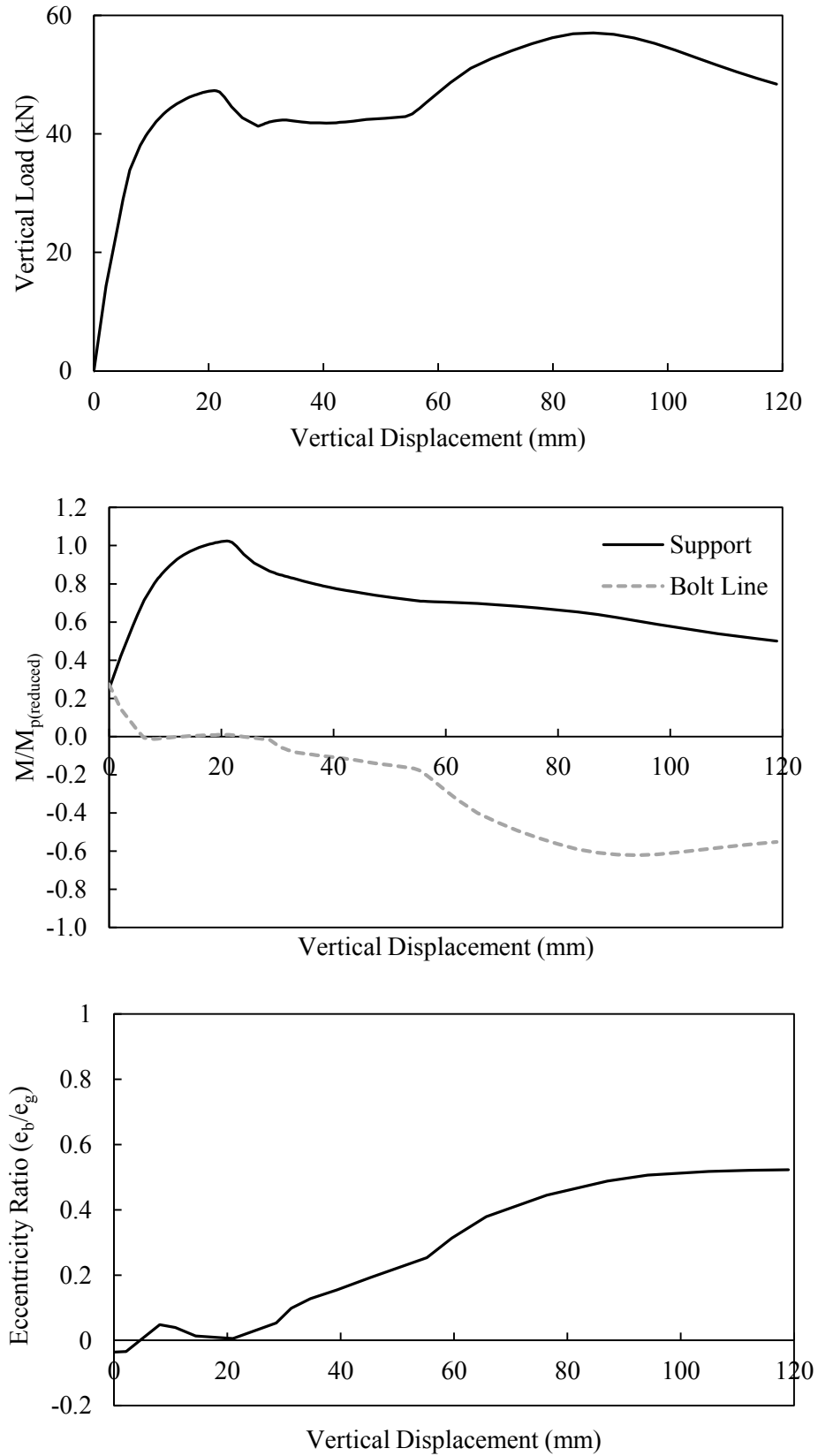
Figure A-15: Model 3B-13-0
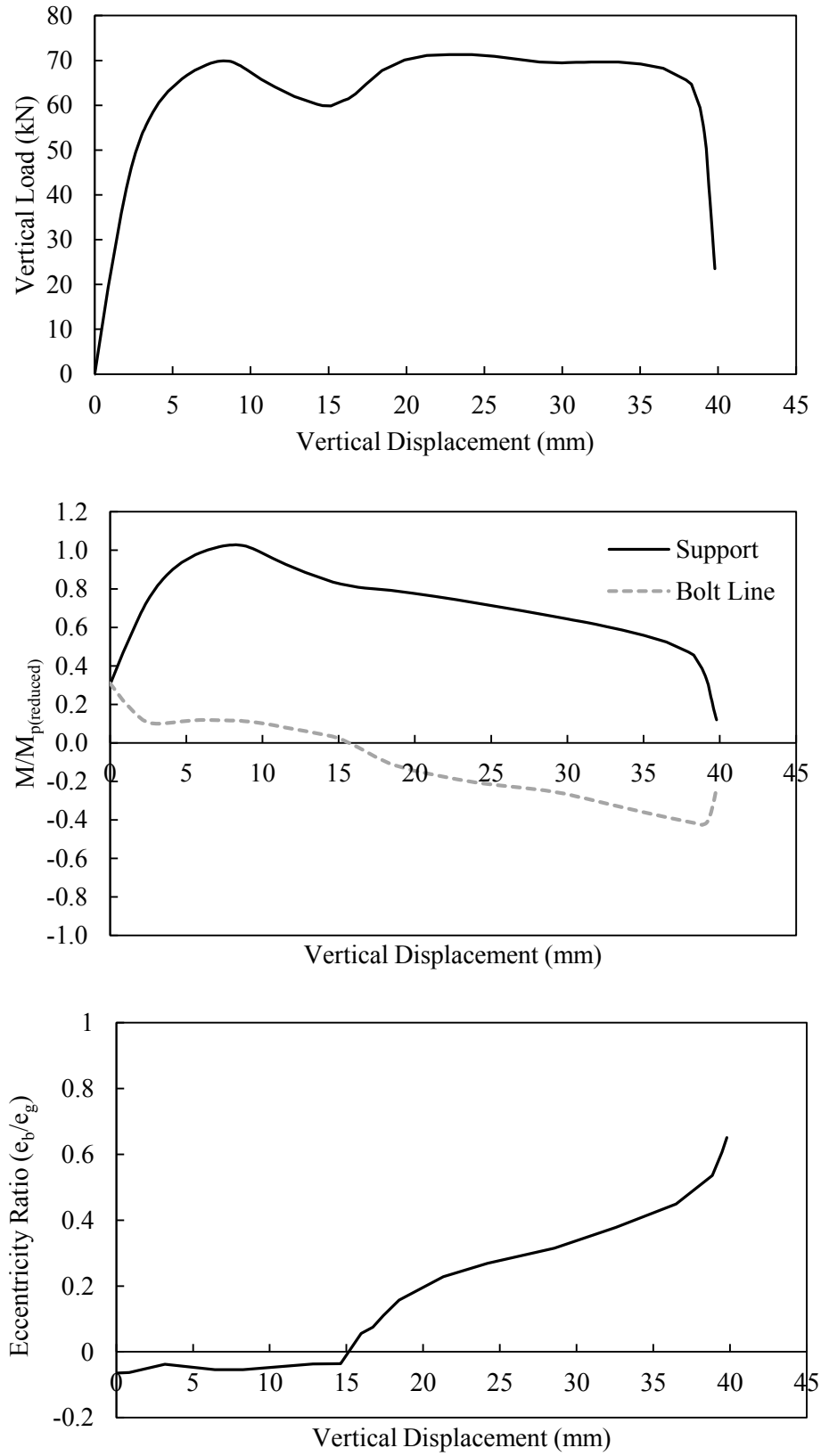
Figure A-16: Model 3B-13-10
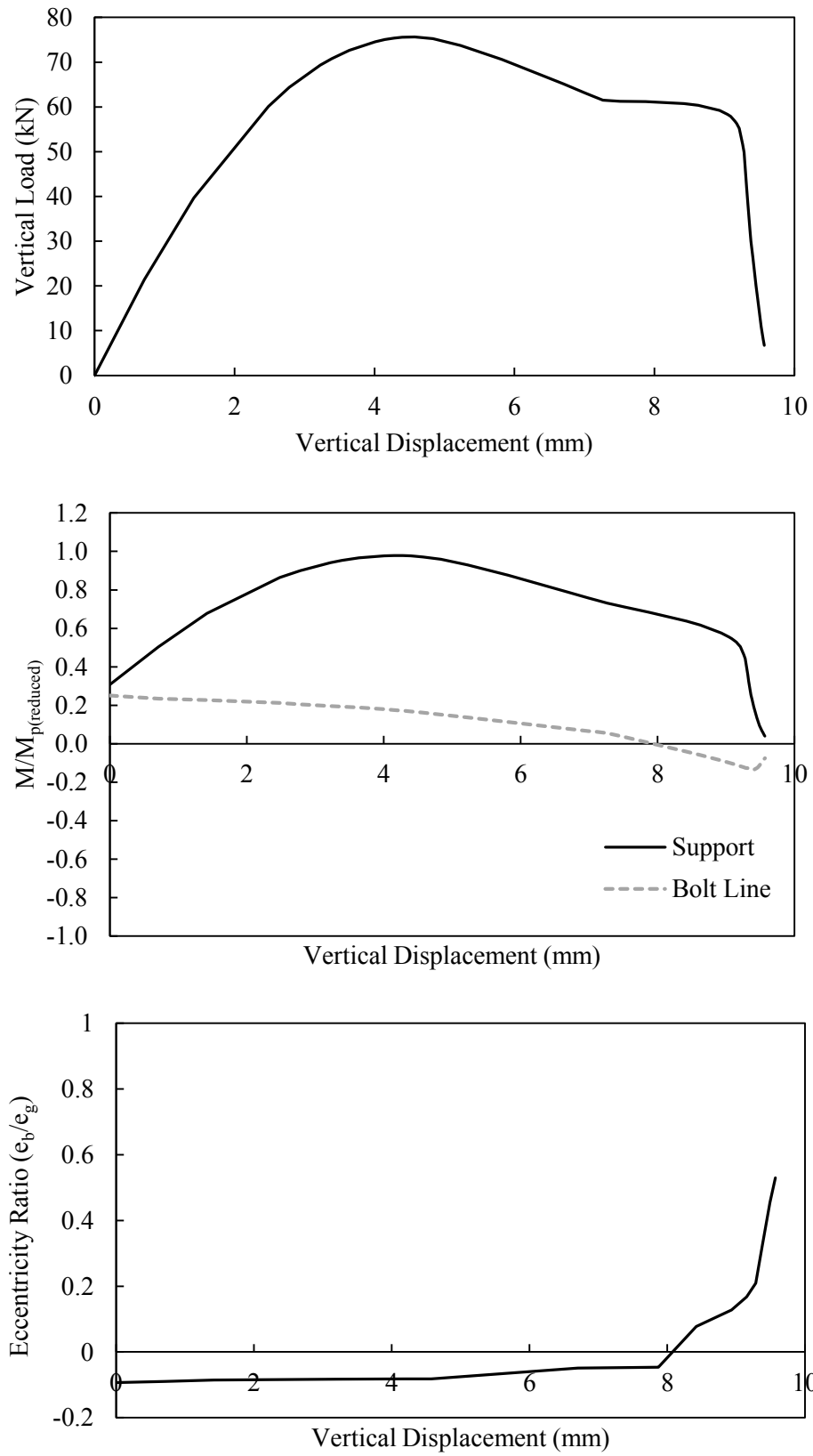
Figure A-17: Model 3B-13-25
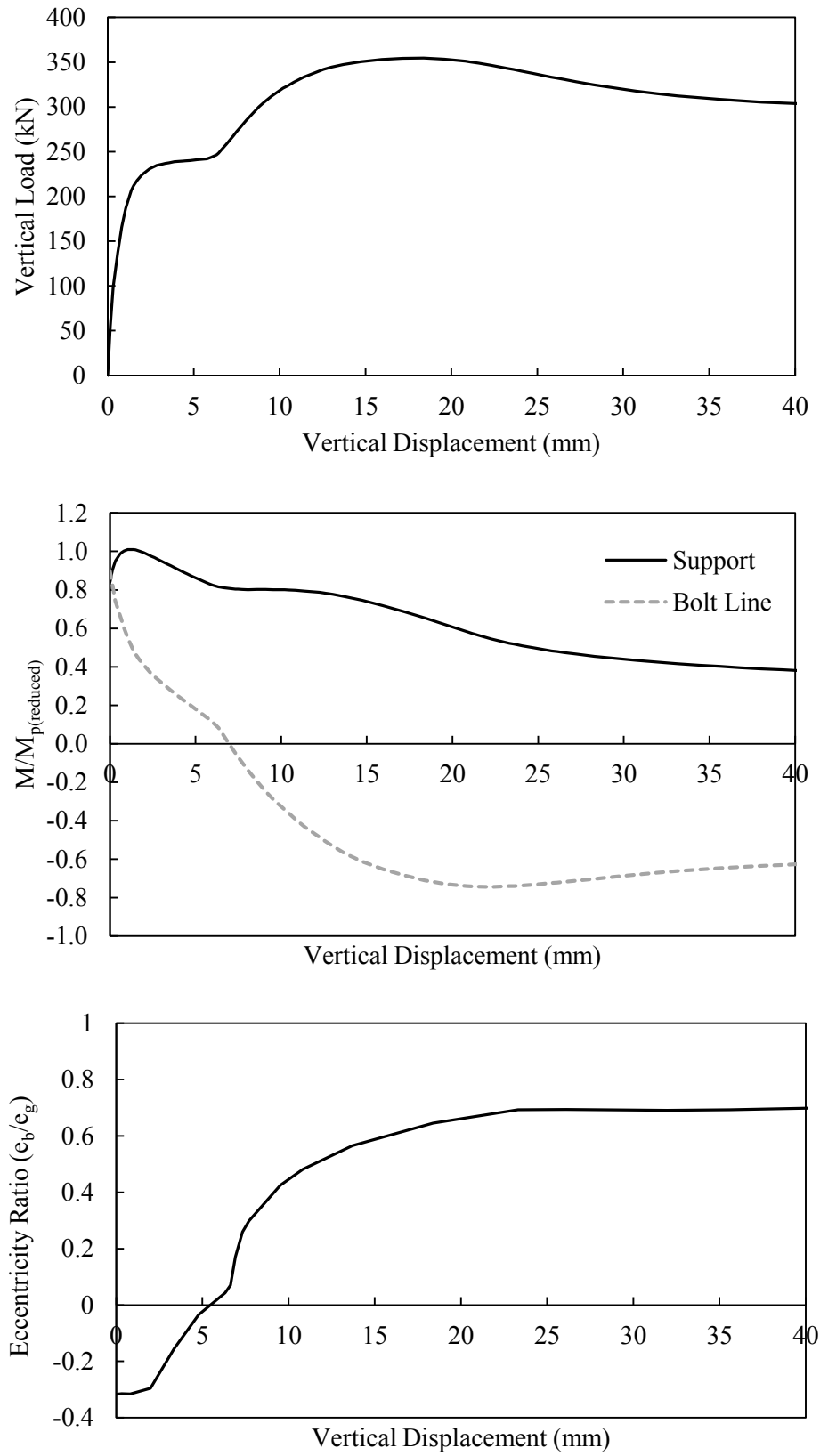
Figure A-18: Model 4B-6-0
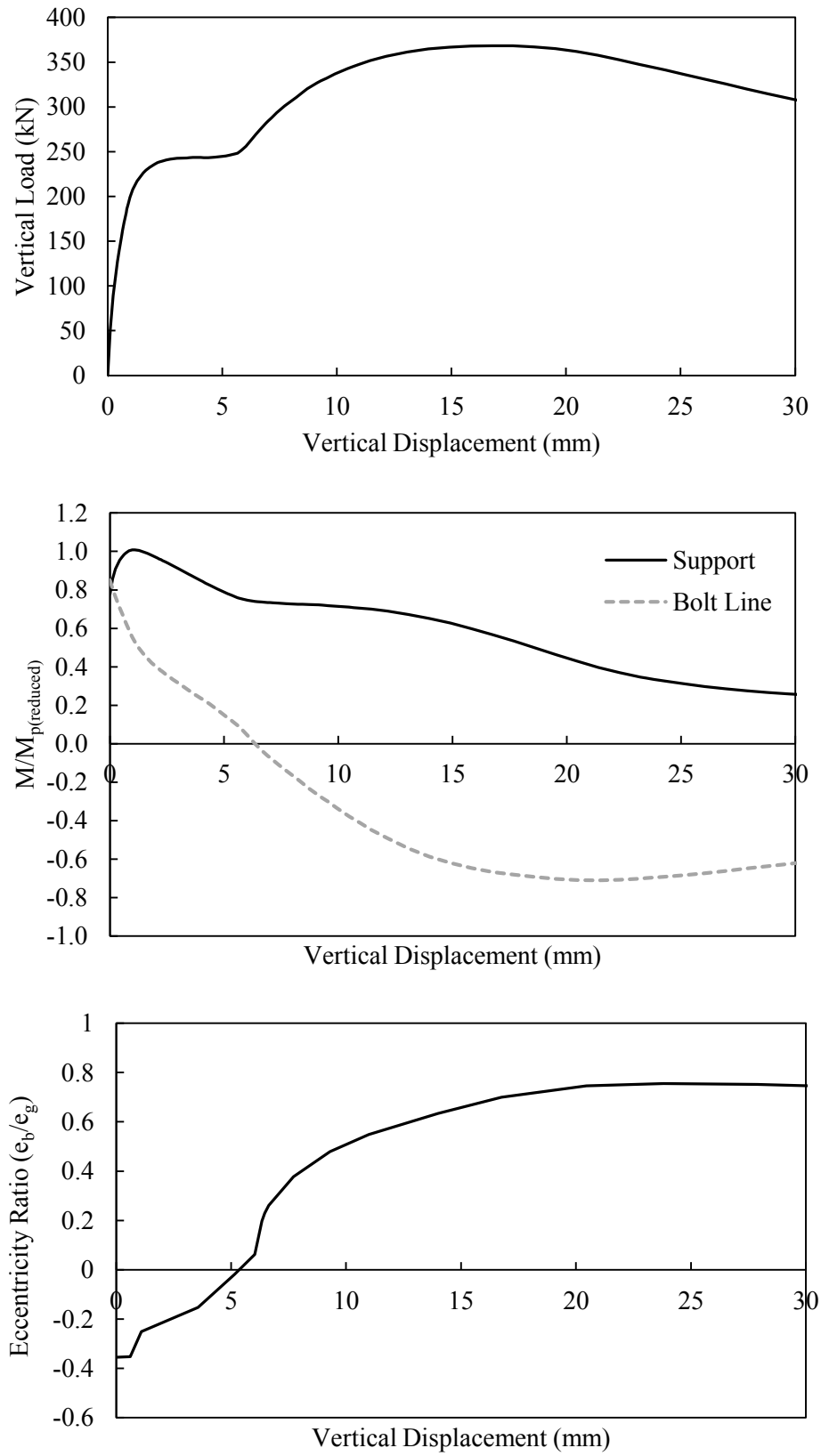
Figure A-19: Model 4B-6-10
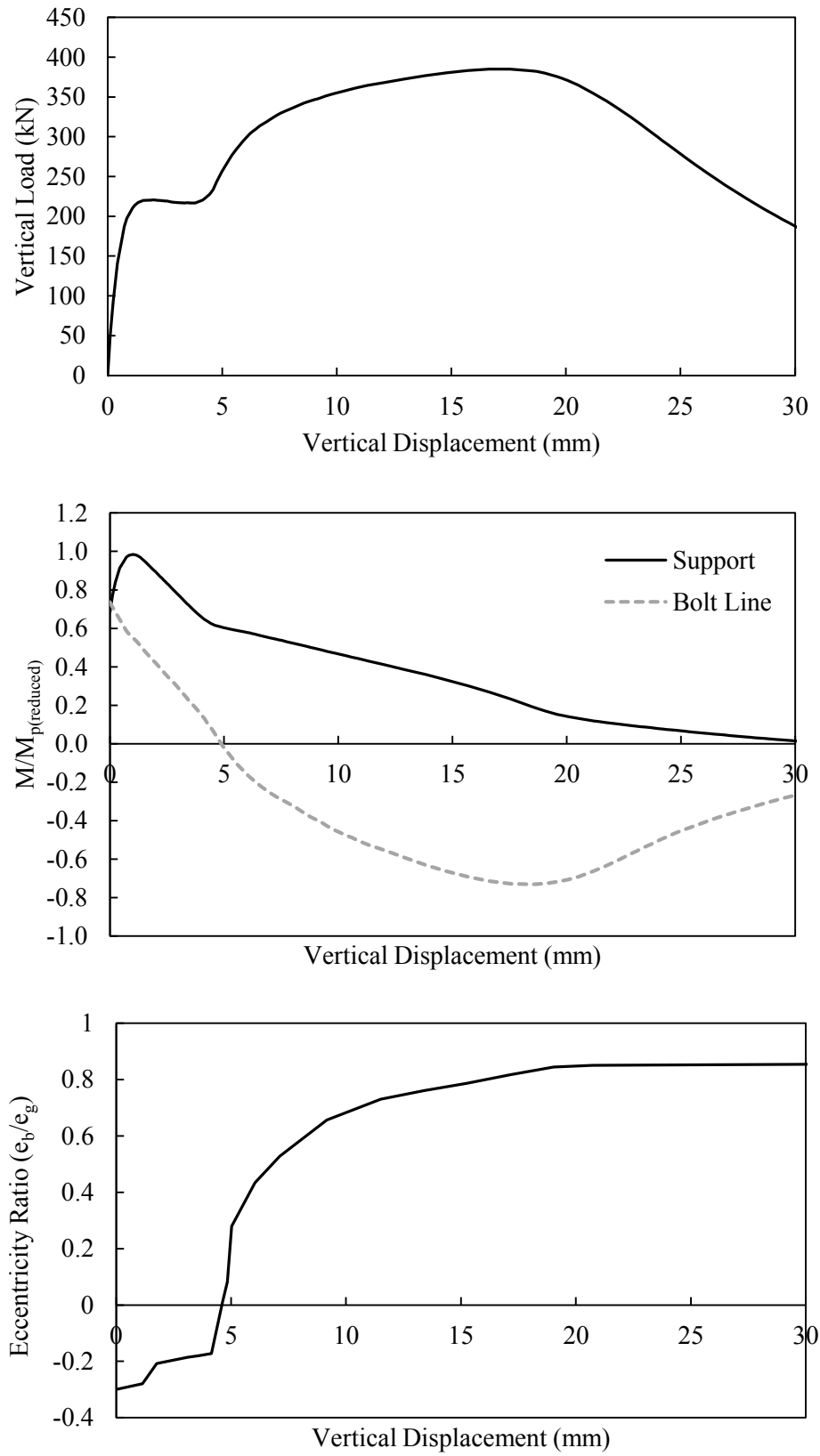
Figure A-20: Model 4B-6-25
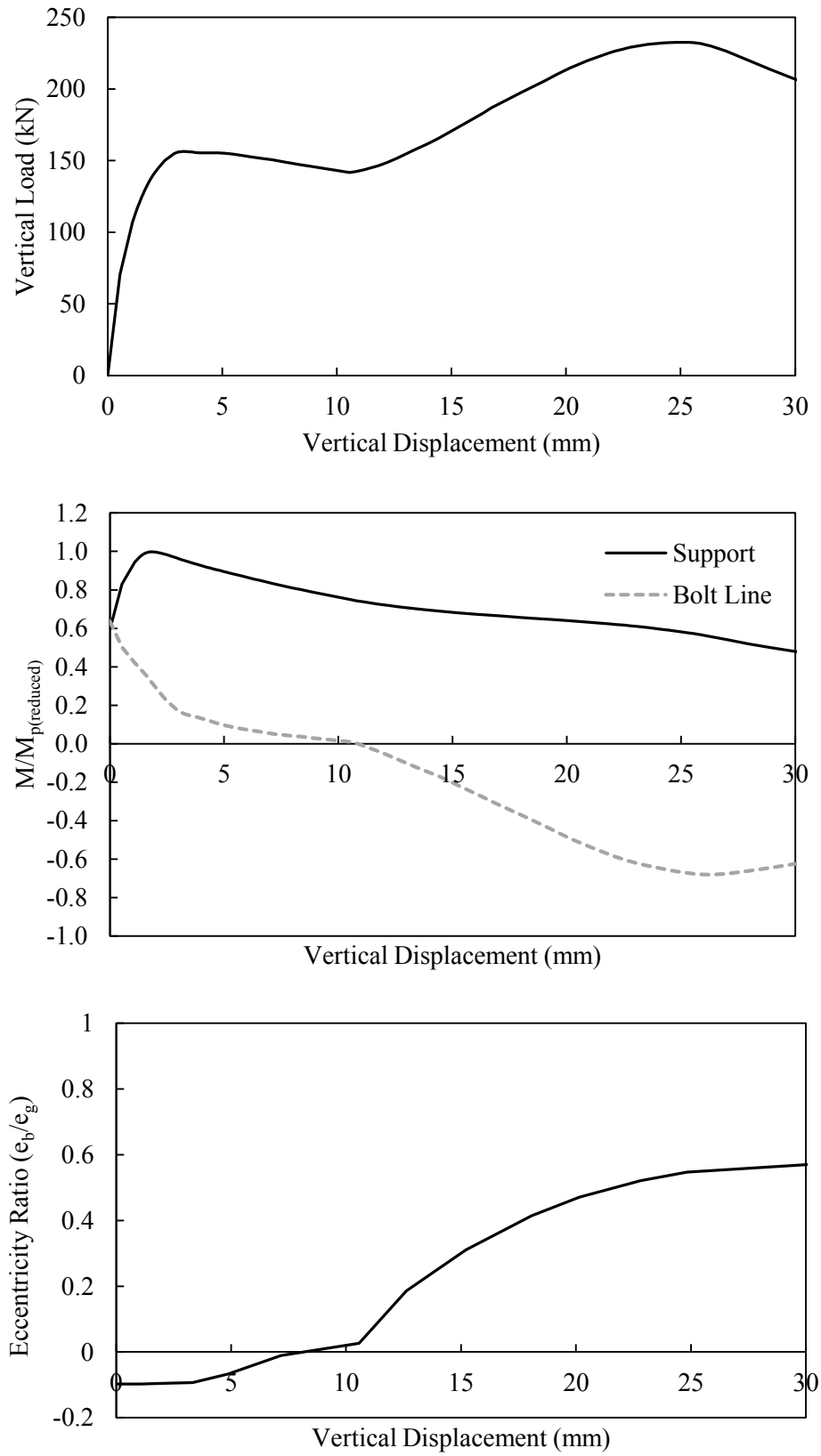
Figure A-21: Model 4B-10-0
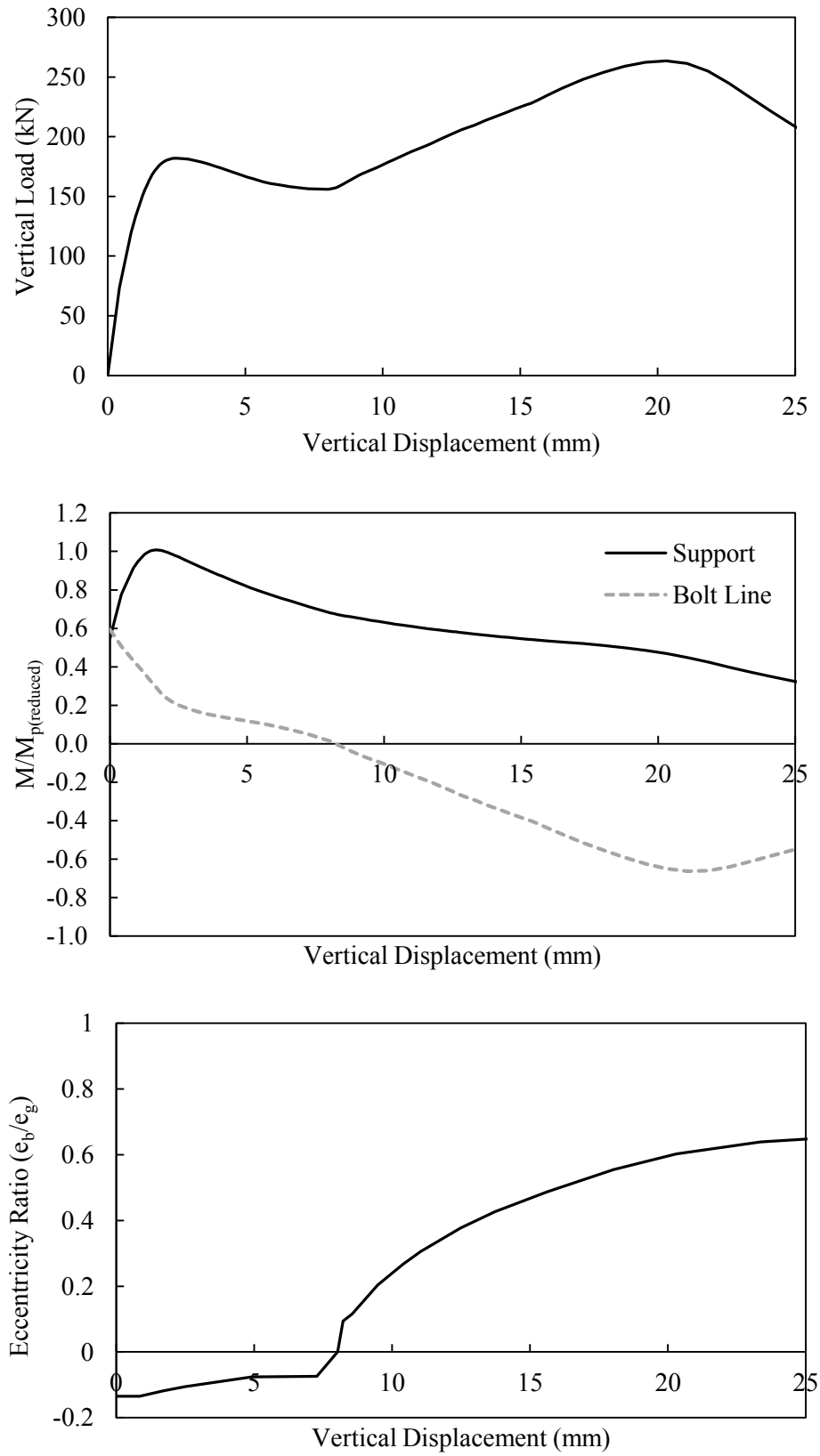
Figure A-22: Model 4B-10-10
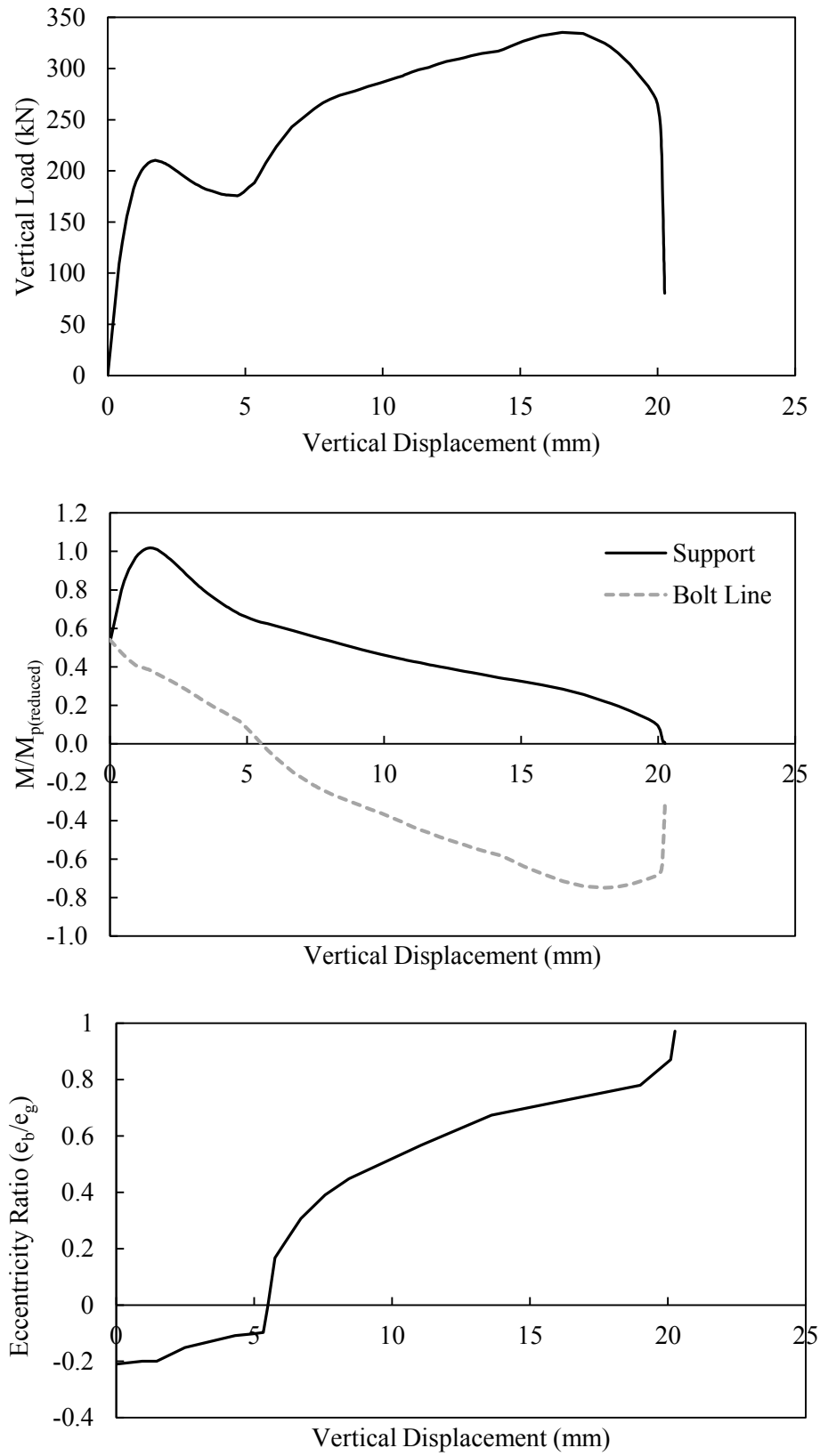
Figure A-23: Model 4B-10-25

Figure A-24: Model 4B-13-0

Figure A-25: Model 4B-13-10

Figure A-26: Model 4B-13-25

Appendix B: Material Test Results
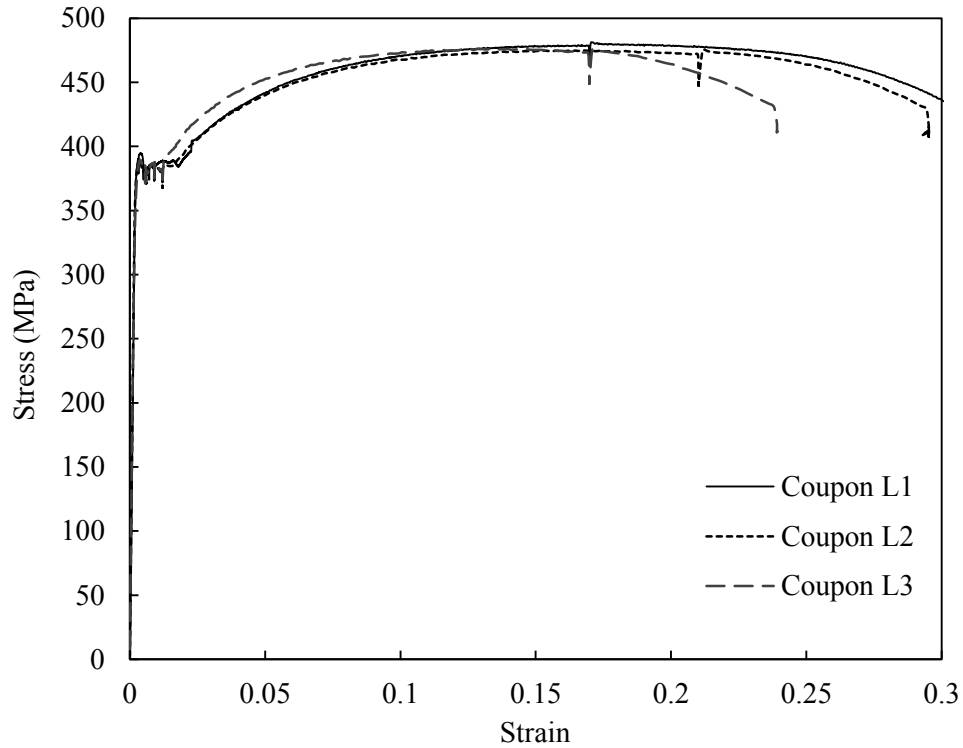
Figure B-1: Engineering stress–strain response of coupons in the longitudinal direction
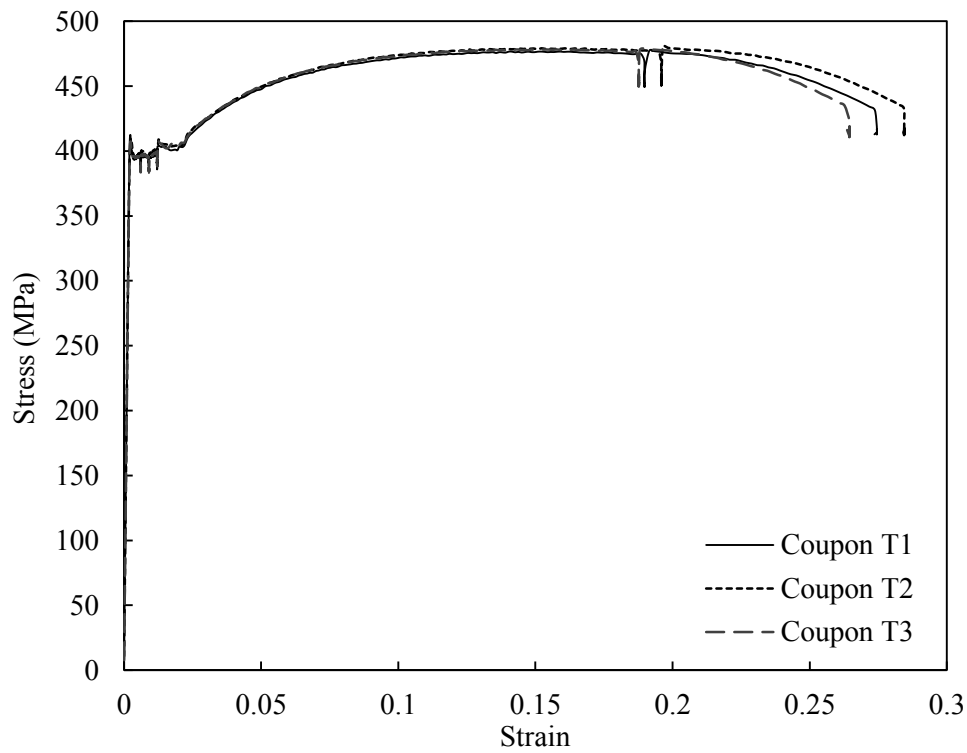
Figure B-2: Engineering stress–strain response of coupons in the transverse direction

Appendix C: Experimental Test Response Curves
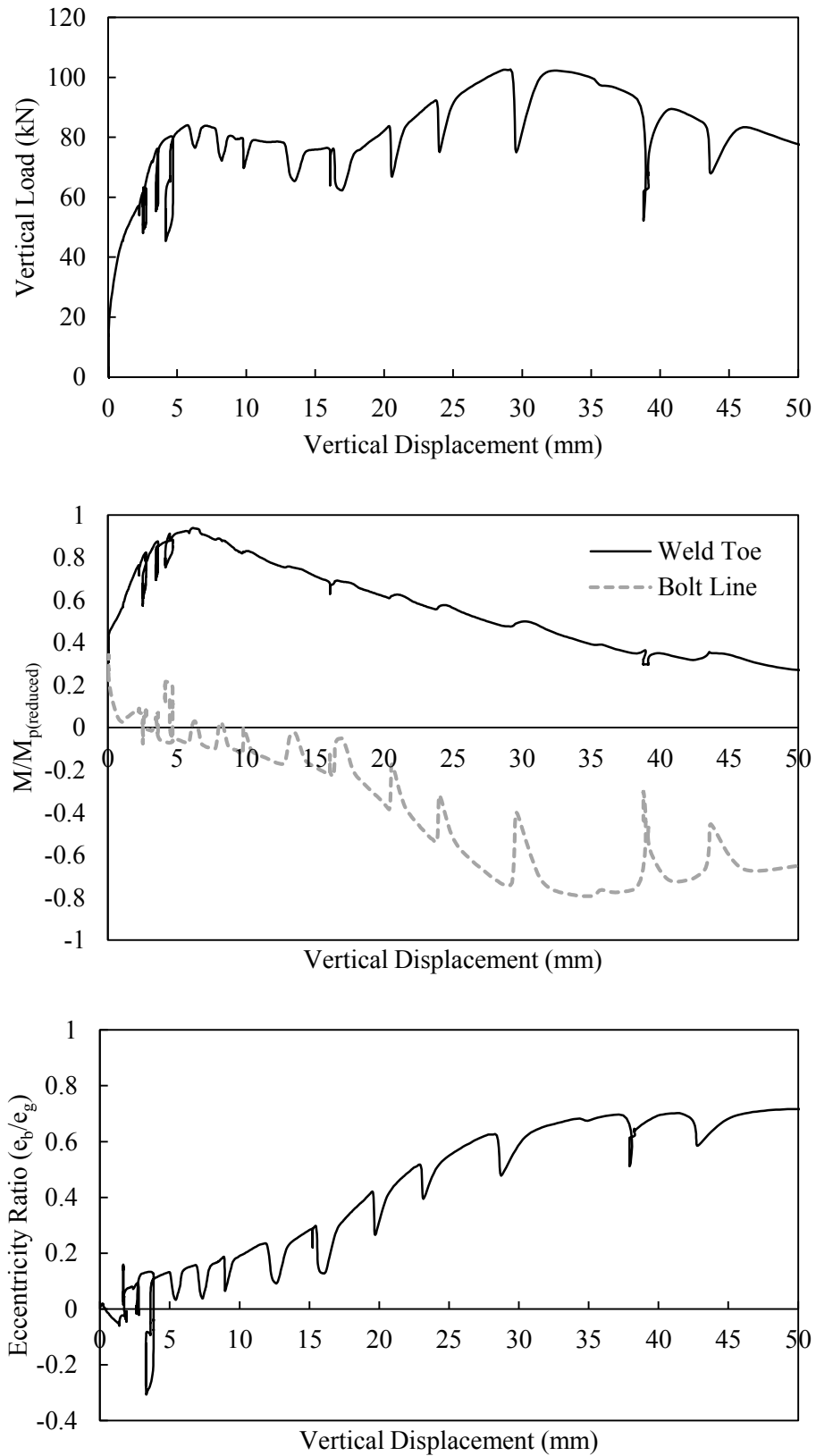
Figure C-1: Specimen 3B-0
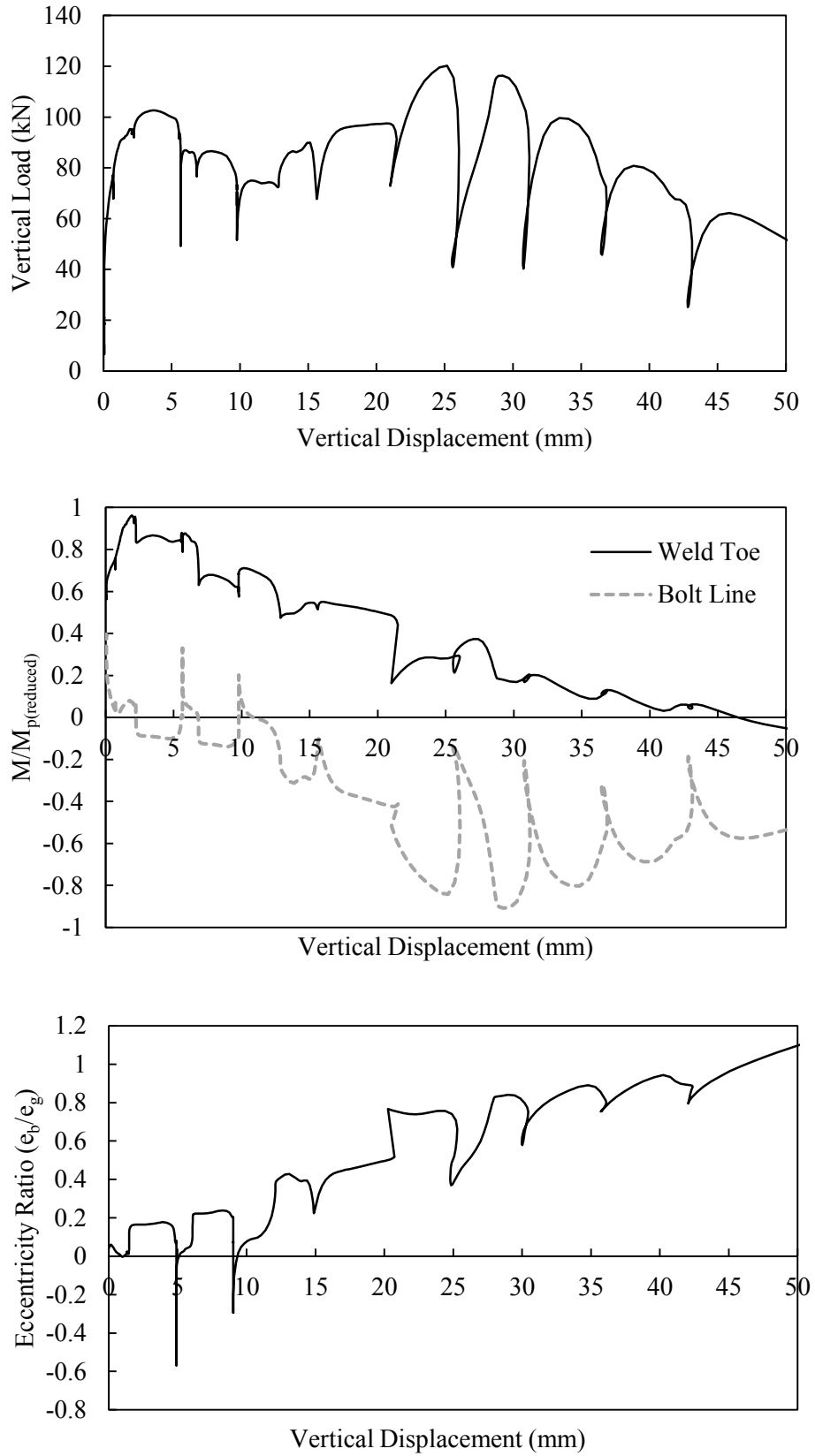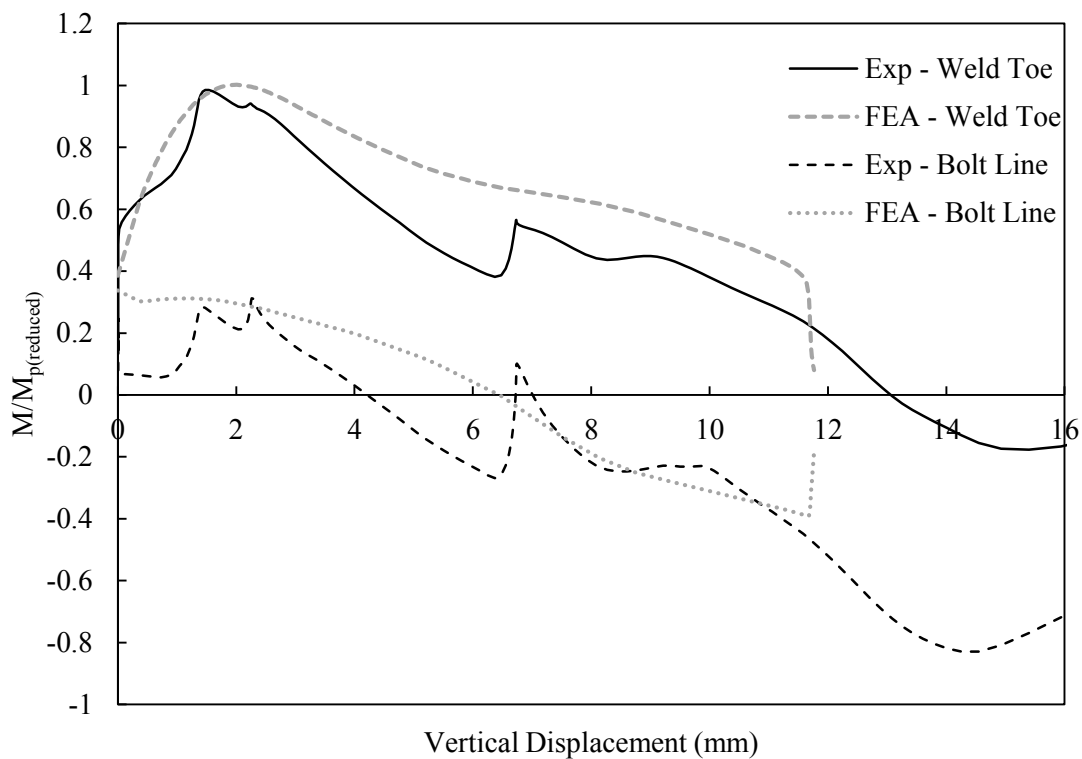
Figure C-2: Specimen 3B-10
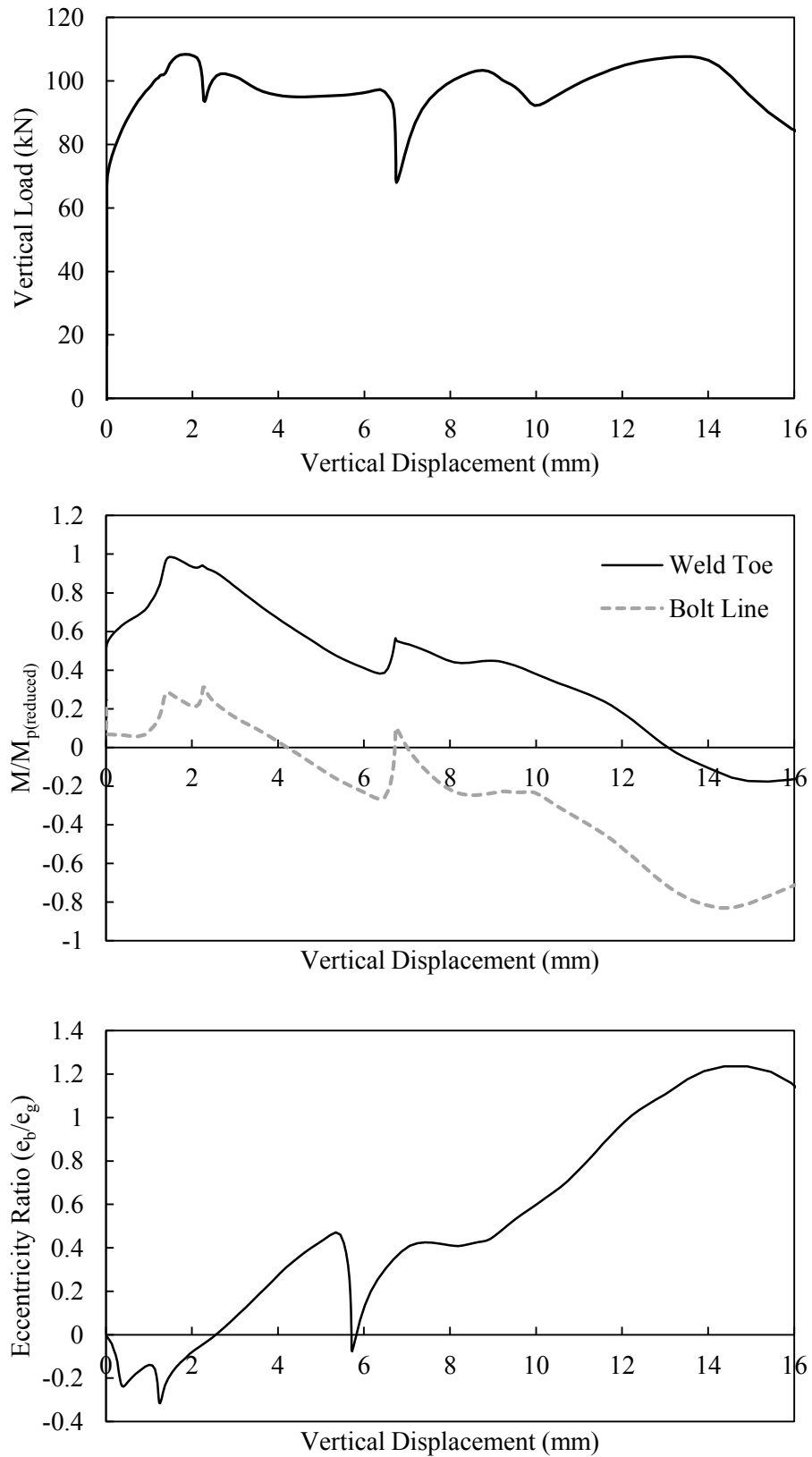
Figure C-3: Specimen 3B-25

147
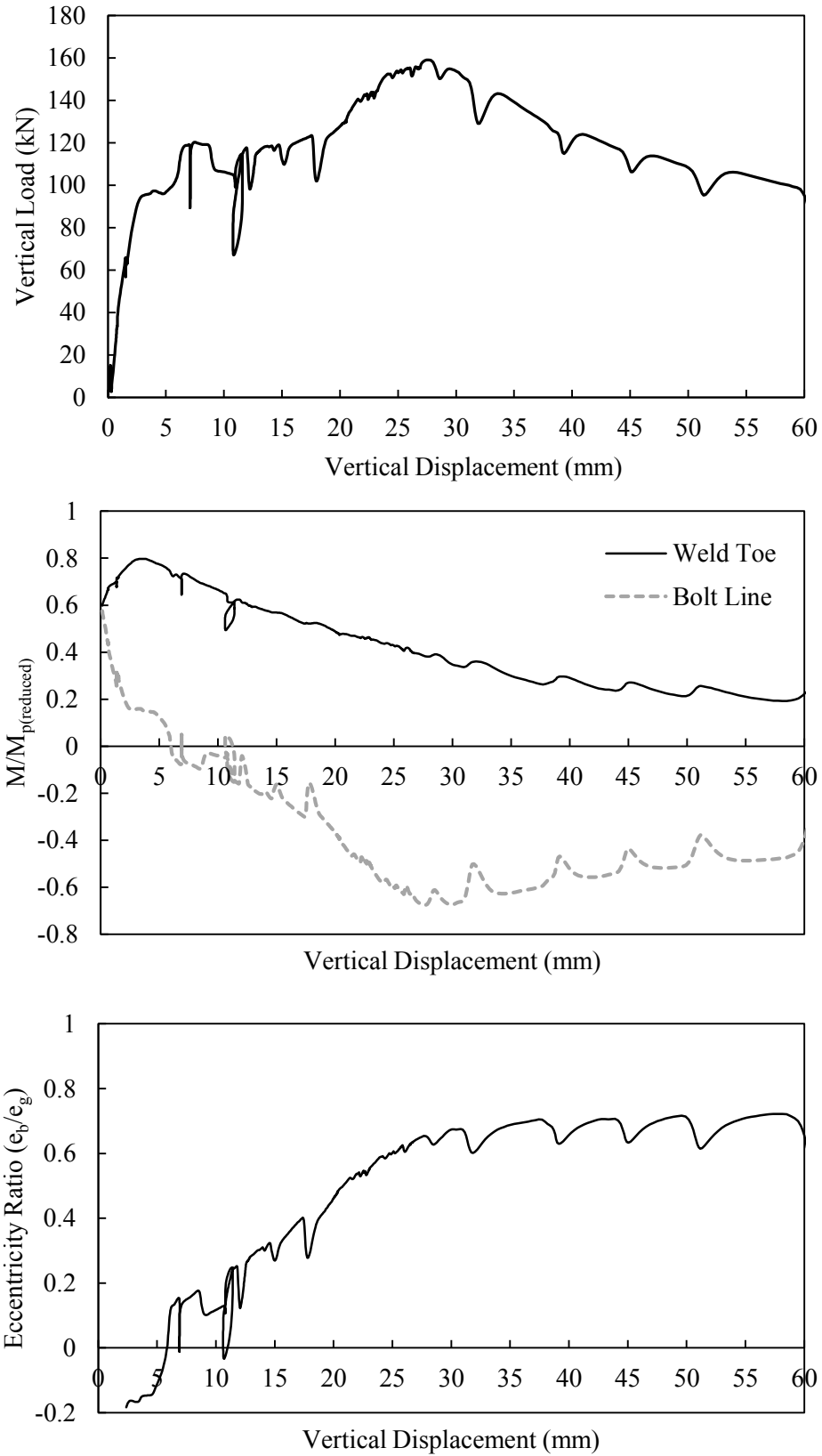
Figure C-4: Specimen 4B-0
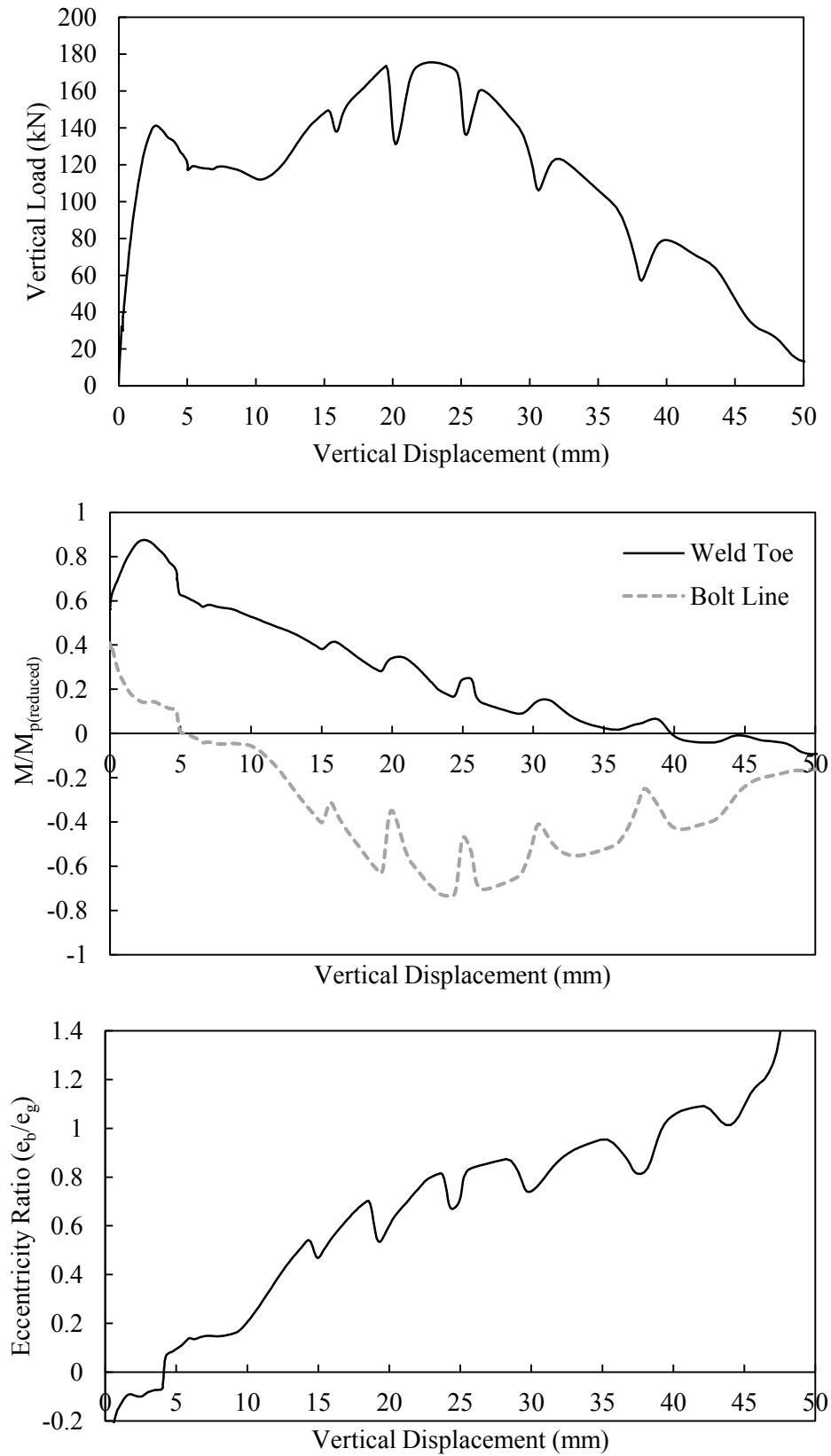
Figure C-5: Specimen 4B-10
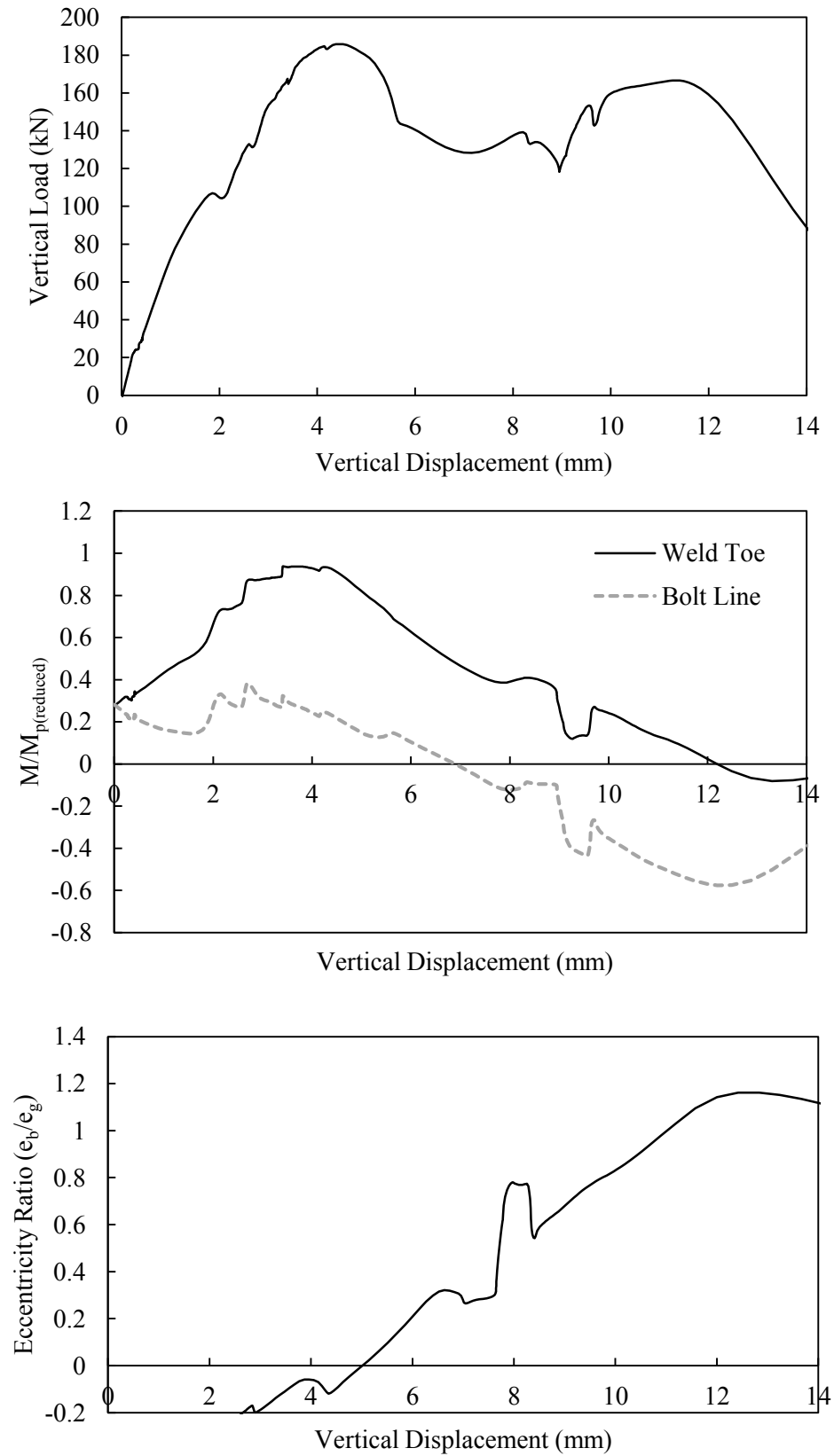
Figure C-6: Specimen 4B-25

Appendix D: Comparison of Bending Moment Response for Numerical and Experimental Tests
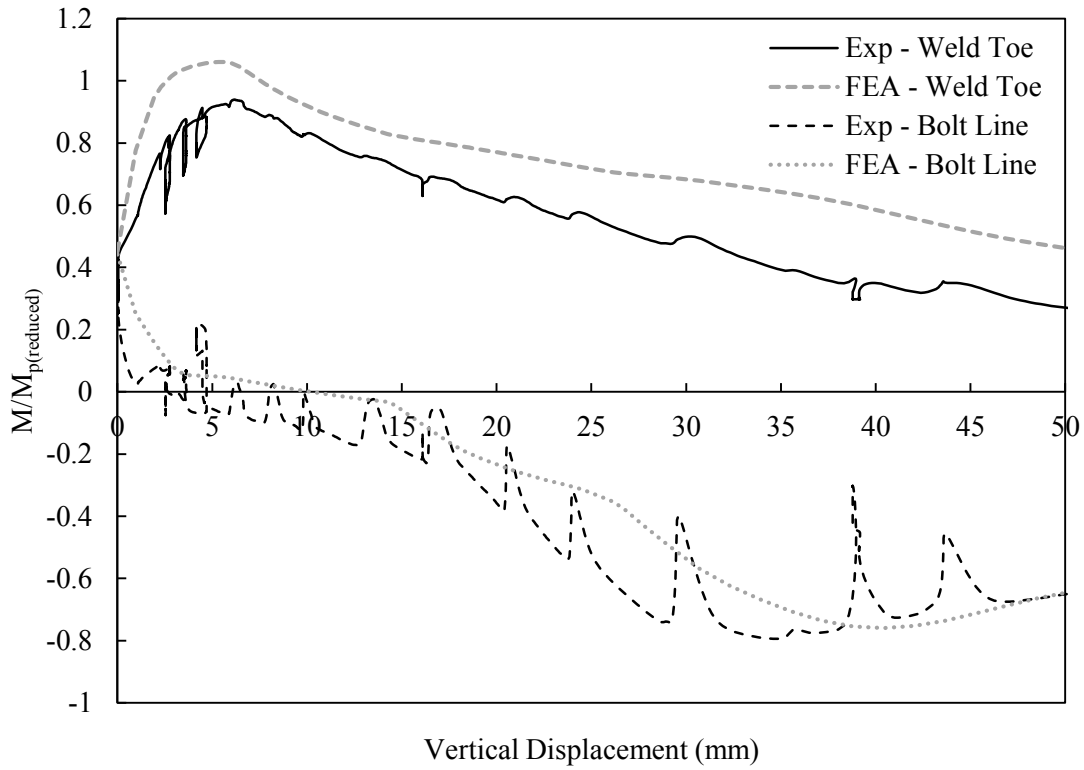
Figure D-1: Specimen 3B-0
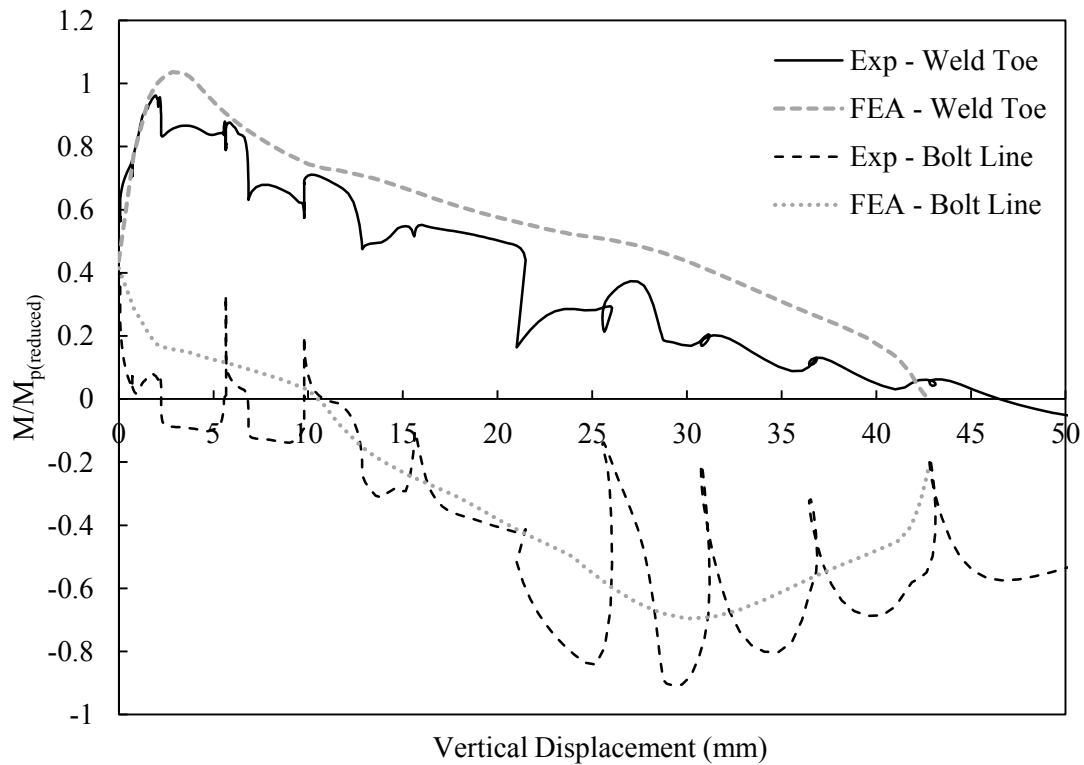
Figure D-2: Specimen 3B-10
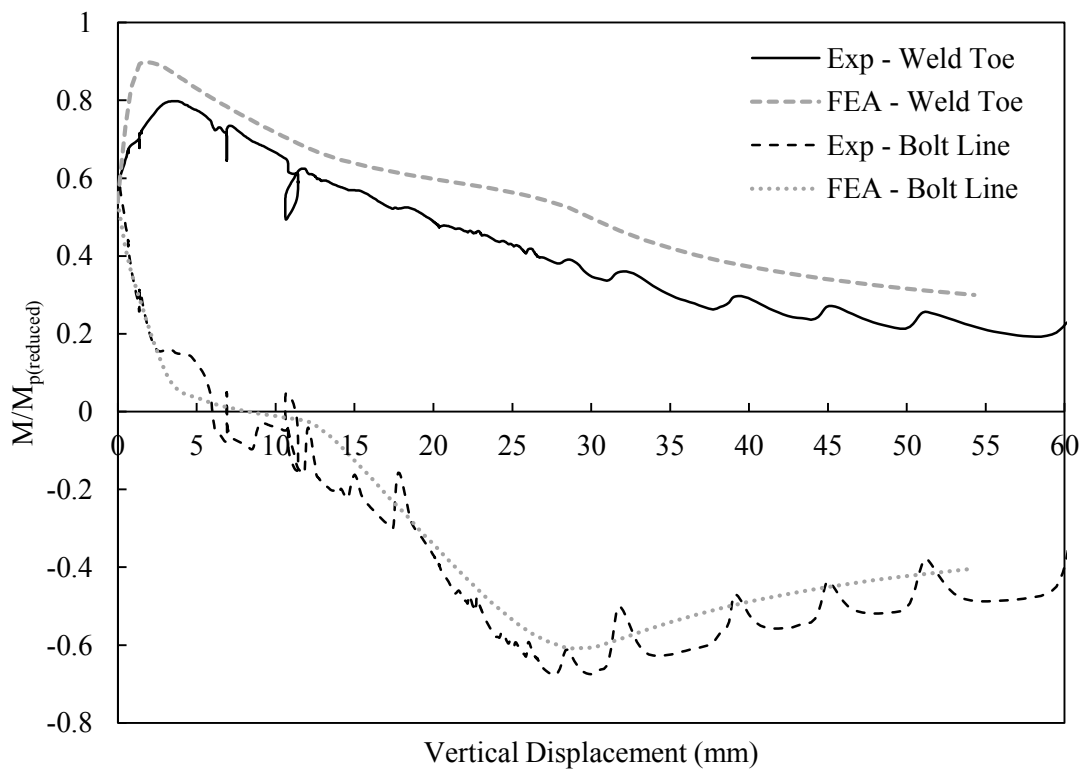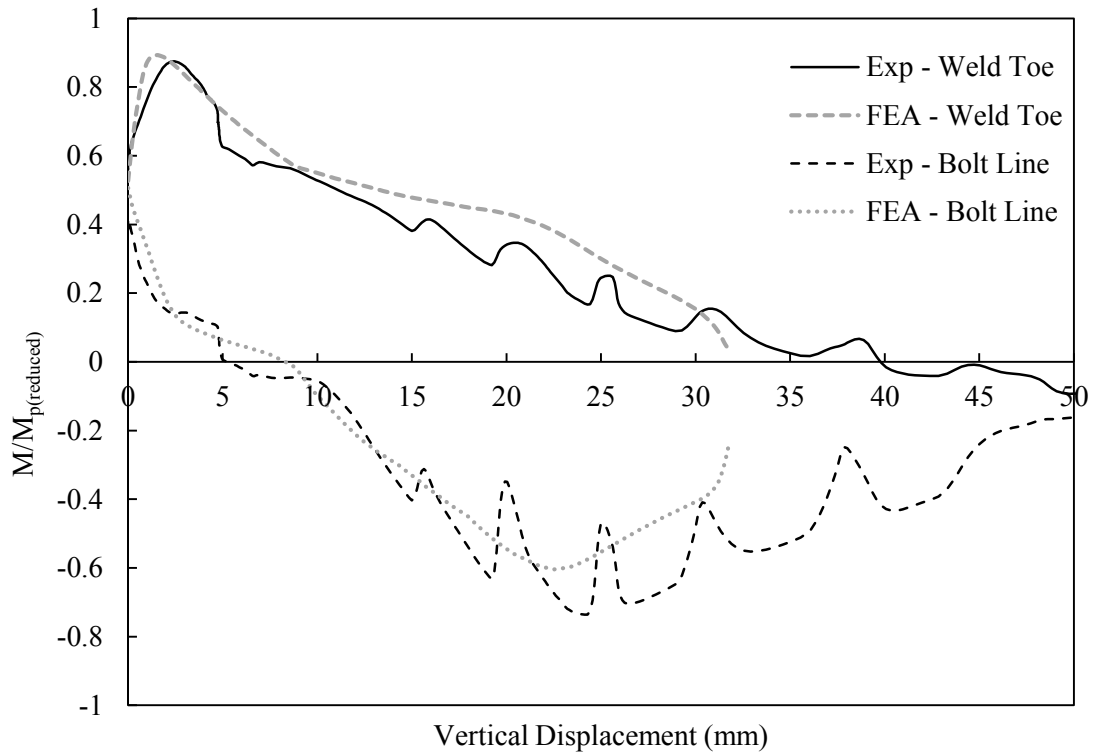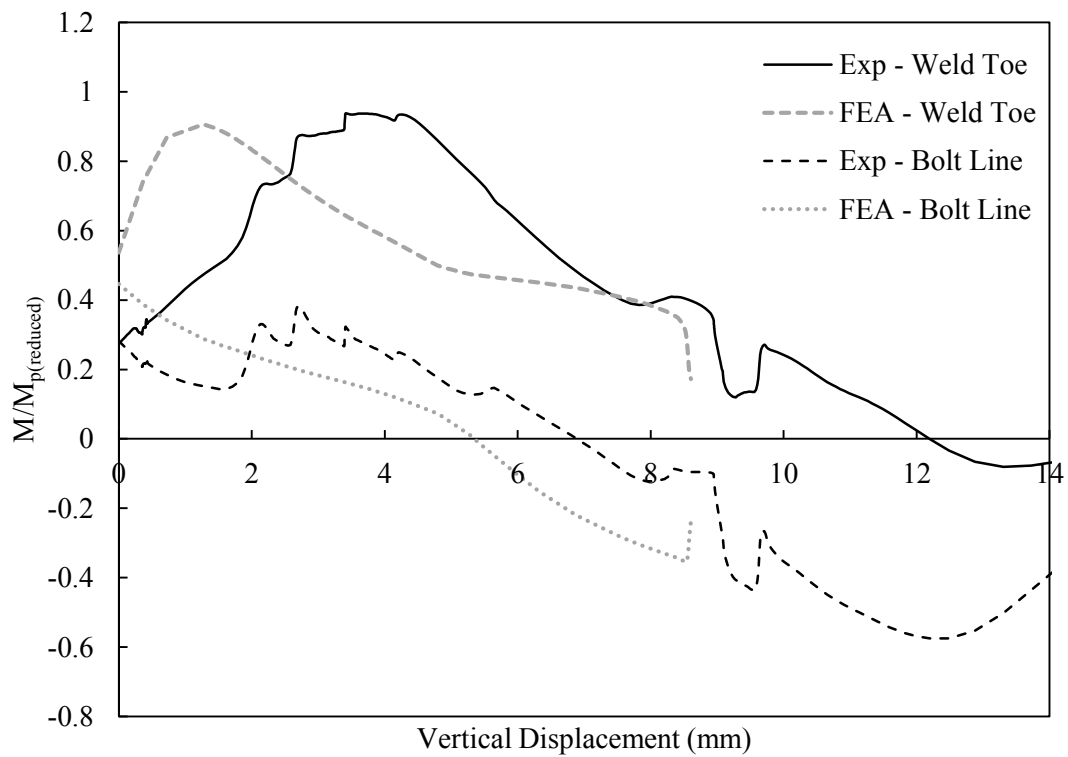
Figure D-3: Specimen 3B-25

Figure D-4: Specimen 4B-0

Figure D-5: Specimen 4B-10

Figure D-6: Specimen 4B-25